Advances in Microreactor Fabrication

Bob Reid
Katrina Sweetland
Martin Ward

LA-UR-23-23350

3/30/2023

Prepared for the U.S. Department of Energy/National Nuclear Security Administration

Los Alamos
NATIONAL LABORATORY

TABLE OF CONTENTS

LIST OF FIGURES

LIST OF TABLES

LIST OF ACRONYMS

AM	Additive Manufacturing
AMI	Arc Machines, Inc.
ANL	Argonne National Laboratory
ASME	American Society for Mechanical Engineers
B&PVC	Boiler and Pressure Vessel Code
CF	ConFlat®
CFD	Computational Fluid Dynamics
EBSD	Electron Backscatter Diffraction
EDM	Electric Discharge Machining
FMEA	Failure Mode and Effects Analysis
HIP	Hot Isostatic Press
HTC	Heat Transfer Coefficients
INL	Idaho National Laboratory
LANL	Los Alamos National Laboratory
MAGNET	Microreactor AGile Non-nuclear Experimental Testbed
MSFC	Marshall Space Flight Center
NASA	National Aeronautics and Space Administration
NIST	National Institute of Standards and Technology
NQA-1	Nuclear Quality Assurance 1
OTW	Orbital Tube Weld
PID	Proportional-Integral-Derivative
SAFE	Safe Affordable Fission Engine
SEM	Scanning Electron Microscope
SME	Subject Matter Expert
SST	Shear Stress Transport
TIG	Tungsten Inert Gas
TZM	Titanium-Zirconium-Molybdenum

UHI	Ultimate Hydroforming, Inc.
UHP	Ultra-High-Purity
US	United States

1.0 INTRODUCTION

The eBlock37 is a subscale electrically heated and heat-pipe-cooled prototype of a fast spectrum microreactor that is under development at Los Alamos National Laboratory (LANL). The prototype consists of an electrically heated core and a gas-cooled heat exchanger. These subassemblies, both built from 316L stainless steel, are thermally linked by an array of 37 sodium heat pipes that transfer a nominal 100 kW from the core at 700°C. An overarching objective of this effort is to overcome challenges associated with core block and heat exchanger manufacture and integration of high-temperature heat pipes into the assembly. Safety-critical components in an actual reactor, such as the heat pipe wicks, are being built under a Nuclear Quality Assurance 1 (NQA-1) quality program. Figure 1 shows an example of design and production steps.

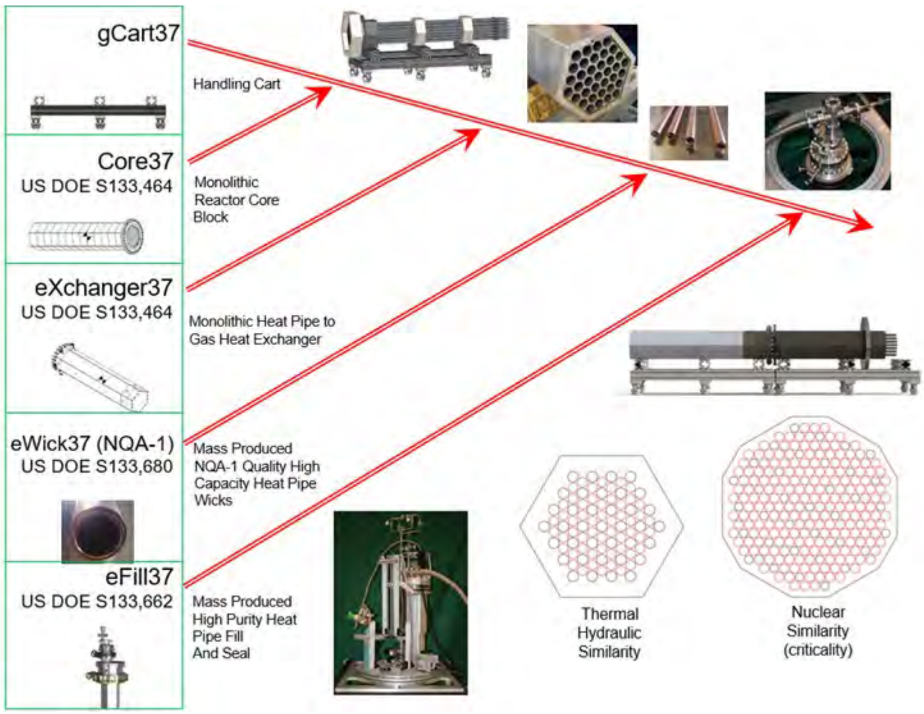

Figure 1. eBlock37 design basis and production sequence.

The eBlock37 assembly was a first-of-a-kind monolithic heat pipe reactor electrical demonstration unit. It is the largest scale high-temperature heat-pipe-cooled nuclear reactor electrical demonstration unit attempted in the United States (US) to date. State-of-the-art design, fabrication, and analysis methods were used to produce the following.

- **Core37 assembly:** This assembly is a fast spectrum heat pipe nuclear reactor 316L stainless steel monolithic core block consisting of an array of close packed high core length to diameter ratio heat pipe cavities. The Core37 is bonded in a high temperature furnace. Several promising fabrication techniques were developed that now exist at varying levels of maturity, including HIP of machined plates, tier welding of additively manufactured blocks, diffusion bonding of machined plates, and vacuum braze of machined plates. The Core37 fabricated for this project we elected to bond plates via vacuum brazing. The Core37 Assembly approach allows for scaling in number of heat pipes (diameter) as well as assembly length. Current high temperature furnaces in the US permit fabrication of cores of up to 10 ft long.

- **eXchanger37 Assembly:** A 316L stainless steel monolithic heat pipe to gas heat exchanger block consisting of an array of high length to diameter ratio annular heat exchanger channel. The eXchanger37 was fabricated by gun drilling ~0.95 in. holes into a block of up to 30 in. long. At the time of fabrication few US manufacturers possessed the capability to gun drill holes of this number and aspect ratio.

- **eBlock37 American Society for Mechanical Engineers (ASME) boiler and pressure vessel code (B&PVC) analysis:** The initial eBlock37 assembly design was informed by analysis conducted by Argonne National Laboratory (ANL) to address potential heat pipe reactor structural design issues. This exercise laid the foundation for an ASME code case for the fabrication of an innovative nuclear reactor type using advanced materials manufacturing methods.

- **eWick37 array:** This array includes commercially manufactured high capacity and temperature (>10 kW/cm^2 above 800°C) wicks for alkali metal heat pipes. We are not aware of any other source of high temperature heat pipe wicks with the axial heat flux capabilities possessed by this design. These wicks are built to NQA-1 quality standards, are now a national resource available to US entities by license through Los Alamos National Laboratory's Feynman Center for Innovation.

- **eFill61 assembly:** This assembly is a high-quality, affordable, and scalable alkali metal heat pipe fill and closure device using off-the-shelf parts that enables rapid production of high-temperature-alkali-metal-heat-pipe-cooled nuclear reactor cores. In its current manually configured mode the eFill61 assembly can charge, close, and seal an array of several dozen alkali metal heat pipes per day. We are unaware of any existing mechanism with similar capabilities in operation at present. The design of the existing eFill61 is fully amenable to automation with stepper motors to move its rotating stages and electrically or pneumatically actuated valves to control vacuum, gas, and fluid flows. Using industrial PLC an automated version of the eFill61 is believed capable of charging and sealing several hundred alkali metal heat pipes per day. This unique capability has only emerged in the last few years through sustained DOE support.

- **Internal orbital tube weld (OTW) technology:** This is an innovative technique that allows rapid integration of alkali metal heat pipes into high-temperature nuclear reactor assemblies. This unique and useful capability was developed through cooperative development with Arc Machines Inc. (AMI).

Development of these technologies enables affordable mass production of alkali metal (potassium, sodium, and lithium) heat-pipe-cooled nuclear reactor cores. To date, all eBlock37 components have been fabricated, including the eWick37 array, the eXchanger37, the eFill61 assembly, and the Core37 assembly. All components, except for the Core37, were successfully fabricated. A setback in the braze of the Core37 that led to high leak rates across the thin web between the heat pipe and the fuel tube holes has rendered it unusable for heat pipe integration. However, the existing Core37 and eXchanger37 can be heated electrically and used to test instrumentation at prototypic temperatures.

2.0 OBJECTIVES

Heat transfer in a microreactor needs to overcome unique challenges because of the compact footprint, radiation field, transportability, and high temperatures present. High-temperature operation of microreactors is preferred to give higher power production efficiencies. Here, novel heat pipe concepts were explored to transport heat and dampen transients affecting structural integrity and performance of core structures and components. Research and testing of non-nuclear components helps increase our understanding of system performance. To help overcome these challenges, the following were the objectives for this work.

- Investigate feasible heat pipe and gas-cooled components; heat exchanger and power conversion units can be integrated for non-nuclear testing easier than in nuclear demonstrations

- Develop and demonstrate techniques for fabricating test articles that include a heat exchanger that gas cools a heat pipe non-nuclear core

3.0 eFill37

Before this effort, low volume production of alkali metal heat pipes reflected their developing technology readiness level. In 2002, LANL built a general-purpose alkali metal fill system for use at the National Aeronautics and Space Administration’s (NASA’s) Marshall Space Flight Center (MSFC). This system allowed the fill of individual potassium, sodium, or lithium heat pipes in a low oxygen, water, and nitrogen inert gas environment (typically <1 ppm). Figure 2 shows a picture of this system configured for the fill of sodium heat pipes for the Safe Affordable Fission Engine (SAFE)-100a technology demonstration. This system was dependable with moderate flexibility and complexity but required a skilled operator. Its design only allowed the fill of a few individual heat pipe modules per day. Although the fill system performed well for low volume development efforts, its methods and techniques were ill-suited for automated industrial fill of alkali metal heat pipe arrays. Recent interest in very small modular nuclear reactors motivates the development of methods to rapidly and cost-effectively fill and seal arrays of heat pipes with high-purity alkali metal, such as sodium, in a mass production environment.

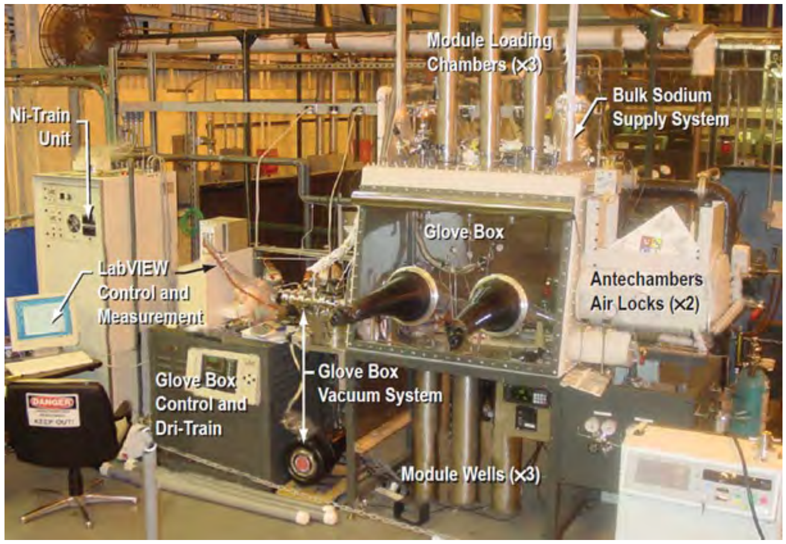

Figure 2. LANL-built heat pipe fill system at NASA's MSFC, 2003.

During the present program, LANL built a scalable, modular alkali metal heat pipe fill system called the eFill61 for use in large-scale heat pipe systems to rapidly charge individual heat pipes in larger monolithic heat-pipe-cooled nuclear reactors. This section describes the product of this effort. The fill system methods used represent a significant departure from earlier approaches to alkali metal fill. Desired attributes for this system include rapid, reliable, and inexpensive filling of a ~103-heat-pipe monolith in several days or less. Simple and flexible filling steps intend to allow system use by normally skilled operators. The design progression centered on successive simplification. Implementation of a failure mode and effects analysis (FMEA) guided process development by identifying least reliable process steps. This permitted selection of a design that allows appropriate levels of product inspection and quality control.

The bulk of the eFill61 development effort consisted of producing a cost-effective and scalable means to fill large heat pipe arrays. Where possible, the eFill61 uses readily procured parts and industry-standard fabrication practices such as vacuum laser welding. A scalable system to fill, plug, and seal an array of heat pipes was developed. To make the system reproducible, the components primarily consisted of off-the-shelf parts. There are separate subassemblies for charging the heat pipes, plugging the heat pipes, and sealing the heat pipes with laser welding. Each subassembly is designed to be able to be removed while dynamic vacuum over the heat pipes is maintained. When using the eFill61 to charge the eBlock37 heat pipes, the system uses two rotatable stages and the theta-theta relation to reach each heat pipe. Figure 3 shows the theta-theta relation that allows the eFill37 to reach each of the 37 heat pipes in the array.

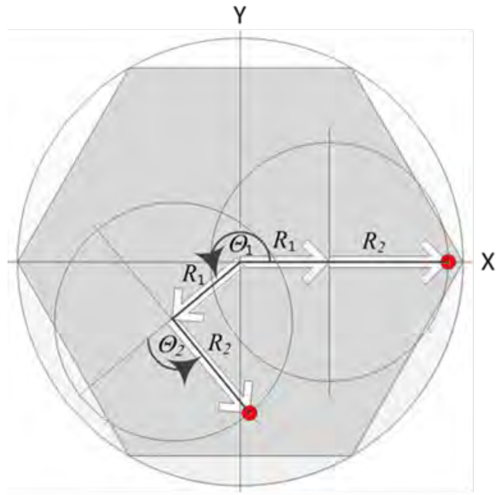

Figure 3. Theta-theta relation used in the eFill37.

The eFill37 attaches to the eBlock37 using a matching ConFlat® (CF) flange that connects to the lowest rotatable stage. After the eFill37 is attached to the eBlock37 and is verified to be leak free using helium leak testing, the three subassemblies can be used to charge each of the heat pipes. These subassemblies consist of a sodium charge subassembly, a plug subassembly, and a laser weld subassembly. The height of the core is approximately 2 m, so a mezzanine was used to provide a support and work area for the eFill37. As a proof of concept, all subassemblies were tested on a “mock block” that consists of a shorter representative heat pipe core on the mezzanine. Figure 4 shows the sodium charge assembly installed onto this mock block.

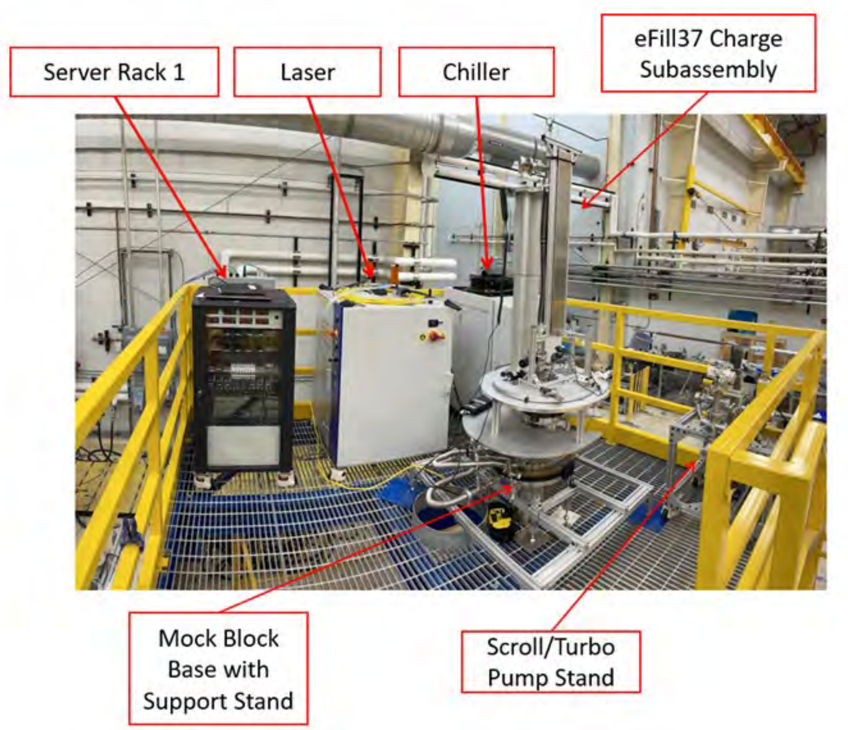

Figure 4. Sodium charge subassembly installed on the mock block.

The eFill37 system is heated with both heat tape and band heaters. The heaters are controlled using over-temperature controllers and proportional-integral-derivative (PID) temperature controllers located in two server racks. One server rack controls the heaters on the top half of the eFill37 and is located on the mezzanine, whereas the second server rack controls heaters wrapped around the eXchanger37 and Core37 under the mezzanine. To maximize the working space available on the mezzanine, the second server rack was placed on the floor. Figure 5 shows the two server racks side by side.

Figure 5. Sodium charge subassembly server racks.

3.1 Sodium Charge Subassembly

The first step of the using the eFill37 is installing and using the charge assembly to charge each heat pipe. After installation, the charge subassembly will undergo a successive dilution with ultra-high-purity (UHP) argon. Figure 6 shows an exploded model of the sodium charge subassembly. In the charge subassembly, the sodium distribution and fill stem are lowered by the linear lifting column until the fill stem is over or even slightly inside a heat pipe tube as shown in Figure 7.

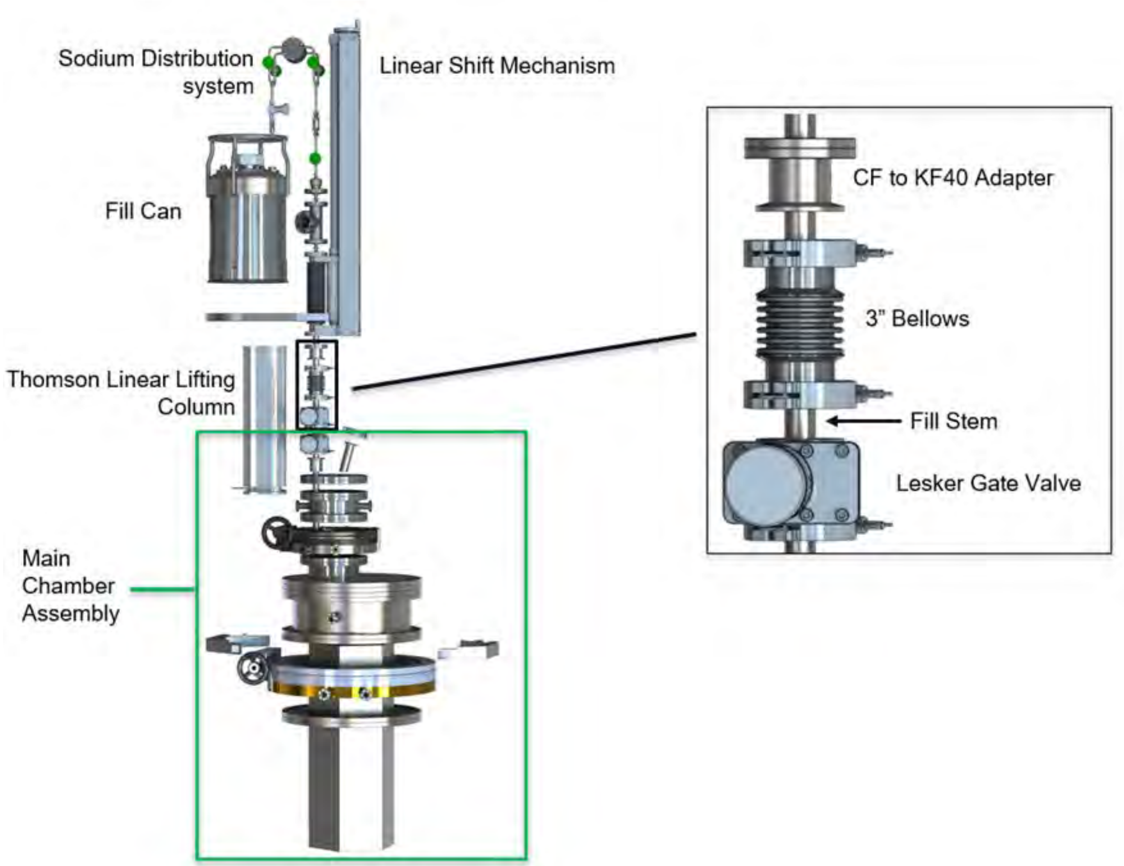

Figure 6. eFill37 charge subassembly.

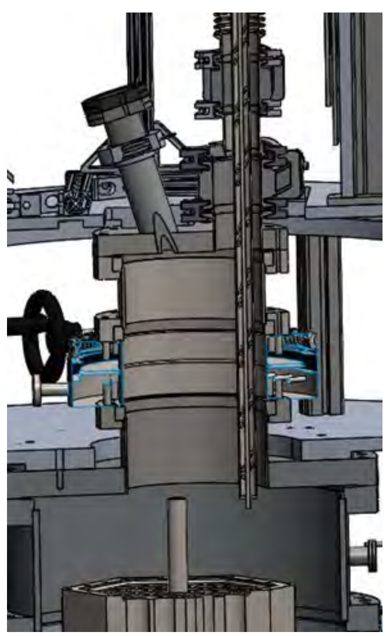

Figure 7. eFill37 fill stem lowered over a heat pipe with an example tube shown for scale.

The sodium distribution system then dispenses a known and repeatable quantity of sodium. The sodium flows down the heated fill stem and into the heat pipe. The assembly is raised and aligned with the next heat pipe. This process is repeated until the desired number of heat pipes is filled. When the process is complete for the desired number of heat pipes, the fill stem retracts into a stow position above both gate valves. The valves are closed, and the sodium charge subassembly is removed from the system by disconnecting the two gate valves. After removal, the sodium charge assembly is replaced with the plug subassembly.

3.2 Plug Subassembly

The plug subassembly is similar to the sodium charge subassembly, with the main difference being a plug feed tube and a spring-loaded arm assembly in place of the fill stem. There is also an additional linear motion actuator that provides enough downward force to move the spring-loaded arms and release a plug. The plug loader is shown in Figure 8 and the subassembly is shown in Figure 9.

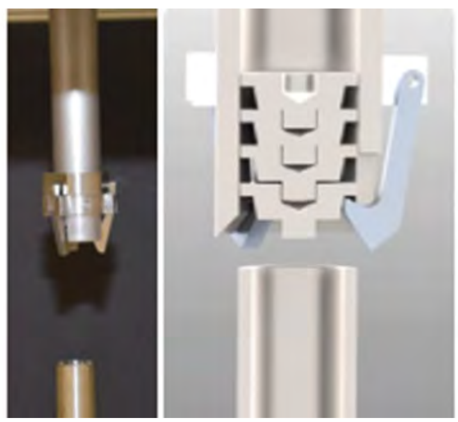

Figure 8. (Left) eFill37 plug loader feed tube with spring-loaded arms and (right) section view of the plug loader feed tube with spring-loaded arms.

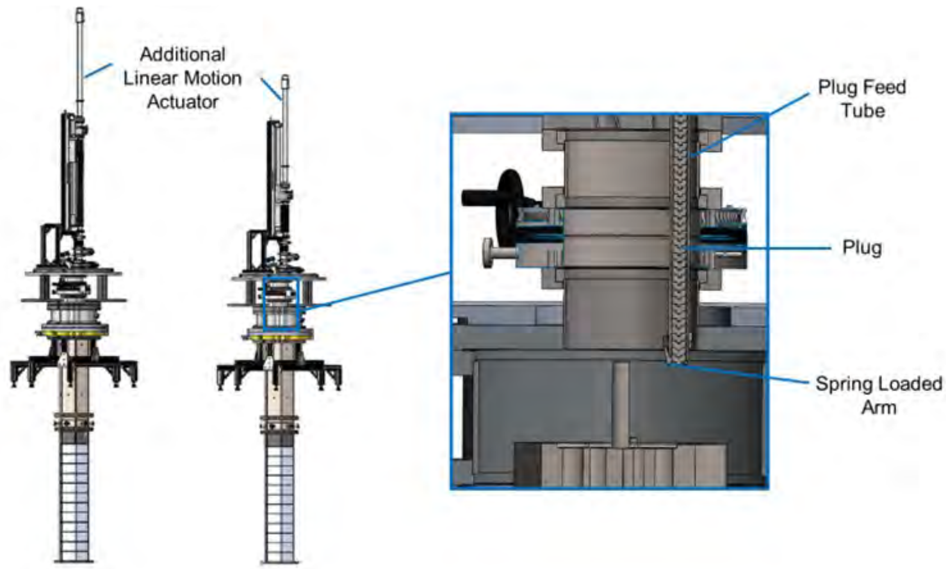

Figure 9. (Left) eFill37 plug subassembly fully in a stowed/raised position, (center) the plug assembly lowered into the plugging position, and (right) a section view of the plug subassembly in its plugging position with an example tube for scale.

After the plug is released, the feed tube is raised and the spring-loaded arms return to their original position, catching the next plug. The system is then rotated to align with the next heat pipe hole and the process is repeated. When all of the filled heat pipes are plugged, the gate valves shown in Figure 6 are closed and the plug subassembly is replaced with the laser welding subassembly.

3.3 Laser Welding Subassembly

After the laser assembly has been installed onto the eFill37 main chamber assembly, the laser assembly is successively diluted with UHP helium. After successively diluted the bottom gate valve is opened and the main chamber is set to a pressure of 0.1 Torr of helium using a needle valve to control the helium flow rate.

A camera with a laser filter and light-tight enclosure is used to verify laser alignment and weld. The camera output can be seen on the upper right monitor in the right image of Figure 10. The weld passes over the plugs in a circular pattern and the wobble head allows the laser to successfully seal larger gaps than a standard laser welder. Figure 11 shows an example laser weld of a representative plug and tube.

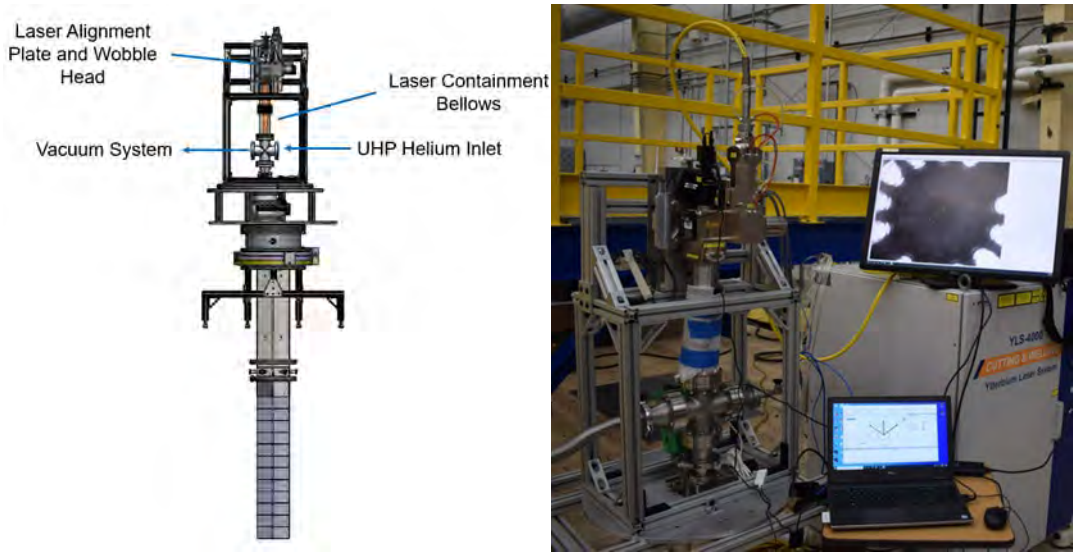

Figure 10. (Left) eFill37 laser weld subassembly model and (right) built laser weld subassembly.

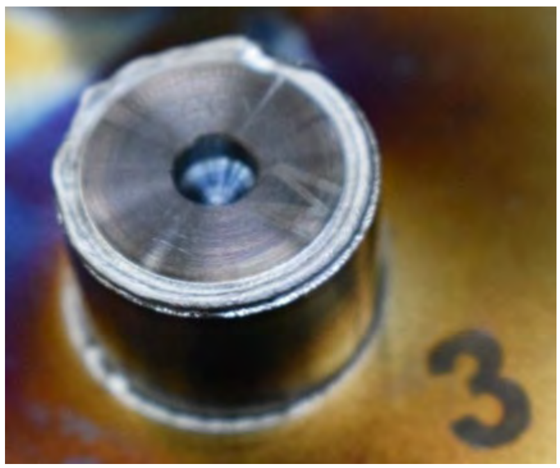

Figure 11. Sample plug and tube after laser welding.

4.0 eWick37

Heat pipes serve in a range of applications such as electronics, spacecraft, and nuclear power conversion. This results from their flexibility in terms of size, heat transfer capability, and angle of operation. Fluid returns to the heat addition zone from the heat removal zone through a high-performance wick that drives the versatility of the heat pipes.

A comparison between thermosiphons and heat pipes demonstrates wick utility and adaptability. A wick creates capillary action that drives fluid circulation, whereas thermosiphons rely solely on gravity to operate. Thermosiphons must operate inclined, with the heated region at the bottom. Because heat pipes rely on capillary action rather than gravity to function, they can operate at any angle within their wicking height and even in microgravity environments, such as in space.

The shape of the heat pipe wick imposes order on a saturated liquid by (1) forming menisci between the condensate and the vapor and (2) allowing condensate to flow toward the heated zone.

Simple heat pipe wicks are homogeneous with a uniform pore structure with condensate to flow axially through the same pore structure that forms the surface menisci. Figure 12a depicts a cross section of a homogeneous wick. A homogeneous wick that produces a high capillary pressure rise typically has high resistance to condensate flow, thus limiting the axial heat transfer rate.

In the heated zone of a heat pipe, evaporation of the liquid produces vapor and increases pressure on the concave side of the wick's meniscus. This pressure rise drives vapor toward the cooled zone and returns condensate to the heated zone through the wick. For a heat pipe to work correctly, the maximum capillary pressure rise, governed by the largest pore in the heated zone, must be greater than the pressure drops in the liquid and vapor regions: $\Delta pmax \geq \Delta pl + \Delta pv$. The pressure drop in the heat pipe wicks, Δpl, is viscous and so is linear with the local mass flow rate. The effects of stable vaporization to the heated region combine with unstable condensation of vapor in the cooled region. Viscous and turbulent inertial effects (with possible pressure recovery) may contribute locally to the vapor zone pressure change, Δpv.

Compound wicks address the performance limitations of homogeneous wicks. Two compound wick geometries appear especially attractive for high-power-density liquid metal heat pipes: an annular gap and an artery wick. Figures 12b and 12c depict cross sections of each of these wicks. The annular wick allows condensate to freely flow toward the hot zone in a gap between the pipe inner surface and the outer surface of the porous material on which menisci form. Artery wicks are similar to homogeneous wicks in that their outer diameter mates with the inner diameter of the heat pipe and the inner diameter sits at the liquid-vapor boundary. Artery wicks may incorporate one or more non-concentric arteries that create channels for free condensate motion. To maintain capillary continuity, a solid plug seals compound wicks on the end nearest the heated zone. A compound wick normally remains open at the cold end to ease fill. As a heat pipe warms, its working fluid expands. When the heat pipe is isothermal, excess condensate (typically 5% of charge) seals the condenser end of the wick and ensures capillary continuity.

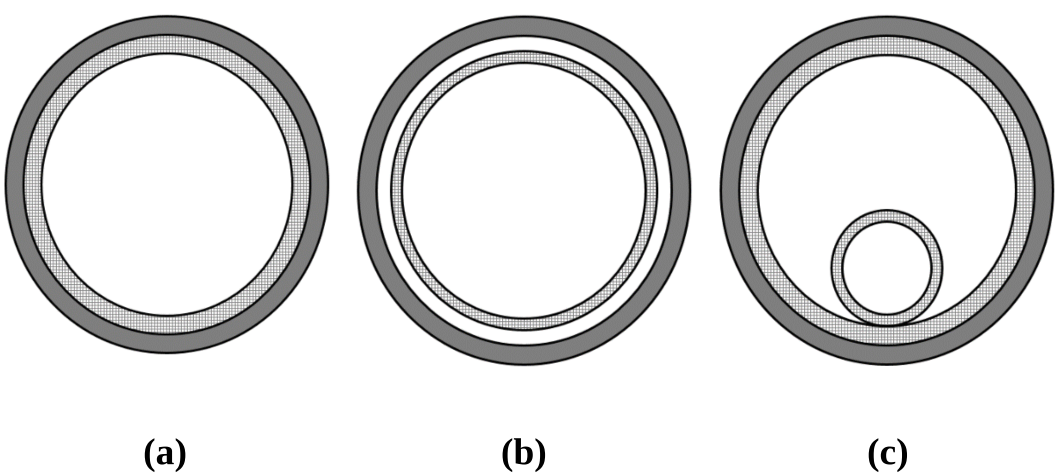

Figure 12. (a) Homogeneous, (b) concentric annular, and (c) artery wick geometries.

The following discussion details wick forming of a concentric annular wick. These steps include procuring raw goods for the wick assembly and bubble point testing of the final product. Though there are many approaches for forming a heat pipe wick, the processes described below represent methods that have proven effective to achieve high-power density.

Ultimate Hydroforming, Inc. (UHI) fabricated and scaled production of the LANL eWick37 design under an NQA-1 certifiable quality assurance program. Fifty-seven wick assemblies were produced through the final assembly and bubble testing. This project was completed under LANL Subcontract No. 570950 on September 30, 2022. UHI formed the wicks as specified by LANL using *eWick Work Instruction for Annular Wick*, Version 1.0, dated July 18, 2019. UHI modified the process in multiple areas to ease production for a larger lot size.

The eWick37 is formed from stainless steel wire mesh encased and diffusion bonded inside copper tubing, both mandrel and sheath. The copper mandrel procured was initially cleaned to remove any impurities. Scotch-Brite pads were used to manually clean the exterior of every copper tube, and a wire brush was used to clean the interior of every copper tube. A heavy-duty degreaser was then used to clean every surface, interior and exterior, of each copper tube, and each copper tube was wiped dry. The copper tubes were then rinsed in methanol and stored in a clean and closed area until the stainless steel screens were ready to be used. Nitrile gloves were used for all material handling through final assembly.

The procured stainless steel screen was initially cut to size. The screen needed to be long enough to produce the final assembly length and wide enough to allow for at least seven wraps around the copper mandrel. UHI confirmed the layer number with LANL before the rolling process. Before insertion into the mandrel and sheath, the stainless steel wire mesh was chemically cleaned, vacuum fired, and rolled. This cleaning was done under a fume hood, as noxious fumes are produced during the process. A stainless steel tank was used to contain the mesh during cleaning. Before use and between operations, the tank was cleaned and rinsed with methanol.

After the stainless steel screen was chemically cleaned, it was placed into the vacuum furnace. This degases and removes impurities from the stainless steel. Before the degassing, the vacuum furnace underwent a burnout to ensure it was clean before starting the screen firing process. The furnace was brought to <10-5 Torr and 750°C and had a run time of 2 h. During vacuum firing, the mesh was folded only once along the length to minimize creases from forming in the material. The vacuum furnace was evacuated with three successive dilutions with argon gas at 10-5 Torr for all firing steps. The furnace pressure did not exceed 10-5 Torr at any point. The screen was then cooled under vacuum conditions. Figure 13 shows a scanning electron microscope image of the stainless steel wick material used.

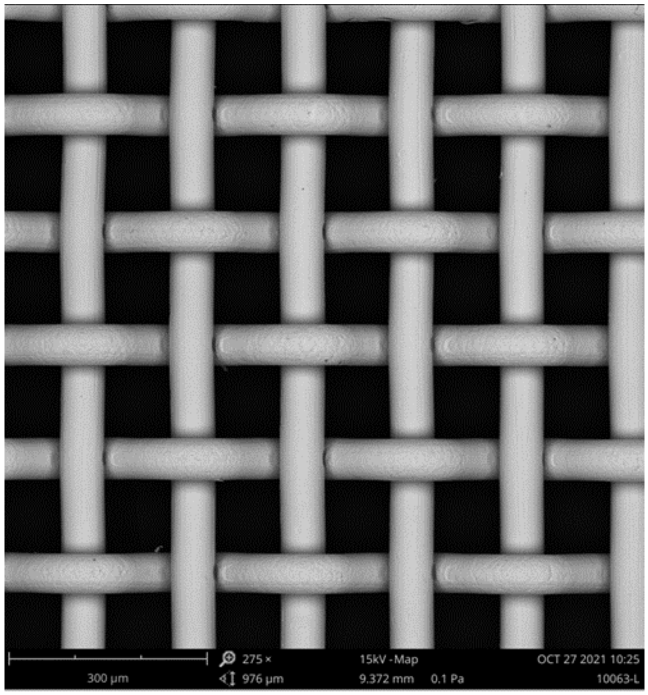

Figure 13. Scanning electron microscope (SEM) image of wick material during manufacture.

The chemically cleaned and vacuum fired screen was then rolled around the copper mandrel. During this process, the screen material was kept taut and uniformly wrapped around the mandrel. Although stainless steel mesh is unrolled in the cleaning process, wrinkles can be ironed out of the material using a clean stainless steel mandrel. This is crucial to ensuring a good diffusion bonding.

After the stainless steel screen was rolled around the copper mandrel and placed inside the copper sheath, the assembly was swaged to a diameter that allowed the finished wick assembly to properly fit within the heat pipe. The swaging brought the wick diameter to the correct size and applied pressure to ensure a proper diffusion bond. This swaging process reduced the diameter of the copper sheath, firmly compressing the stainless steel wick in between the two layers of copper tubes. A target sheath outer diameter of 0.667 in. +0.005/-0.000 in. ensured the wick produced would be the proper size. Initially, small trial batches of three to five assemblies were tested before swaging all 57 eWick37 assemblies.

The interiors and exteriors of the swaged assemblies were then cleaned of oil and other contaminants that remained from the swage. The assemblies then underwent a diffusion bonding process to allow the screen layers to bond and to prevent delamination of the final wick product. A furnace burnout was required to ensure cleanliness before the diffusion bonding process. The furnace was taken to a vacuum pressure of <10-5 Torr at 900°C and had a run time of 3 h. The cold furnace chamber was successively diluted by introducing argon gas into the chamber and then pumping the furnace down to 10-5 Torr three times before firing. The wick assemblies were then diffusion bonded under vacuum conditions.

Copper was then removed from the diffusion bonded stainless steel wick assemblies by a chemical etching process using a nitric acid solution. The copper undergoes more active dissolution than the stainless steel, allowing the copper to be completely removed without damaging the stainless steel wick. This process produces nitrogen oxide vapor, a heavy brown vapor, and must be performed under a fume hood in a PVC tank. The process also required a peristaltic pump, an in-line heater, and a PID temperature controller. After all of the copper was removed, the bonded wicks were straightened by placing a clean stainless steel mandrel inside the length of the tube. The wicks were then rolled on a flat and clean surface to remove kinks from the outer surface. After being straightened, the wicks were inspected to ensure complete removal of copper and to ensure they were free of any damage or delamination that would prevent them from functioning. Figure 14 shows a subset of the completed wicks.

Figure 14. Subset of eWick37 batch following manufacture.

The bonded stainless steel wicks were then pressure-tested using a bubble point test. This bubble point test determined the approximate size and location of the largest pore and the general pore size distribution. The same bubble point test was performed following diffusion bonding of the end plugs. Table 1 shows measured maximum pore radii for each of the completed wick assemblies following diffusion bonding of the end plug. These maximum pore radius values allow for precise estimates of heat pipe capillary limits.

In Table 1, the cells are color-coded with a scale between red and green. Green cells highlight the higher performing results, whereas red cells highlight the wicks that have lower performance. The colors show that the lowest performing wicks had an effective pore radius of 15.1 μm, which exceeds the goal of an effective radius equal to 32 μm.

Table 1. Measured Pore Radii of Manufactured Stainless Steel Wicks.

Serial Numb	Pressure At First Bubble (in H2O) - Test One	Pressure At First Bubble (in H2O) - Test Two	Total Number Of Bubbles At Cutoff Pressure - Test One	Total Number Of Bubbles At Cutoff Pressure - Test Two	Rmax(µm) - Test
2	13.0	12.5	103	97	13.9
3	12.0	15.5	180	35	15.1
4	12.0	12.0	125	25	15.1
5	12.5	11.0	198	31	14.5
6	12.0	10.0	175	21	15.1
7	13.0	15.0	293	27	13.9
8	15.0	16.3	24	28	12.0
9	13.0	14.0	41	23	13.9
10	14.0	15.0	62	8	12.9
11	14.0	15.0	101	41	12.9
12	13.0	13.5	55	92	13.9
13	14.0	13.5	37	62	12.9
14	14.0	14.0	174	41	12.9
15	15.0	13.0	34	67	12.0
16	17.5	16.0	10	47	10.3
17	16.5	15.0	17	21	10.9
18	14.5	16.0	40	9	12.5
19	14.0	14.0	44	20	12.9
20	15.0	15.5	30	30	12.0
21	15.5	15.0	47	34	11.7
22	15.5	14.0	55	24	11.7
23	16.0	16.0	33	93	11.3
24	13.5	14.5	22	37	13.4
25	15.5	15.0	15	19	11.7
26	16.5	16.5	22	24	10.9
27	15.5	16.0	19	173	11.7
28	14.5	14.0	27	129	12.5
29	15.0	14.0	53	103	12.0
30	12.0	16.0	23	65	15.1
31	14.5	11.5	34	132	12.5
32	15.0	11.0	57	202	12.0
33	15.0	14.0	91	89	12.0
34	12.0	15.5	21	28	15.1
35	18.0	18.0	1	2	10.0
36	15.0	17.0	22	23	12.0
40	15.0	17.5	5	10	12.0
42	19.0	15.0	4	23	9.5
43	17.0	17.0	2	21	10.6
44	20.5	19.0	2	2	8.8
45	17.0	15.0	22	20	10.6
46	19.5	19.0	2	3	9.3
48	16.0	15.0	4	9	11.3
49	17.5	19.5	1	3	10.3
50	16.0	16.5	36	16	11.3
51	18.0	17.0	1	1	10.0
52	17.5	16.0	2	13	10.3
53	17.5	17.5	7	3	10.3
54	15.0	15.0	47	21	12.0
55	15.5	16.0	40	37	11.7
56	17.5	18.5	3	1	10.3
57	18.0	19.0	1	1	10.0
58	19.0	19.5	1	3	9.5
59	13.0	14.0	19	20	13.9

Bar stock for the total plug quantity needed was obtained and machined to mate with the inner diameter of the stainless steel wick (0.561-in. outer diameter). After being machined, the plugs' tops were laser etched with serial numbers before cleaning. The newly machined plugs were chemically cleaned before vacuum firing. This process was the same as that used for the stainless steel screens. After the stainless steel plugs were chemically cleaned, they were vacuum fired using the same process as the stainless steel screen before the assembly step. After removal from the furnace, the plugs were stored in a clean location to ensure they remained clean before the diffusion bonding process. When the plugs and wicks were ready to be diffusion bonded, the plugs were installed into the wicks. The wick was then diffusion bonded to plugs as shown in Figure 15.

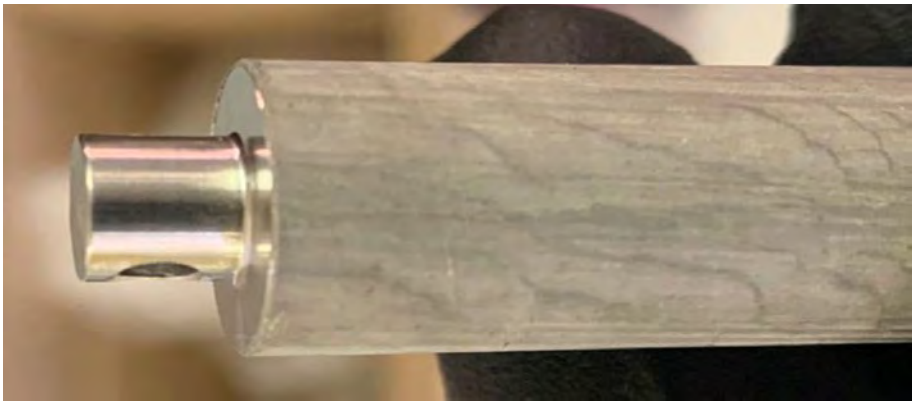

Figure 15. Detail of eWick37 with diffusion bonded plug.

Final assemblies were packaged in a way to prevent damage to the wicks. UHI used foil wrapped tightly around the wick with foam wrap around the foil. The wrapped assembly was placed in a triangular box just over the length of the finished assembly (the box was sized based on the wick assembly dimensions). The wrapped final assembly fit tightly, but there was no compression damage done to the wick. The triangular boxes were stacked inside a wood crate, and foam was placed in between the wall and the stacked boxes. Additional foam was placed over the top of the cardboard boxes before the top of the crate was nailed shut. This, along with a dedicated truck, was used to ensure multiple layers of protection for the fragile final assemblies. Figure 16 shows the wooden crate full of wicks being loaded into the dedicated shipping truck.

Figure 16. eWick37 shipment via air-ride van from Michigan to New Mexico.

5.0 WELDING ADVANCES

During this project, several advances in LANL welding capabilities supporting microreactor technology have been made. First, a method and mechanism for welding a large array of heat pipes in a high vacuum/inert atmosphere was developed using a high-power laser weld head capable of X/Y scanning. Second, a first-of-its-kind internal orbital arc welder, procured through a development with Arc Machines, Inc. (AMI), was demonstrated to produce hundreds of repeatable welds over 1 m deep into tube structures.

5.1 Laser Welding

Laser welding was developed using an IPG Photonics YLS-4000 yitterbium fiber laser system with an IPG Photonics D50 Wobble Head scanner integrated into a custom vacuum chamber structure. The 1-m focal distance, 30×30-mm working area, and 4-kW laser power enable a variety of welds for heat pipe sealing and other applications.

Initial weld development began with three test samples representing the condenser plug of the eBlock37. Laser parameters were iterated over the samples until the weld appeared visually conformant. The samples were then sectioned with wire electric discharge machining (EDM) and sent for metallurgical analysis. Figure 17 shows the progress of the welds, which all passed a helium leak test with a leak rate less than 1E-9 Torr L/s. The final basic weld parameters were 1.5 kW with a speed of 3 mm/s and a wobble diameter of 1.5 mm.

Figure 18 shows the cross-sectioned sample and the full penetration of the weld. Further refinement of the weld parameters to increase uniformity and penetration will be done during the trial fill procedure.

Figure 17. Laser weld sample development.

Figure 18. Sectioned laser weld sample showing penetration.

5.2 Internal Orbital Tube Welding

The AMI internal orbital arc welder was initially developed to enable the attachment of the high-density Core37 condenser tubes to the block. There was insufficient space between the tubes to allow for a manual tungsten inert gas (TIG) weld. The internal weld head is based on a traditional external orbital welder with a modified rotor, a collet attached that connects to the tube to be welded, and an extended copper torch with a purge gas path. At the end of the torch, a flat-tipped tungsten electrode sits in a ceramic cup. A cutaway diagram is shown in Figure 19.

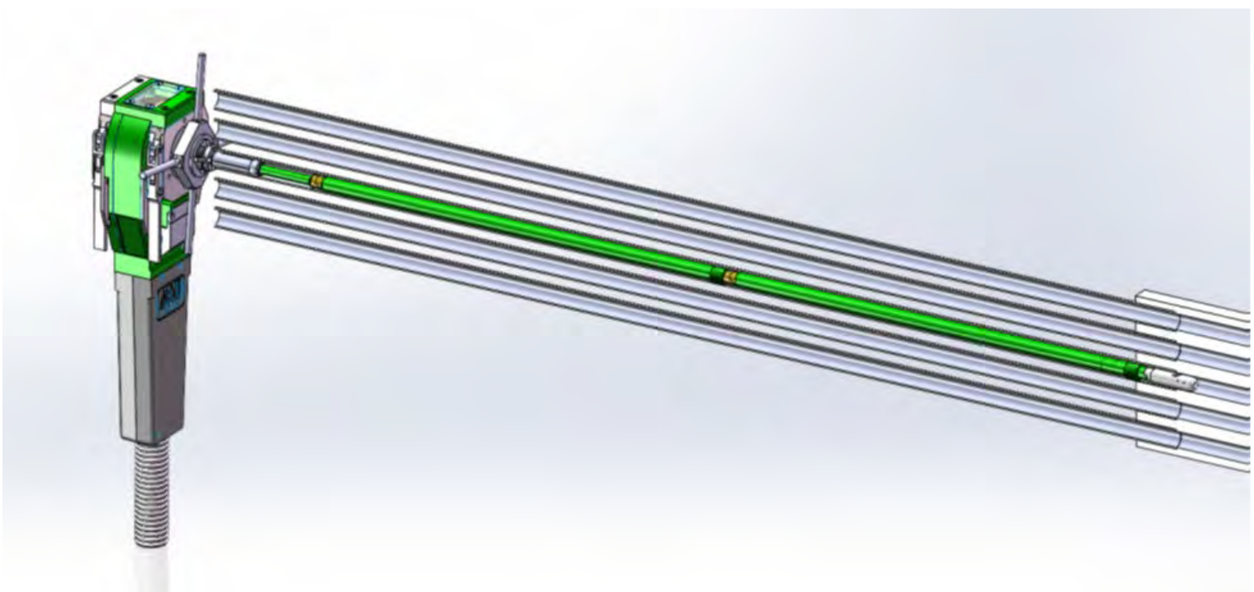

Figure 19. AMI internal OTW torch inserted into eBlock37 condenser tube.

The condenser welding process was developed using several test samples representing the block socket and condenser tubes. The weld schedule was adjusted over the samples until the weld passed a visual inspection. The samples were then sectioned with an abrasive saw and polished for metallurgical analysis. Figure 20 shows the sectioned weld sample and the polished and etched microscope image showing full penetration.

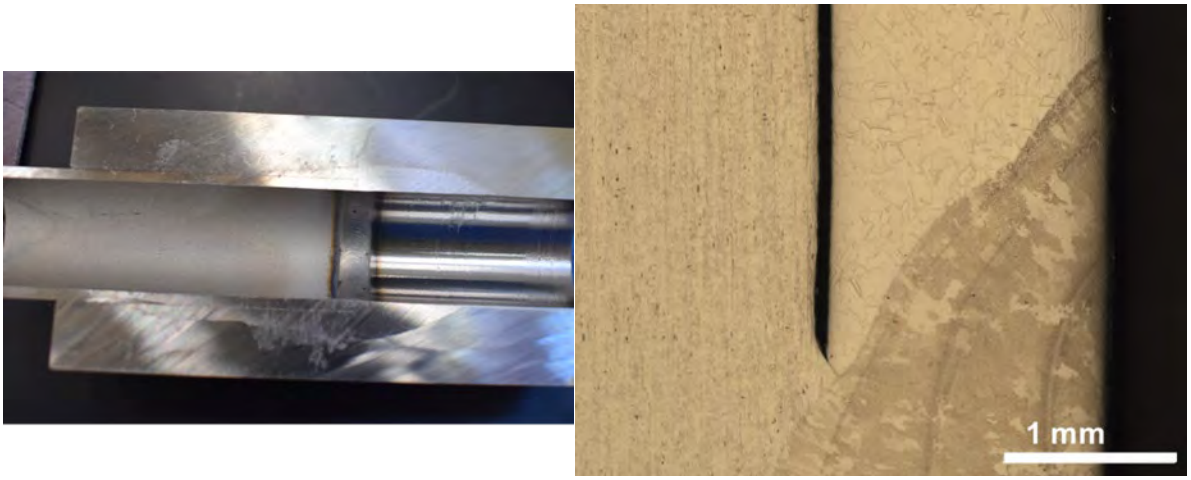

Figure 20. Core37 condenser weld sample analysis showing full penetration.

After the welder and welding process were proven, they were used in an attempt to repair the Core37. See Section 7.8, “Braze Repair.”

6.0 eXchanger37

The heat exchanger is a shell and tube-type exchanger with 37 channels that surround the heat pipe tubes. At the inlet and outlet, the gas will be in crossflow with the outlet closest to the core. Figure 21 depicts the completed eXchanger37. Appendix A shows release drawings of the eXchanger37 base assembly. Thermal analysis was conducted on the Core37 and eXchanger37 in ANSYS to evaluate the expected temperature distribution and thermally induced stresses under steady-state operation. This analysis revealed that rigid coupling of the Core37 to the eXchanger37 yielded high stress levels near the interface between the Core37 and eXchanger37. To mitigate this problem, the eBlock37 design was changed to place the Core37 in sliding contact with the eXchanger37 via a high-temperature (head gasket) seal. The analysis below covers the design state before this mitigation was implemented as it was presented in a paper published in *Nuclear Technology*.[1]

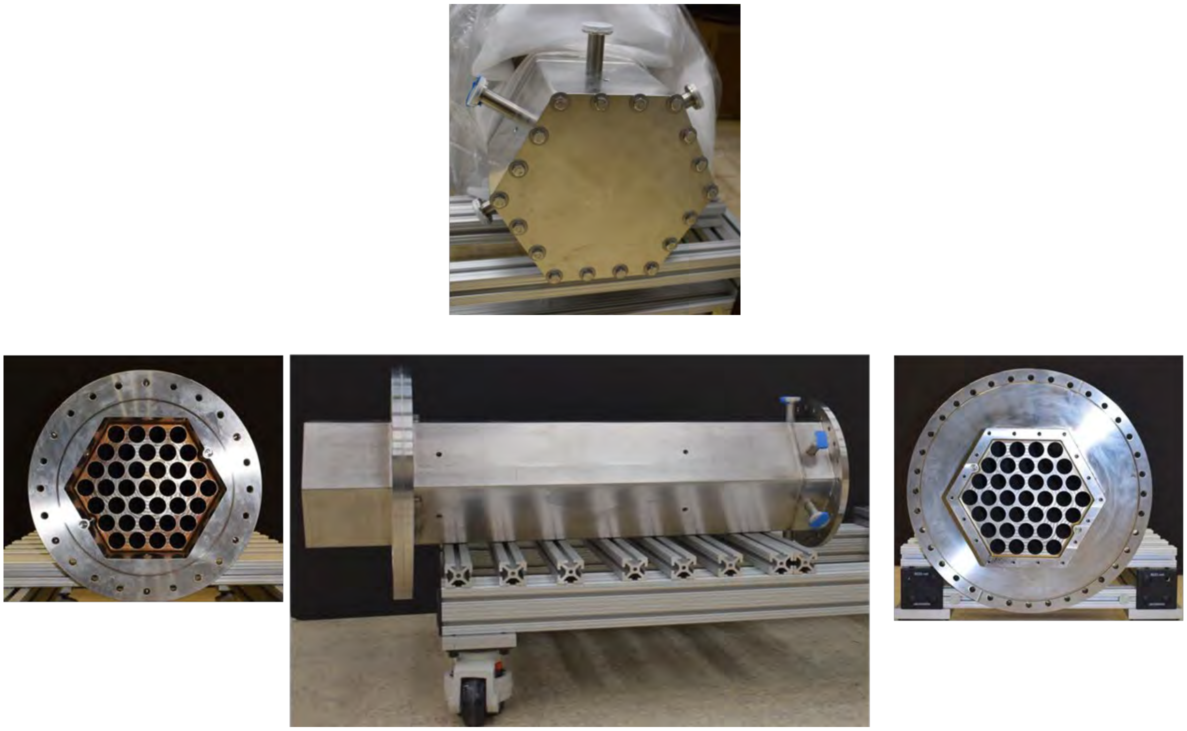

Figure 21. (Top) eXchanger37 end cap and (bottom) completed eXchanger37 body.

Temperature-dependent bilinear elastic-plastic material properties were used to represent the 316L stainless steel eBlock37. Preliminary analyses were conducted to obtain further insight into where the largest stress concentrations were expected to occur, and meshing was refined in regions deemed to be of concern. Fillets were incorporated at vertices within the heat exchanger to reduce incurred stresses in regions where initial assessments showed large temperature gradients and thermally induced stresses. Top and bottom views of the meshed assembly are shown in Figure 22, and an overview of the analysis model parameters is provided in Table 2.

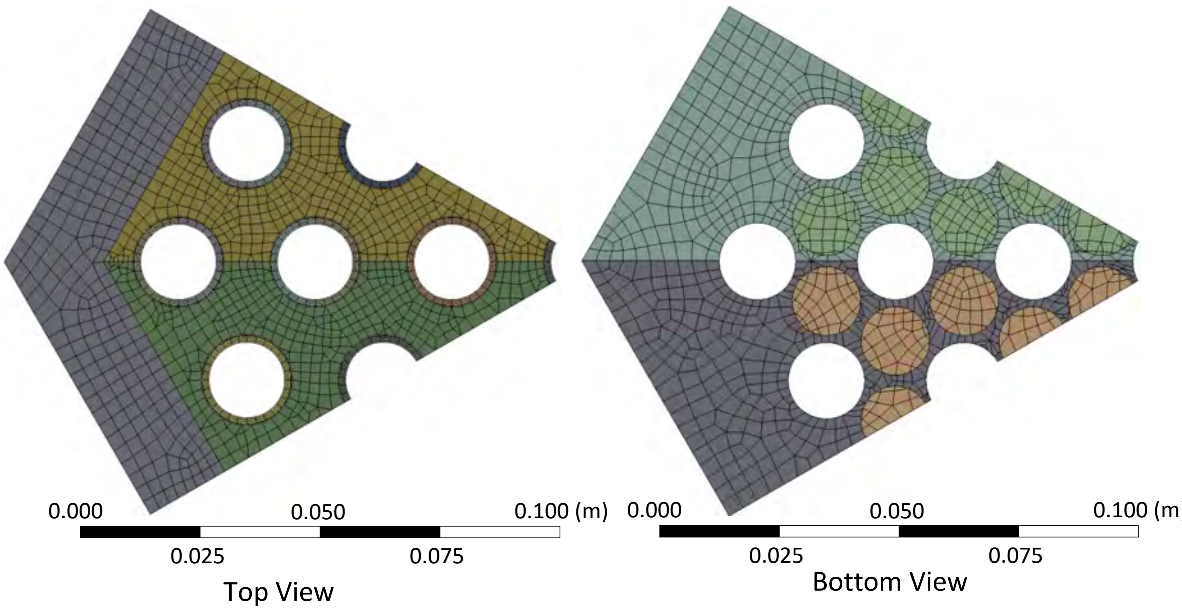

Figure 22. (Left) top and (right) bottom views of meshed ANSYS model.

Table 2. eXchanger37 Model Parameters.

Analysis Software	Symmetry	Analysis Type	Element Type	Number of Elements	Number of Nodes
ANSYS 2019 R1	One-sixth	Steady-state (thermal and structural)	Primarily hexahedral and tetrahedral	217,817	985,310

Thermal boundary conditions within the eXchanger37 were determined by evaluating fluid temperature and heat transfer coefficients (HTCs) for each of the heat exchanger regions [i.e., inlet (crossflow), annular flow, and exit (crossflow)]. Crossflow occurring in the eXchanger37 inlet and exit was assumed to have a uniform fluid temperature and HRC on the heat pipe walls. Values for these parameters are shown in Table 3.

Table 3. eXchanger37 Crossflow Zone Thermal Boundary Conditions.

Heat Exchanger Zone	Inlet	Outlet
Fluid Temperature	350°C	686°C
HTC	311.3 W/m^2 K	303.2 W/m^2 K

Fluid temperatures and HTCs in the annular region are based on parallel flow heat exchanger relations such that each is a function of position along the length of the channel. The plots in Figures 23 and 24 show the fluid temperature and HTC based on location, with the starting position (y = 0 m) being at the entrance of the annular channel, furthest from the reactor interface.

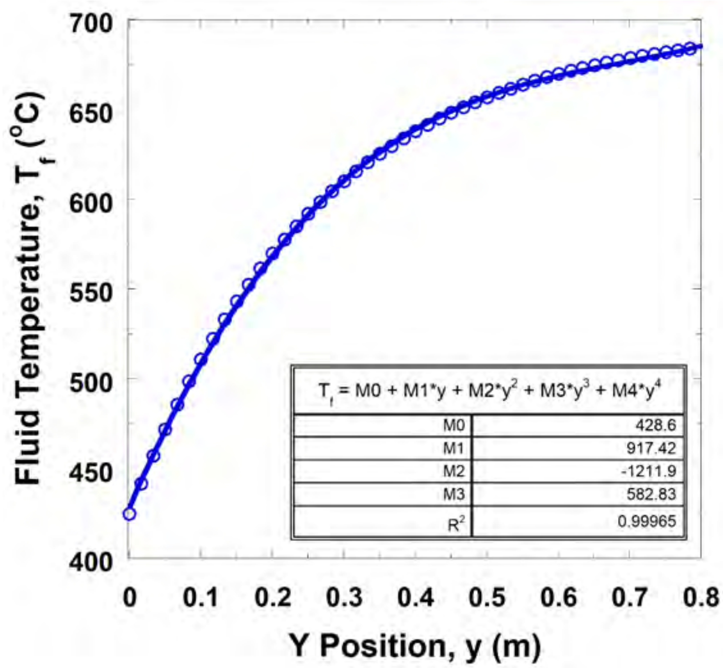

Figure 23. Fluid temperature as a function of channel position.

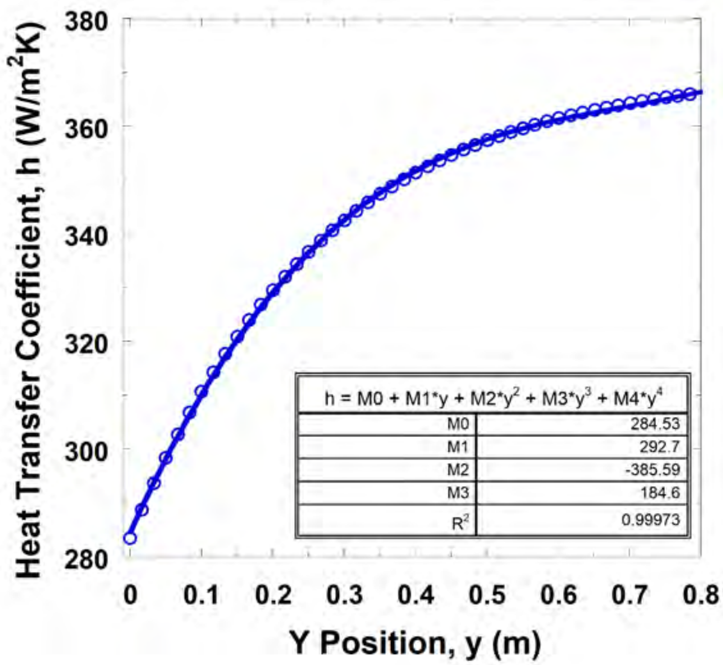

Figure 24. HTC as a function of channel position.

Several assumptions were made to allow for solution of the thermal model. First, internal heat pipe temperatures were defined as isothermal with a constant temperature of 700°C. All external surfaces of the eBlock37 were considered perfectly insulated. Additionally, each fuel rod was assumed to have a heat flux of 22.5 kW/m^2, which was determined by energy balance.

Temperature and heat flux contours determined using the aforementioned thermal boundary conditions are shown in Figures 25 and 26, respectively.

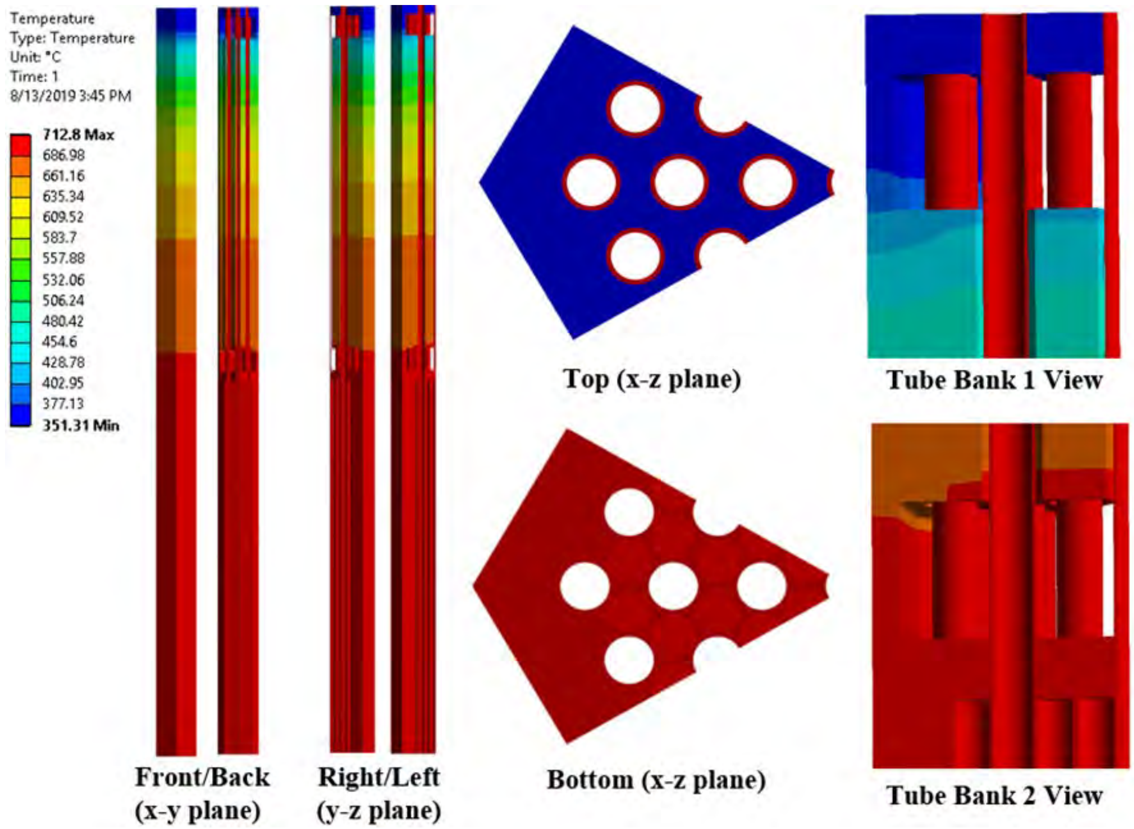

Figure 25. Heat exchanger and reactor assembly steady-state temperature distribution.

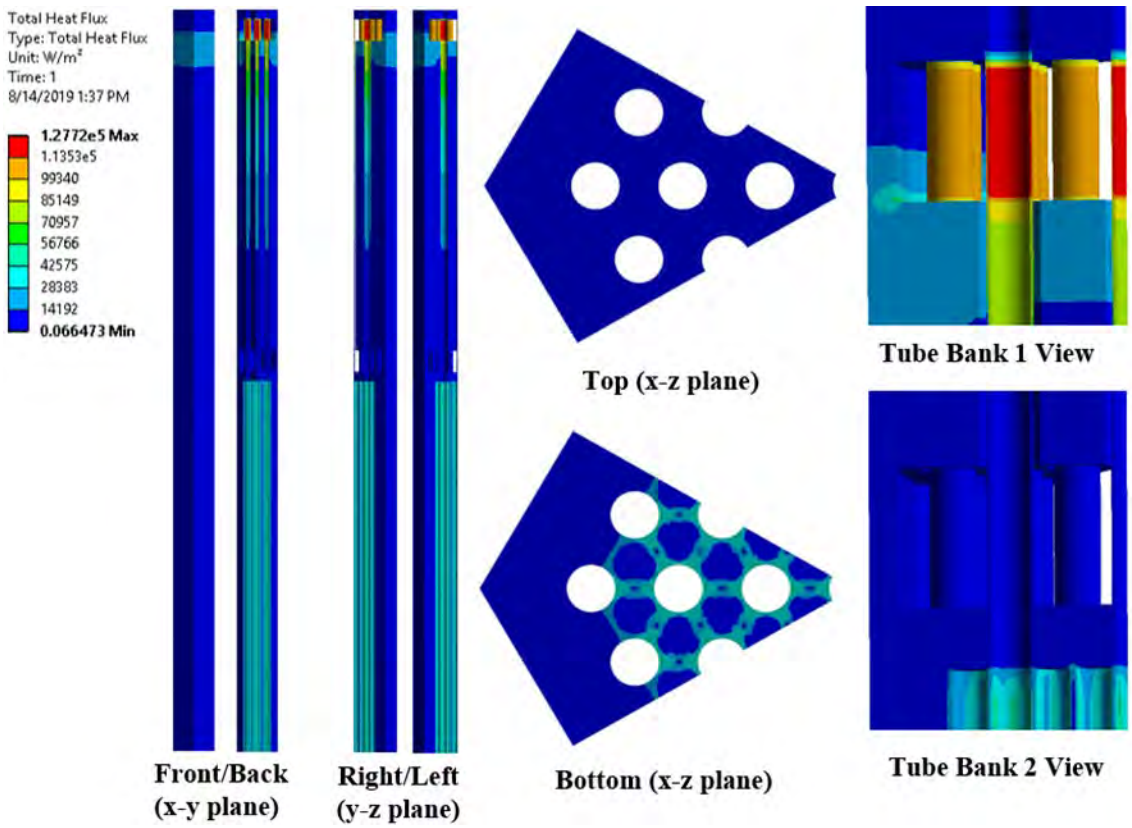

Figure 26. Heat exchanger and reactor assembly steady-state heat flux distribution.

6.1 Structural Analysis

Upon completion of the previously described thermal analysis, structural boundary conditions were applied to the eBlock37 to evaluate the stresses incurred by the combination of thermal loading and an internal fluid pressure loading of 2 MPa. The structure was fixed in the x-z plane at the base of the Core37 subassembly, allowing for deflection only in the y-direction (i.e., parallel to the heat pipe axes). Additionally, a cylindrical support was applied to the inner surface of the centermost heat pipe to prevent rotation of the assembly. Deformation and stress results can be found in Figures 27 and 28, respectively.

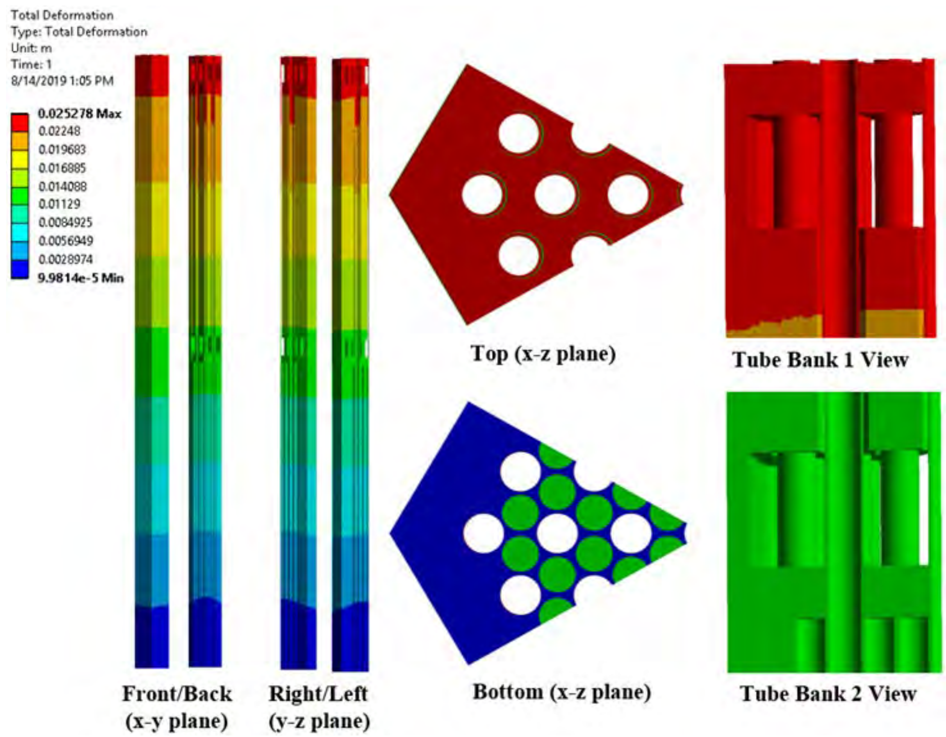

Figure 27. Heat exchanger and reactor assembly steady-state deformation.

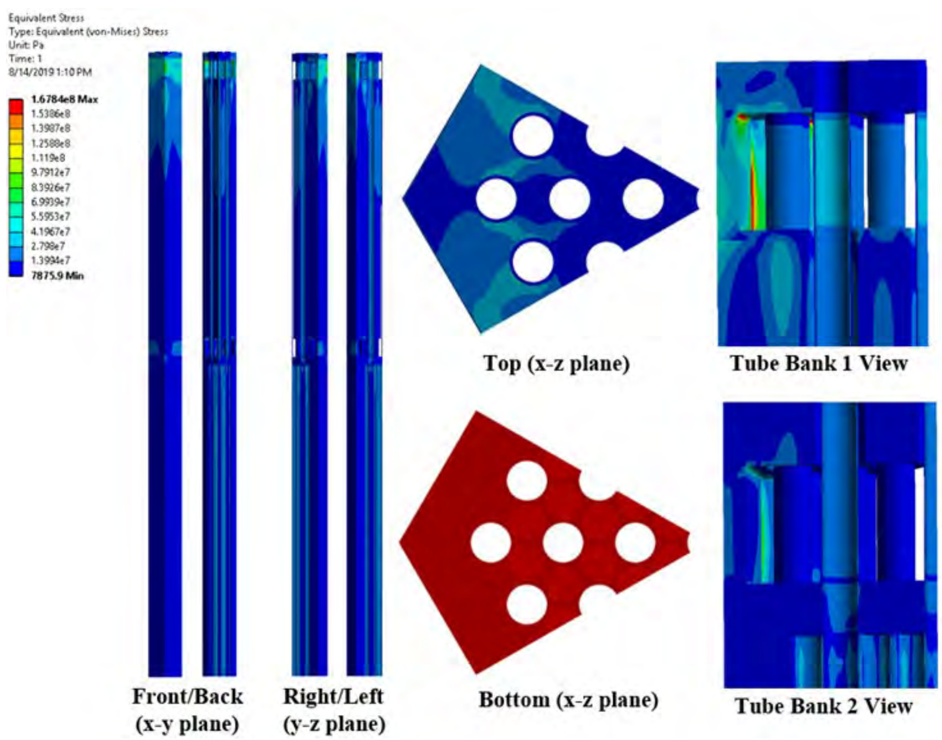

Figure 28. Heat exchanger and reactor assembly steady-state stress distribution.

6.2 Computational Fluid Dynamics Analysis

Computational fluid dynamics (CFD) analyses were conducted in Starccm+, Version 15.06.007-R8, to provide a higher fidelity assessment of flow distribution and heat transfer within the eXchanger37. Initial design iterations contained only three inlet and three outlet ports. After some consideration, additional ports were added to enable a more uniform flow distribution and corresponding heat transfer. Figure 29 shows the model used for CFD analysis, which includes six inlet and six outlet ports.

Consistent with the previous analysis, inlet air temperature was assumed to be 350°C, heat pipe surface temperatures were assumed to be 700°C, and all other surfaces were considered adiabatic. Isobaric (0.1 MPag or 15 psig), temperature-dependent air properties were defined, with relationships based on National Institute of Standards and Technology (NIST) data.[3]

Figure 29. eXchanger37 CFD fluid model.

A grid sensitivity study was performed with four different meshes (M1 = 2-million cell, M2 = 6-million cell, M3 = 13-million cell, and M4 = 25-million cell), shown in Table 4, to quantify the optimal mesh specification for the current application. The outlet coolant temperature and pressure drop were evaluated along with different mesh sizes, showing an asymptotic behavior beyond Mesh M3. Mesh M3 was therefore deemed the optimal mesh for analysis of the eXchanger37. Hereafter, all results presented in the paper are based on the optimal mesh defined from the grid sensitivity study.

Table 4. Mesh Statistics for Grid Sensitivity Study.

	M1	M2	M3 (optimal)	M4
Mesh Count	1,998,722	6,273,881	13,508,921	25,010,982

A hexagonal mesh was chosen as a base mesh with seven layers of the prism mesh along the heat transfer surface to resolve the viscous boundary layer in the flow channel and help produce a well-converged energy equation in the stimulation. After several turbulence model tests, Menter's k-w Shear Stress Transport (SST) turbulence model was employed in the simulation.

A series of iterative simulations was conducted using the meshed model shown in Figure 30 to evaluate inlet flow conditions needed to achieve the desired 100-kW cooling capacity. This was accomplished by incrementally increasing inlet air flow rate until the target thermal energy dissipation was achieved. Results showed that a total air mass flow rate of 0.33 kg/s was required.

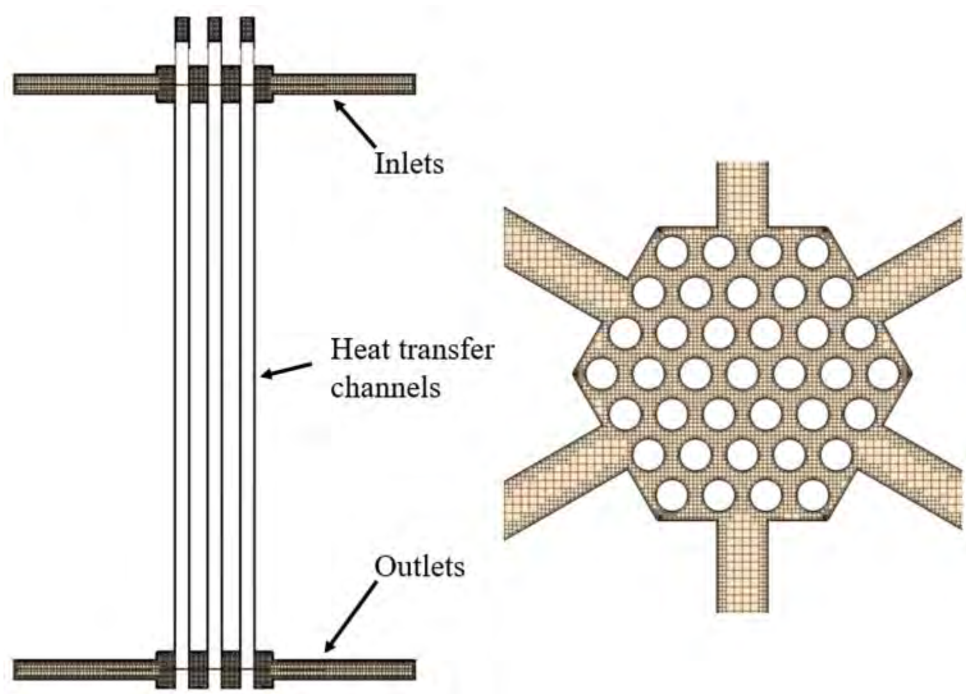

Figure 30. (Left) cross-sectional view and (right) top view of meshed CFD model.

Velocity profiles through the eXchanger37 are displayed in Figures 18 and 19. No critical stagnation or recirculation was observed in either the inlet or outlet crossflow regions. However, it was noted that air velocities at the outlet were nearing supersonic velocity, which implies that other cooling mediums may need to be considered to meet the desired thermal target.

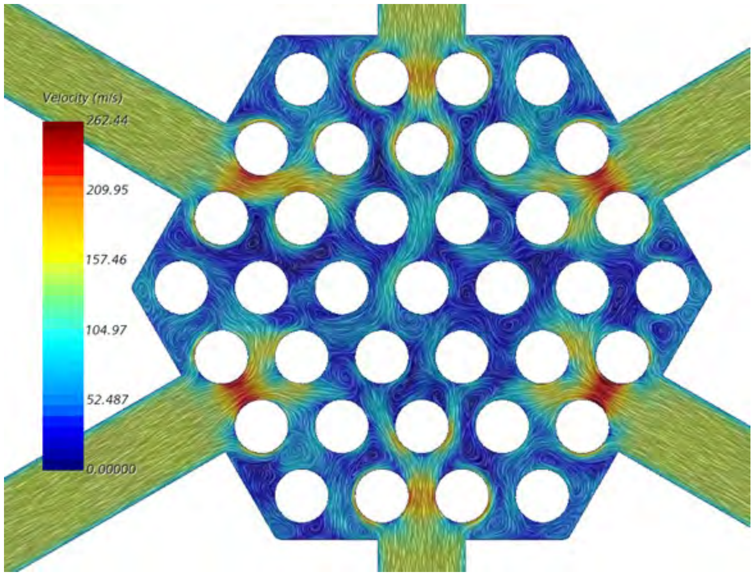

Figure 31. A flow visualization of the air flow mixing distribution in the upper plenum.

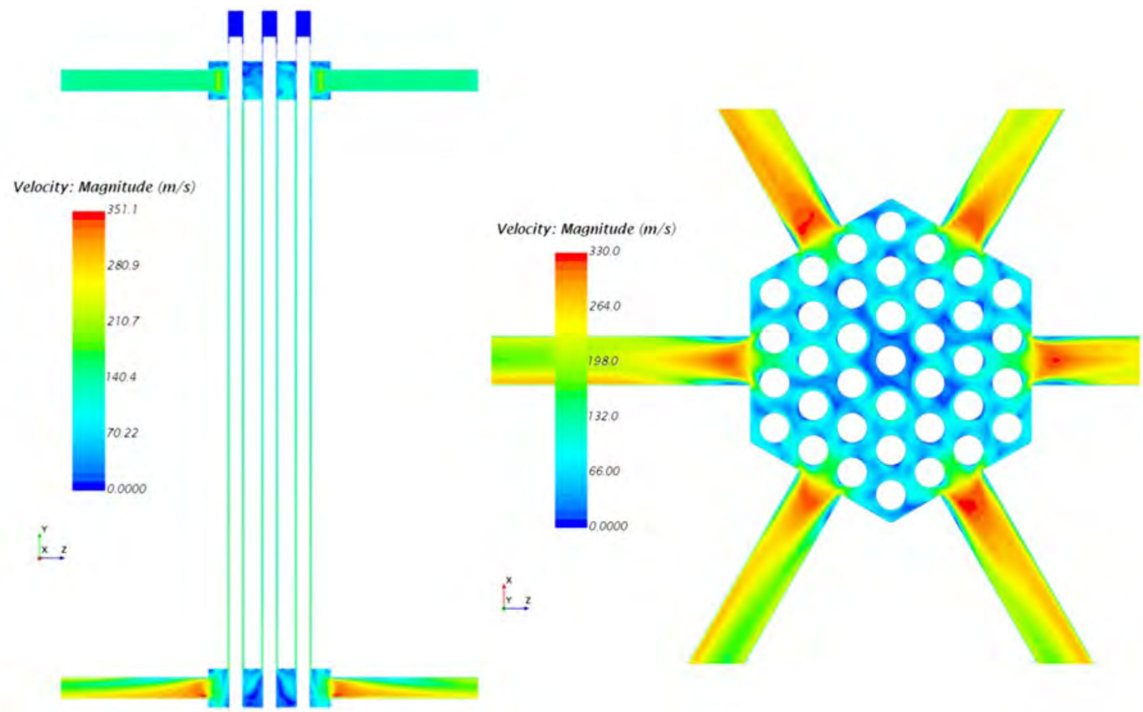

Figure 32. (Left) side view and (right) bottom view in the lower plenum of air velocity profiles.

As intended, stagnation was observed in the heat exchanger cap as a result of narrow channels preventing upward flow. The heat exchanger cap was designed with narrow openings to accommodate heat pipe thermal expansion. Openings were made as narrow as possible to ensure that the path of least resistance for fluid flow was through the heat exchanger. Figure 33 shows that the heat exchanger cap design effectively mitigates unnecessary thermal capacity losses at the heat exchanger inlet.

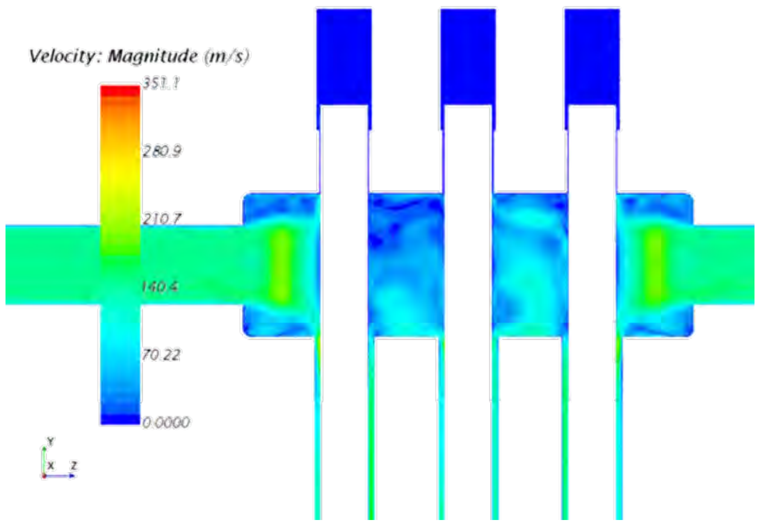

Figure 33. Heat exchanger cap stagnation for air working fluid.

Stagnation of air in the cap creates an increase in fluid temperature as shown in Figure 34. This potentially reduces the severity of temperature gradients and corresponding thermal stresses observed at the heat exchanger inlet in the previous analysis.

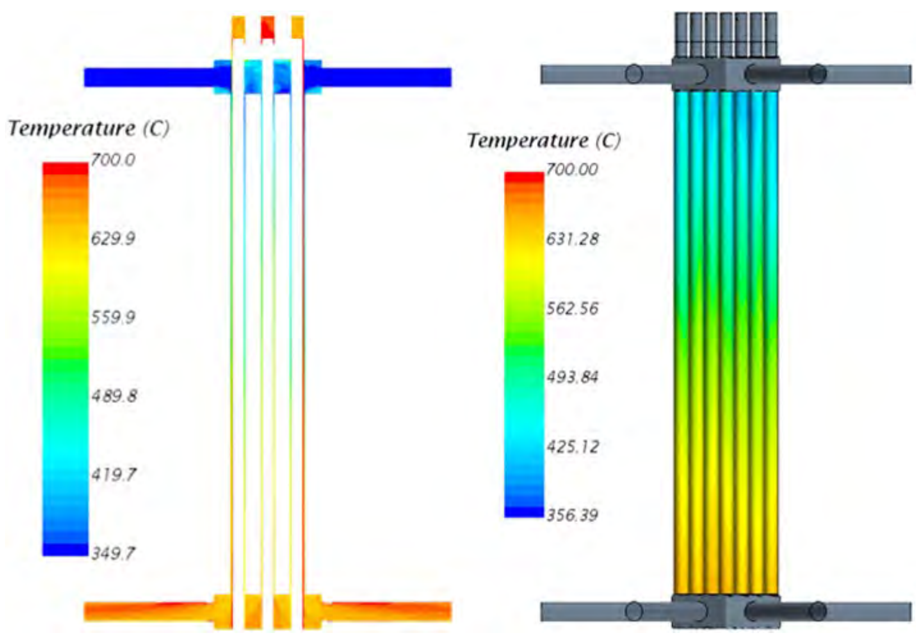

Figure 34. (Left) cross-sectional view and (right) side view of air temperature profiles.

Figure 34 also shows the expected gradual increase in air temperature between the entrance and exit of the annular flow region. Though relatively minor, some variation in air temperature profiles can be seen in heat pipes located on the perimeter of the eXchanger37. The most notable difference occurs in annular channels located at vertices of the heat exchanger, which appear to increase in temperature further down the length of the channel than those adjacent as shown in Figure 34.

Figure 35 shows the air temperature and velocity profiles at the center of the annular flow region. The flow distribution feeding into each of the 37 annular channels is non-uniform because of the abrupt transition and structural obstacles in the inlet crossflow region as shown in Figures 18 and 19. Channels with higher air velocities experience higher heat transfer rates and exhibit a correspondingly greater temperature drop as demonstrated in Figures 21 and 22.

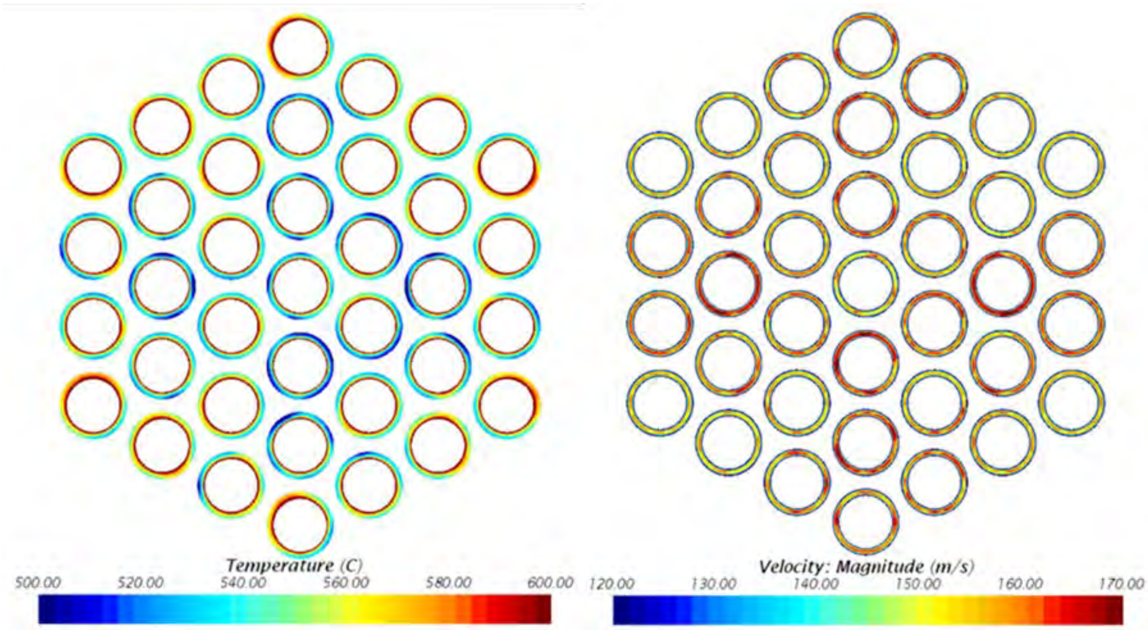

Figure 35. (Left) mid-plane air temperature and (right) velocity profiles.

Local HTCs were evaluated in the baseline air flow condition and are illustrated in Figure 36. High HTC values were observed upstream in the annular channel because of the large temperature gradient between the flowing air and heat pipe surface. HTC values became saturated in the middle of the annular flow channel and transitioned to a constant value in the downstream side.

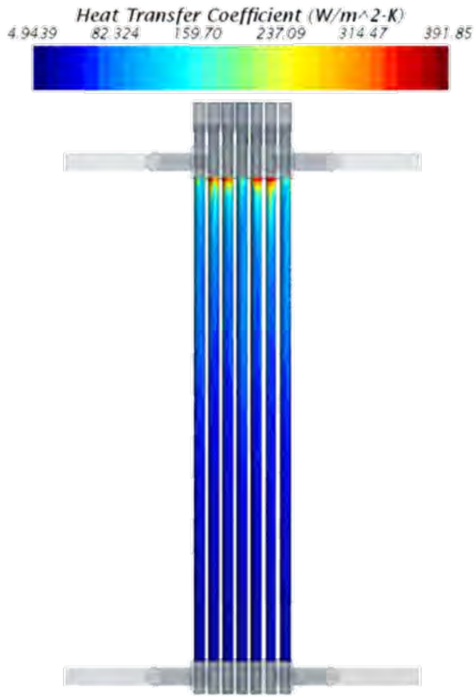

Figure 36. Side view of annular channel air HTC profiles.

It is worth noting that heat transfer performance over the 37 channels is not uniform and that flow distribution in the current design dictates the initial heat transfer performance of individual channels. This is particularly true at the transition from the inlet crossflow region to the annular flow channel and can be seen by comparing the air velocity distribution in the inlet crossflow region (Figure 31) to HTCs at the entrance of the annular flow region (Figure 36). Channels located directly in front of the air inlet, where velocities are largest, exhibit the highest HTCs.

An overall assessment of individual heat pipe performance is shown in Figure 37. Reiterating previously discussed findings, analysis results showed that annular channels closest to the center (i.e., HP12,13,20,26,25,18,19) and at the vertices of the eXchanger37 (i.e., HP01,04,22,37,34,16) exhibited lower than average power dissipation. These heat pipes are denoted by the red dotted lines in Figure 37. Thermal energy dissipation ranged from just under 2 kW at the center of the heat exchanger (i.e., HP19) to approximately 3.25 kW for heat pipes directly in front of the heat exchanger inlet ports.

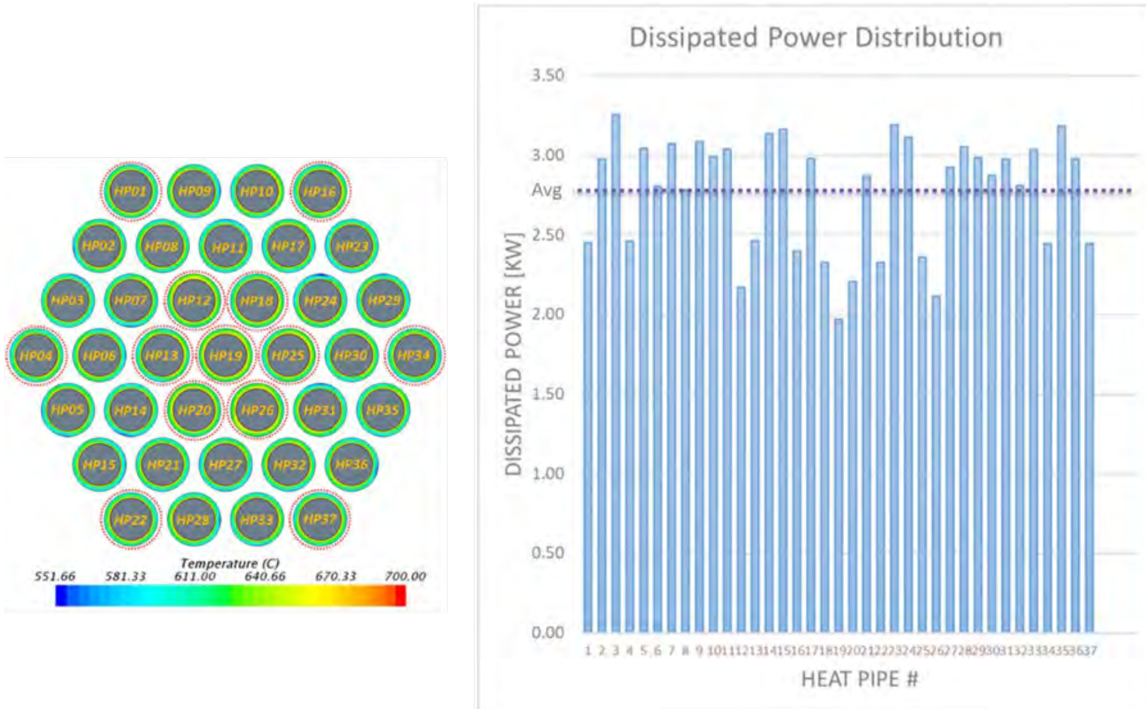

Figure 37. Heat pipe power dissipation by location for air working fluid.

To demonstrate the capacity of the eXchanger37 with desirable target thermal energy while alleviating engineering concerns regarding air flow approaching supersonic velocity, the CFD analysis was also conducted using helium as a cooling fluid. Again, iterative analyses were performed to identify the helium flow rate necessary to achieve the desired 100-kW thermal energy dissipation. Results showed that a total helium mass flow rate of 0.06 kg/s could achieve the same cooling capacity as a total air mass flow of 0.33 kg/s. Figure 38 shows that although magnitudes differ, the overall flow distribution was found to be similar to that shown in Figure 32 for air. Additionally, the distribution of thermal energy dissipation was found to be comparable to that shown in Figure 37. Although the capacity of the eXchanger37 with both cooling fluids was found to be satisfactory for the current application, improvements to the channel flow design may be implemented to further reduce thermal-mechanical stress and lifecycle limitations.

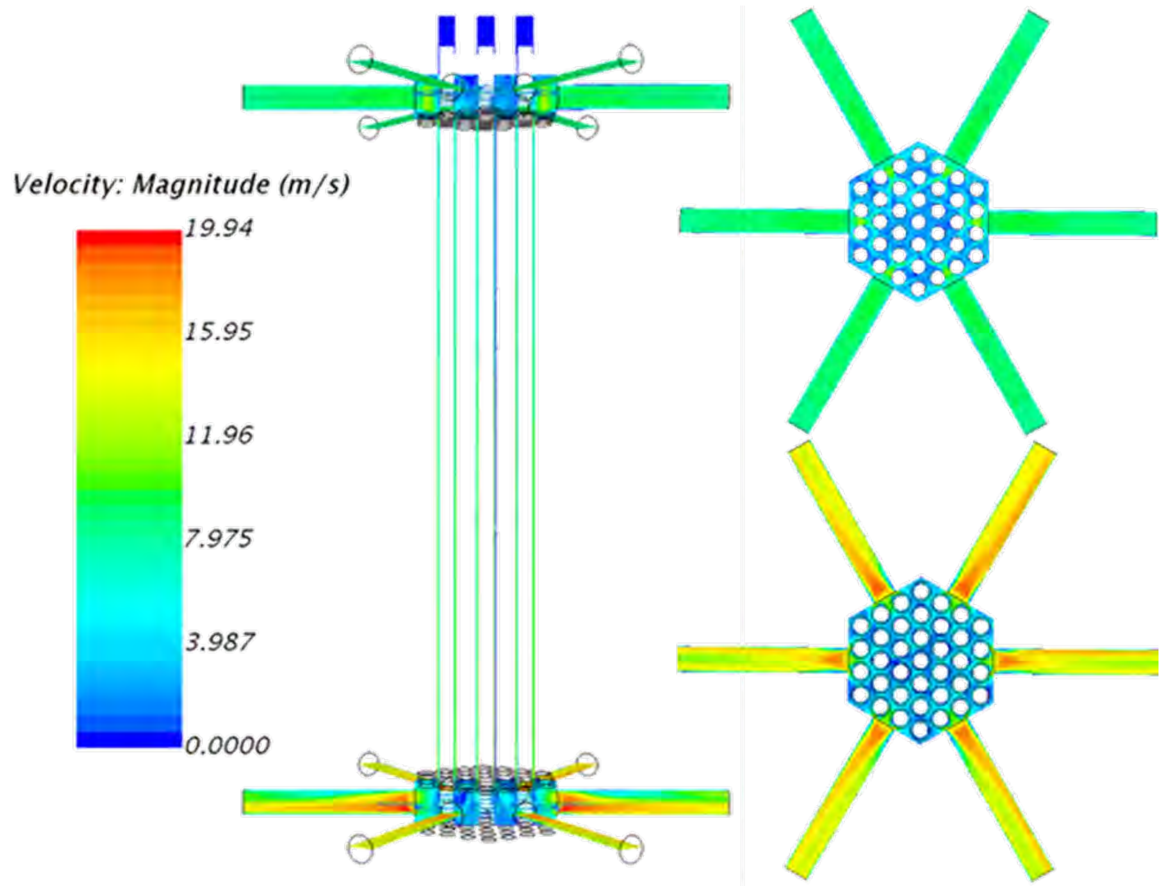

Figure 38. (Left) helium velocity profiles in the overall heat exchanger, (top right) inlet crossflow region, and (bottom right) outlet crossflow region.

7.0 Core37

The Core37 is a 316L stainless steel block approximately 1 m long and contains a total of 91 holes: 37 house sodium heat pipes linked to the eXchanger37 and 54 are intended for electrical cartridge heater installation. The web thickness between each of the holes is approximately 1.5 mm. Closures (not shown) welded to the end of the Core37 subassembly seal the heat pipes while allowing the electrical cartridge heaters to be inserted into the adjacent fuel pin holes. A variety of fabrication techniques was considered to form the subassembly, including conventional machining and additive manufacturing (AM) of various length segments. Gun drilling was considered as a conventional method for manufacturing, but it was determined that gun drilling could not maintain the 1.5-mm web thickness over the 1-m length, thus, segments would be manufactured and joined together. Segment joining by hot isostatic pressing (HIP), tier welding, diffusion bonding, and brazing was tested. Both diffusion bonding and brazing trials proved more successful than other bonding methods.

7.1 Additive Manufactured Core

A laser powder bed was used to complete AM of both the subscale 7-hole core block and the larger 37-heat-pipe core block sections from 316L powder. Two 37-heat-pipe core sections were printed simultaneously in the configuration shown in Figure 39.[2] An electron backscatter diffraction (EBSD) test was completed on the printed material to analyze the base microstructure; see Figure 40.

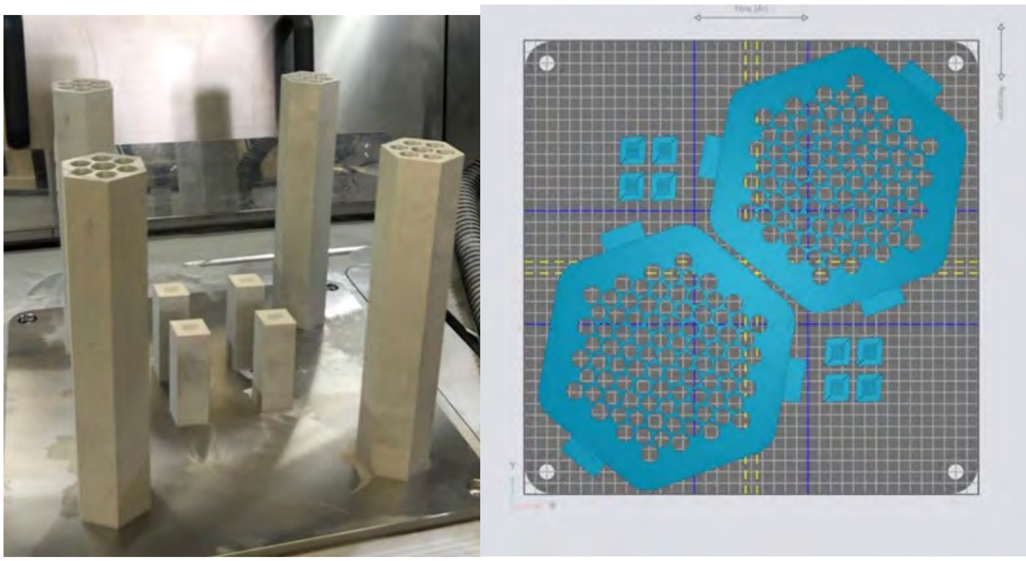

Figure 39. (Left) seveneBlock7 subscale test and (right) Core37 AM configuration with test coupons. (Image from Colt Montgomery.[2])

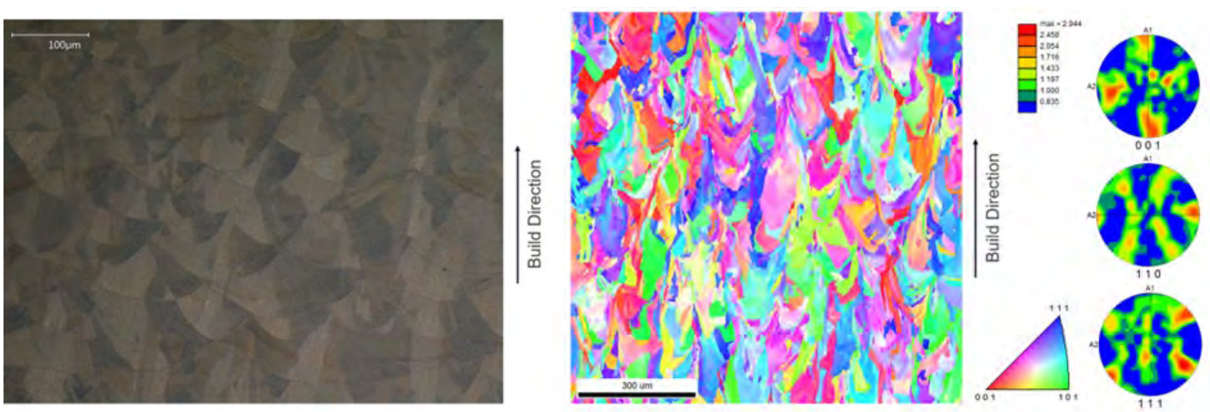

Figure 40. Printed eBlock7 microstructure. (Image from Michael Middlemas.)

The AM eBlock7 was within tolerances and had a microstructure that was typical of the direct metal laser sintering process, so the project was scaled up. During fabrication of the 37-heat-pipe core section, thermal stresses caused the part to warp and go out of tolerance. Because these blocks were out of tolerance, traditional manufacturing methods used with a variety of bonding methods were investigated.

7.2 Traditional Core Fabrication

To maintain tolerances throughout the Core37, traditional machining methods were used to produce 13 Core37 segments that would later be bonded together. Alignment pins were pressed into each of these segments to ensure the alignment of each segment was maintained during the bonding process. Figure 41 shows the 13 Core37 segments stacked together.

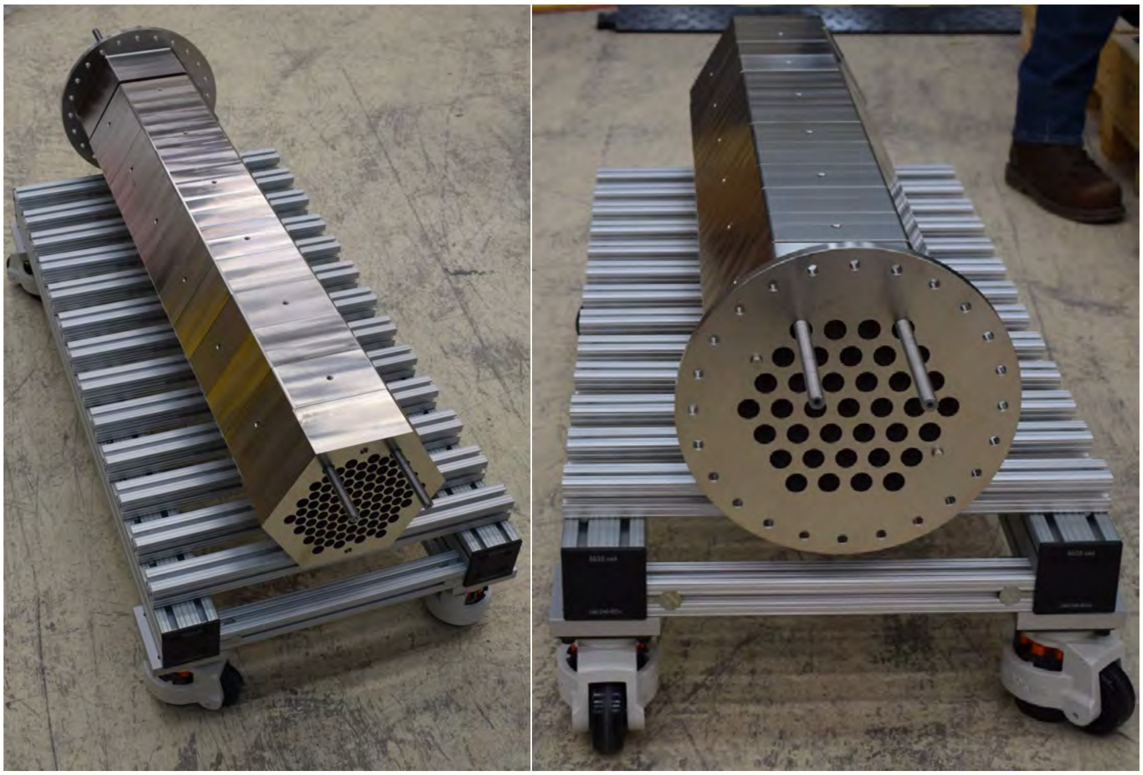

Figure 41. Thirteen-segment Core37 stack-up.

7.3 Hot Isostatic Press

The HIP method was considered as a bonding method for the core. The HIP block was produced from six 1-in.-thick 316 stainless steel plates. 316 stainless steel tubing was inserted through each hole. The ends of the tubes were swaged and orbital welded to the end plates. The assembles were canned while the HIP process took place. After the process, the can was machined off of the remaining block. The resulting HIP block was analyzed with both metallography and a Faro arm after the bond process. Metallography samples were taken from the corners of the block. Figure 42 shows the location of the metallography and both the best and worst bonds present in the blocks.

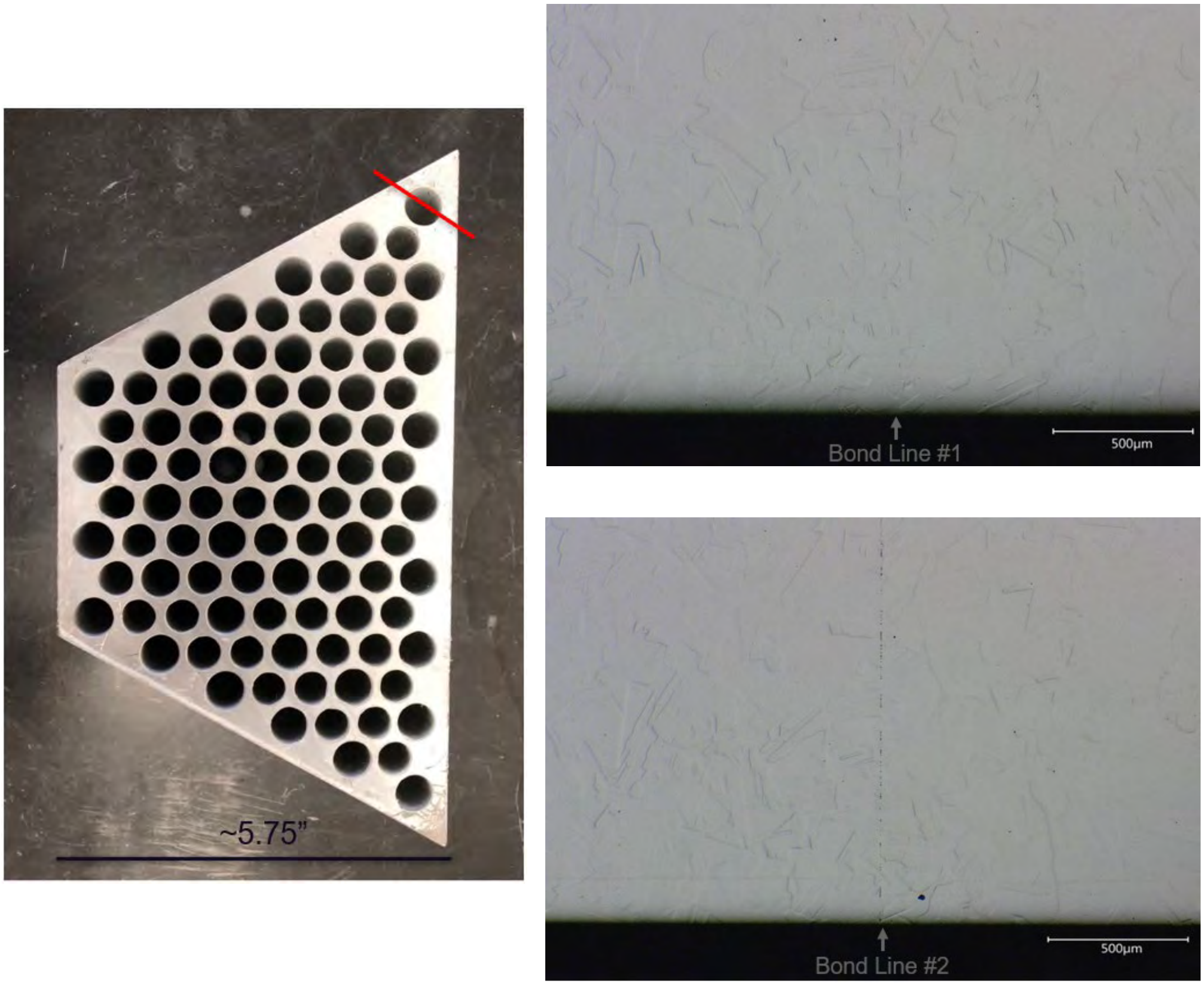

Figure 42. (Left) metallography sample location, (upper right) best bond line in sample, and (lower left) worst bond line in sample.

It is suspected that the worst bond line (bond line 2) shown in Figure 42 was a result of poor surface finish or contamination. Other challenges with the HIP process include ensuring all of the can material is removed from the block. After the sample was polished and etched, it was apparent that residual can material and tube material remained in the block. This extra material is shown in Figure 43.

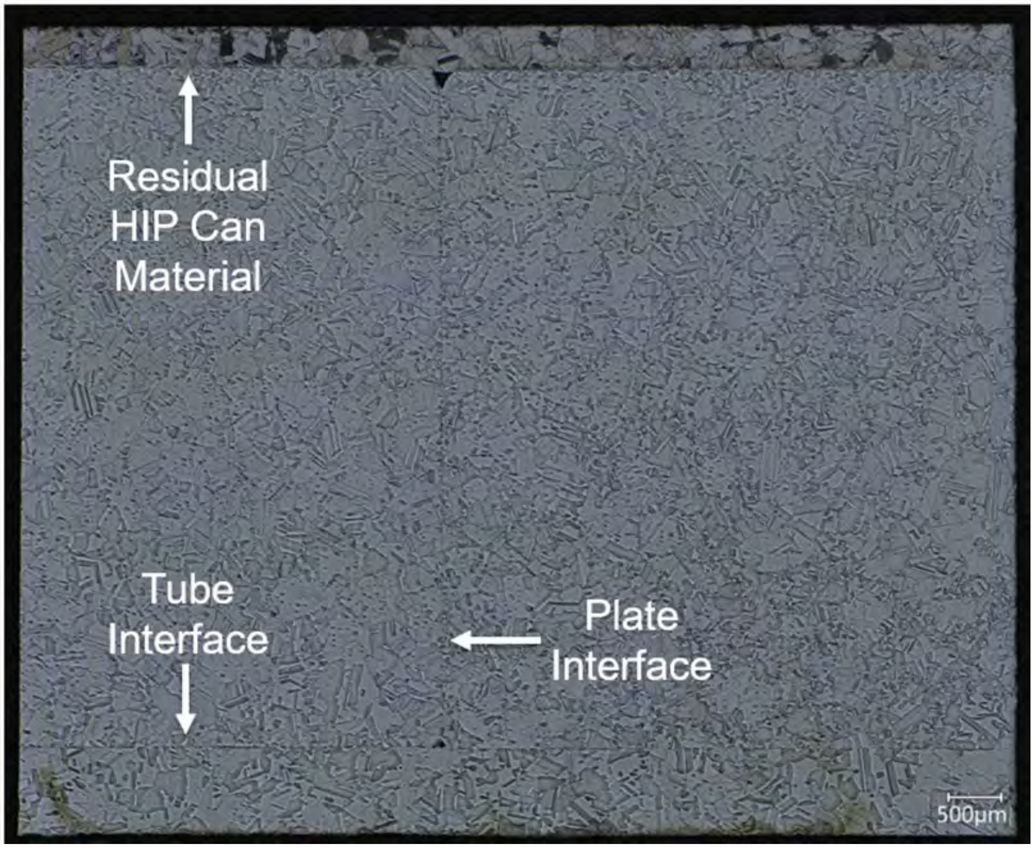

Figure 43. Etched and polished HIP core sample showing residual material.

Although the HIP bond method produced adequate bonds, the blocks that were bonded shifted during the process. To analyze this shift, a Faro arm was used to compare the bonded block to the original set of dimensions. Figure 44 shows point cloud data and a schematic of some example holes, whereas Table 5 shows the measurement point cloud and schematic of the sample hole locations.

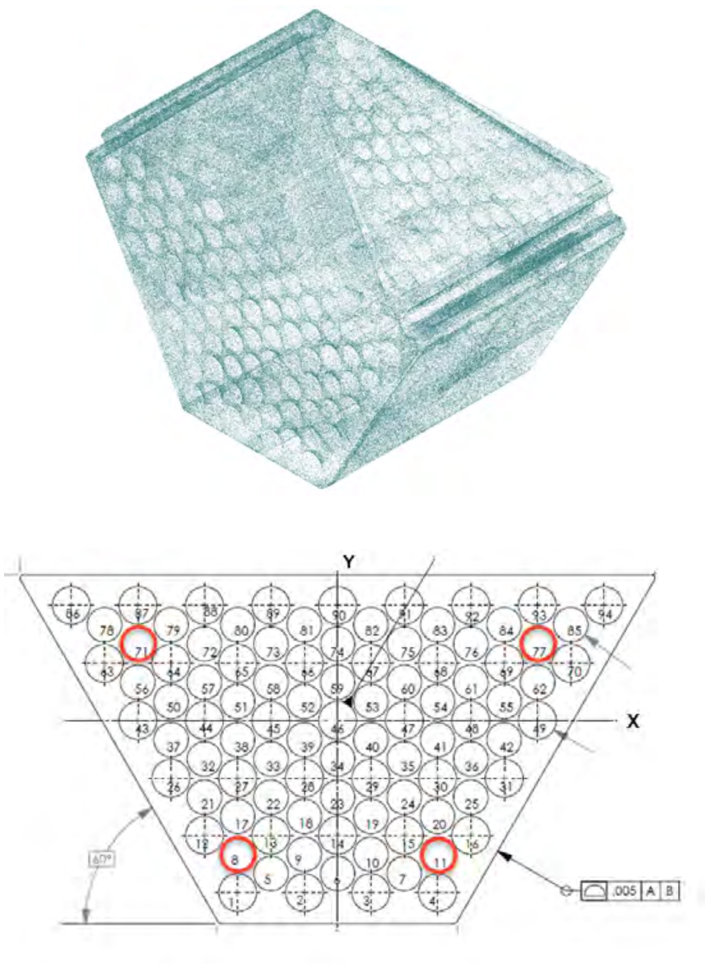

Figure 44. (Top) measurement point cloud and (bottom) schematic of holes measured for positional tolerances.

Table 5. Measured Position Shift Experienced by Selected Holes of the HIP Block.

Hole Number	Shift in X Direction (mm)	Shift in Y Direction (mm)
71	-0.652	0.489
77	-0.043	0.544
8	-0.04	0.67
11	-0.029	0.768

Although the HIP bond method produced good plate-to-plate bonds, the positional shift experienced by the holes during the bonding process is too large for this application. Alternate bonding methods including tier welding, diffusion bonding, and brazing were investigated.

7.4 Tier Weld

Tier welding the core section with an electron beam welder was considered. Several welding trials were conducted on the eBlock7 using a Probeam K110 system.[2] Results of a weld parameter trial are shown in Figure 45.[2]

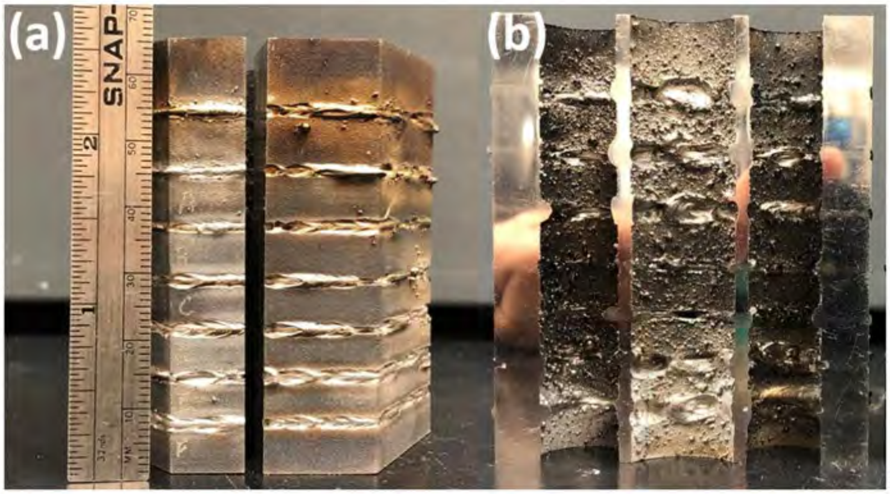

Figure 45. (a) Image of tier weld development on a portion of an AM-fabricated Block 7 article. Currents varied between 35 mA and 17 mA. (b) Cross section showing penetration and spatter from each tier weld seen in (a). (Image from Amber Black.)

The trial shown in Figure 45 included varied currents throughout the process. During welding, alignment pins were used in between sections and clamps were used to hold the part together for a tracking pass.[2] After refining the process, an additional sample was formed; see Figure 46. This sample underwent visual inspection, where it was noted that there was less splatter but some porosity. In addition to the visual inspection, metallography was performed on this sample using an optical microscope and a SEM. Figure 47 shows the locations of the section planes used in the metallography. Before the analysis, the samples were polished and etched.

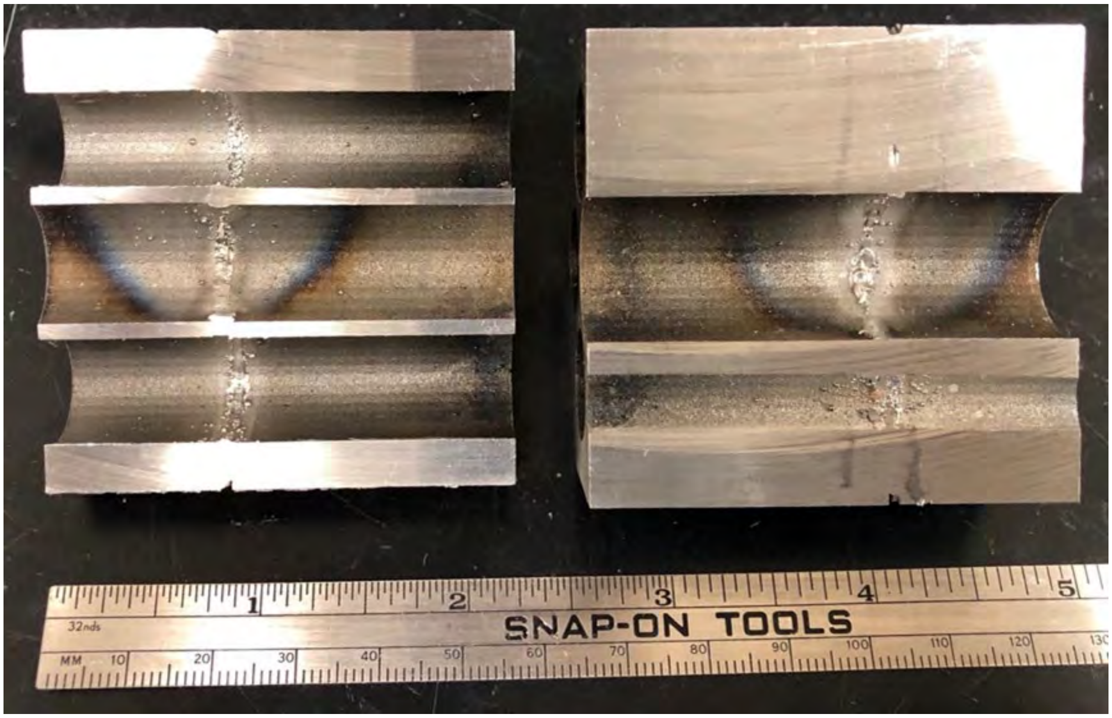

Figure 46. Electron beam tier welding eBlock7 sample used in metallography.

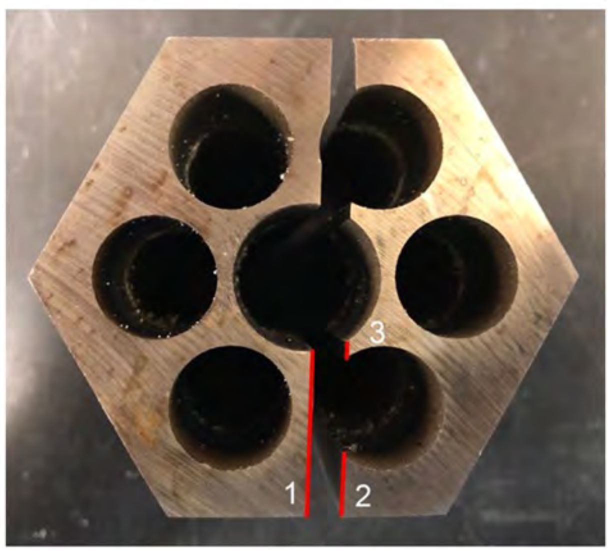

Figure 47. Locations of metallography samples on tier welded eBlock7.

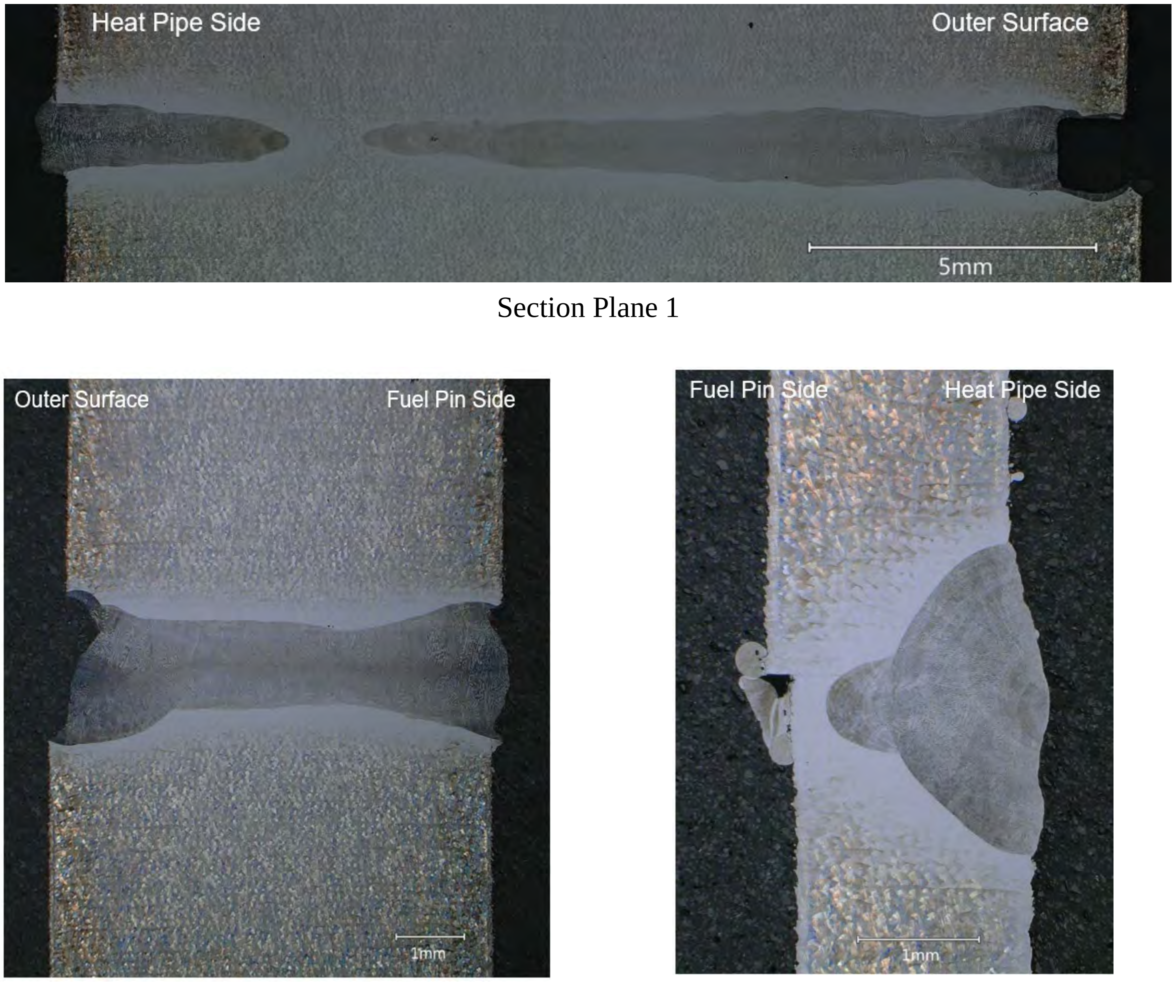

Figure 48. Metallography results from tier welded eBlock7.

From Figure 48 the metallography shows one minor pore in the weld and an inconsistency in weld penetration depth across the sections. The welding procedure produced splatter and the weld bead formed both noticeable convex and concave profiles inside the heat pipe tube. These profiles and splatter would need to be reamed out to successfully install a wick without damaging it. Because of the sizing and tolerances needed for the webbing present in the Core37, this process would be difficult.

7.5 Uniaxial Diffusion Bond

Uniaxial diffusion bonding was explored as a method of bonding the sections of the core block together. Initial tests were conducted by bonding two eBlock7 core block sections together. To provide enough pressure, threaded rods in combination with titanium-zirconium-molybdenum (TZM) plates were installed onto the blocks. Figure 49 shows a picture of the bonding assembly for the eBlock7 while Figure 50 shows the assembled eBlock7 in the vacuum furnace. To prevent the TZM nuts from galling and bonding to the threaded rods, boron nitride was used to lubricate the threads. A calculation was completed to determine a gap size of 0.140 in. between the eBlock7 and the plates. This gap allowed the stainless steel to undergo limited thermal expansion before contacting the top plate. After the gap was sized using gauge blocks, the assembly was torqued down to 29 in.-lb. The goal bonding pressure of this method was 92 MPa, which would allow the asperities to yield and bond while preventing the whole assembly from yielding.

The trials took place at Bodycote Rancho Dominguez in southern California. During the trials, the furnace was successively diluted with argon to reduce oxygen concentration and was then evacuated to 0.1 mTorr or better. During the first diffusion bond trial, the test article underwent three heating phases. In the first phase, the test article was heated to 990°C at a maximum ramp rate of 5.5°C/min. In the second phase, a lower ramp rate of 0.3°C/min was used to bring the test article to 1020°C, and the final phase brought the test article up to 1050°C with a ramp rate of 0.9°C/min. When it was at this temperature, the test article was allowed to soak for 311 min. For the second diffusion bond trial, a continuous ramp rate up to a temperature of 1100°C was used. This was thought to keep the block under constant pressure from the thermal expansion. This trial had four heating phases. The first phase used a ramp rate of 5.5°C/min to bring the test article to 990°C, the second phase reduced the ramp rate to 0.3°C/min until the temperature reached 1020°C, the third used a ramp rate of 0.9°C/min until the test article reached 1050°C, and the final used a ramp rate of 3.8°C/min to bring the test article to 1100°C.

Figure 49. eBlock7 bonding assembly with threaded rods and plates.

Figure 50. eBlock7 position in the furnace.

Figure 51 shows the eBlock7 after the bonding process. The white appearance of the nuts and bolts on the top of the block was caused by the boron nitride. The blocks were successfully bonded together, meaning that the segments did not separate from each other. When the bonded eBlock7 was received, the bonding assembly was disassembled by removing the plates and threaded rods. The bonded blocks from each trial were leak checked to determine if the holes were sealed. To identify leak positions, faces were labeled with letters and holes were labeled with numbers as shown in Figure 52.

Figure 51. eBlock7 after bonding.

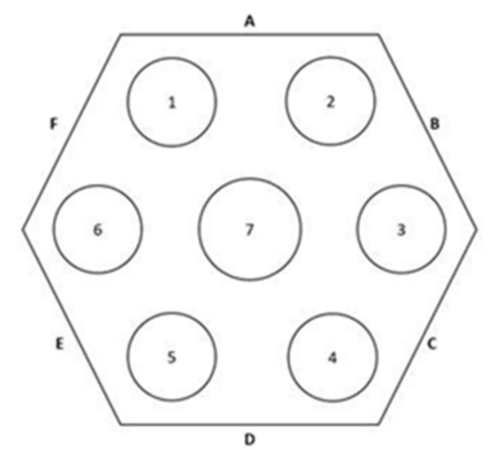

Figure 52. eBlock7 labeling schematic.

Seals for leak checking were created by using rubber stoppers as shown in Figure 53. The first trial block had significant leaks, with the outside holes having a baseline leak rate (without helium sprayed around down the hole) of 2E-6 atm cc/s and the center hole having a leak rate of 7E-8 atm cc/s. The leak rate in the center hole increased to 5E-5 atm cc/s when helium was sprayed into the surrounding holes. To locate the leaks, a positive pressure leak check was conducted by submerging the block in water and flowing 3 PSIG of helium into each of the holes, which were sealed with rubber stoppers. Holes 1–7 produced a large leak along the seam at face A, a medium leak at the seam on face B, and a small leak at the seam on face F. When the center hole was tested, there were not any visible bubbles from the seam.

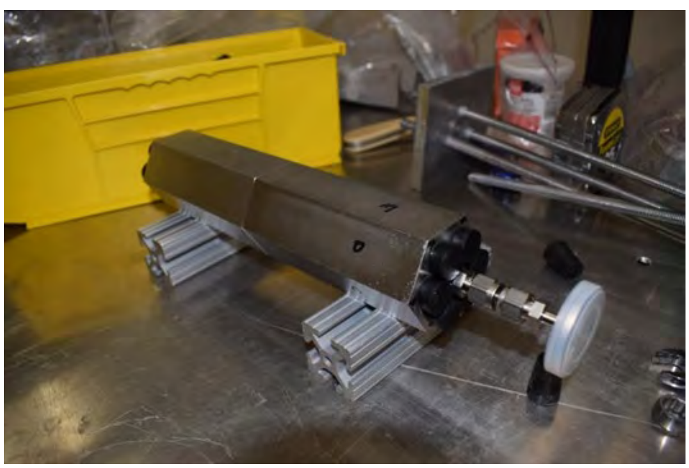

Figure 53. eBlock7 leak testing setup.

The second diffusion bond trial performed better than the first by having a leak rate of 2E-9 atm cc/s when measuring leaks from Hole 7 and spraying into Hole 4. The largest leak occurred when measuring from Hole 7 and spraying into Hole 1 (a leak rate of 2E-6 atm cc/s).

The leak tests suggest the asperity closure was incomplete because of pressure relaxation following initial asperity crush. A temperature ramp that applies a consistent uniaxial compression during diffusion bond may be sufficient to close asperities. Post-trial analysis indicated that the Arrhenius diffusion time constant is shorter than the thermal diffusion time constant between 1000°C and 1100°C. This time constant mismatch may have led to uneven contact across the bond line.

Matching the Arrhenius diffusion rate with the thermal diffusion rate requires longer furnace operation time at lower temperature. To close the 56-mil asperity stack-up in the eBlock37 segments, a ramp that starts near 900°C and ends at 1000°C was considered. To get the equivalent Arrhenius diffusion of 100 min at 1040°C, the eBlock37 requires up to multi-day exposure over at a temperature between 900°C and 1000°C. Although this option may be applicable in future designs, a brazing bond method was considered as a faster alternate bond technique.

7.6 Subscale Braze

To reduce technical risk for the electrical demonstration, an alkali metal–compatible braze bond was investigated. Two braze trials were conducted on the eBlock7 at Bodycote Rancho Dominguez in southern California. In the first trial, AMS 4778 braze foils were used, and in the second, AMS 4777 braze foils were used. Additionally, in the first trial, no alignment pins were present between the blocks, whereas the second trial had alignment pins.

During the trials, the furnace was heated to 1040°C at a rate of 5.5°C/min and held at that temperature for 2.5 h. The furnace was allowed to cool under vacuum to 500°C and then was cooled with argon gas to below 200°C. The parameters for these trials were determined using guidance from industry experts.

As shown in Figure 54, although both trials bonded the segments together, the first trial's seven-hole block segments rotated some whereas the second trial's remained aligned. Both of the brazed seven-hole blocks were helium leak checked. Helium leak check results for Trials 1 and 2 are shown in Tables 6 and 7, respectively. The holes and faces were labeled as shown in Figure 52.

Trial 1: AMS 4778 Braze Foil

Trial 2: AMS 4777 Braze Foil

Figure 54. eBlock7 braze trial results.

Table 6. Helium Leak Check Results for Trial 1 with AMS 4778 Braze Foil.

Leak Detector Hole	Hole Where Helium was Sprayed	Baseline Leak Rate (atm cc/s)	Leak Rate After Spray (atm cc/s)	Leak Detector Pressure (Torr)
7	1	0.0E-10	0.0E-10	5E-3
7	2	0.0E-10	0.0E-10	4E-3
7	3	0.0E-10	2.3E-9	3E-3
7	4	0.0E-10	0.0E-10	3E-3
7	5	0.0E-10	1.1E-8	3E-3
7	6	0.0E-10	0.0E-10	3E-3
1	2	0.0E-10	0.0E-10	4E-3
1	6	0.0E-10	0.0E-10	4E-3
3	2	1.1E-9	1.1E-9	4E-3
3	4	2.2E-9	2.2E-9	4E-3
5	4	0.0E-10	0.0E-10	4E-3
5	6	0.0E-10	0.0E-10	4E-3

Table 7. Helium Leak Check Results for Trial 2 with AMS 4777 Braze Foil.

Leak Detector Hole	Hole Where Helium was Sprayed	Baseline Leak Rate (atm cc/s)	Leak Rate After Spray (atm cc/s)	Leak Detector Pressure (Torr)
7	1	0.0E-10	0.0E-10	4E-3

7	2	0.0E-10	0.0E-10	4E-3
7	3	0.0E-10	0.0E-10	4E-3
7	4	0.0E-10	0.0E-10	4E-3
7	5	0.0E-10	0.0E-10	4E-3
7	6	0.0E-10	0.0E-10	4E-3
1	2	0.0E-10	0.0E-10	4E-3
1	6	0.0E-10	0.0E-10	4E-3
3	2	2.0E-9	2.2E-9	4E-3
3	4	2.0E-9	2.5E-9	4E-3
5	4	0.0E-10	0.0E-10	4E-3
5	6	0.0E-10	0.0E-10	4E-3

The maximum leak rate in Trial 1 was 1.1E-8 atm cc/s and occurred in the webbing between Holes 7 and 5, whereas the maximum leak rate in Trial 2 was 2.3E-9 and occurred in the webbing between Holes 3 and 2. Given the results of the leak checking and the fact that both trials successfully bonded the block segments together, additional subscale tests with thin Core37 segments were performed. The first subscale Core37 trial consisted of two approximately 1-in.-thick Core37 segments. Two AMS 4777 braze foils were used in this test. Upon visual inspection, there was some discoloration from something off gassing in the furnace. Even with this potential off gassing, the blocks bonded together. This discoloration is shown in Figure 55.

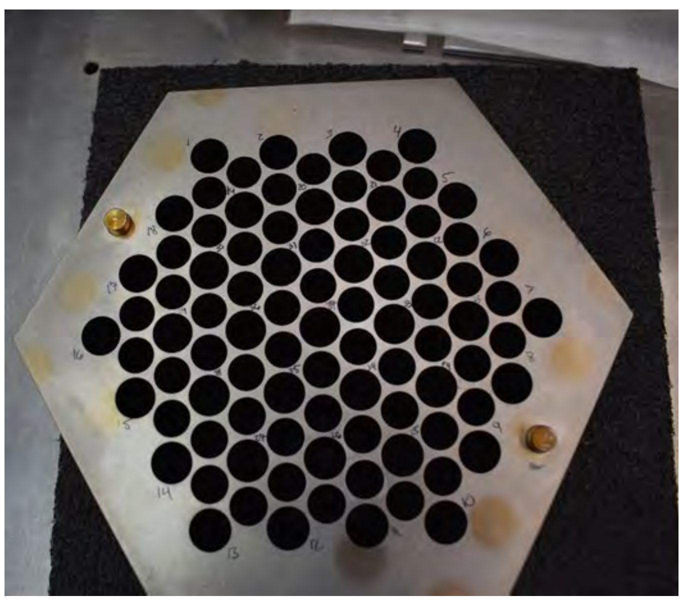

Figure 55. Brazed subscale Core37 with discoloration and labeled holes.

After a visual inspection, select holes were leak checked because of the increased number of holes and a limited timeline. Figure 56 shows a schematic of the holes selected for leak checking. The leak-checked holes were sealed with rubber stoppers. During the leak check, helium was sprayed around the seam and in each of the surrounding heater holes and heat pipe holes. For example, if Hole 1 was being leak checked, helium would be sprayed in all of the unlabeled surrounding heater holes and in Holes 2, 18, and 19. Several holes were tested twice one day apart to let any residual helium that was sprayed into the hole the day before to dissipate. Figure 57 shows the leak checking process and Table 8 shows the results of this leak check.

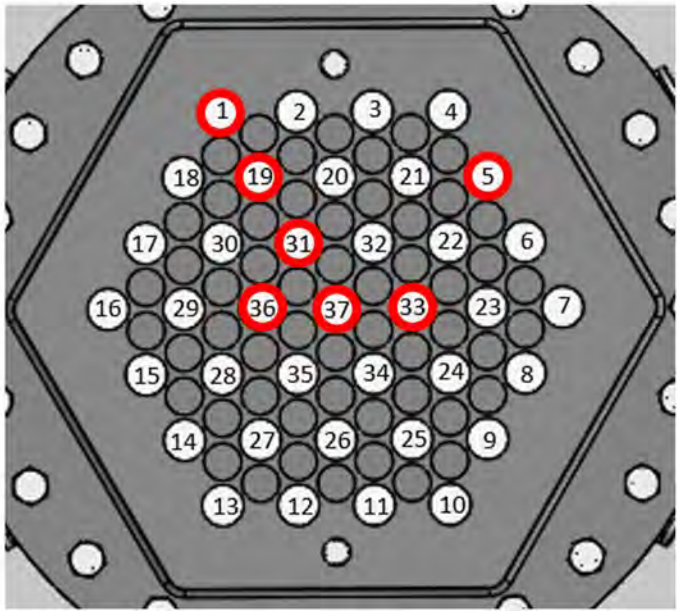

Figure 56. Schematic of selected heat pipe holes that underwent helium leak checking.

Figure 57. Leak checking process for Hole 31.

Table 8. Helium Leak Check Results for Subscale Core37 Braze Trial.

Hole Number	Baseline (atm cc/s)	Surrounding Hole Test (atm cc/s)	Seam Test
1	Initial Test: <4×10^-9	<4×10^-9	<4×10^-9
5	Initial Test: <2×10^-9	<2×10^-9	Increase to 1×10^-8 (disappeared with pressure applied to stopper)
19	Initial Test: <4.7×10^-9	<4.7×10^-9	<4.7×10^-9
30	Initial Test: <2×10^-9 Second Test: <7×10^-10	Initial Test: 3×10^-7 max. Second Test: <7×10^-10	Initial Test: <2×10^-9 Second Test: <7×10^-10
36	Initial Test: <3×10^-9 Second Test: <7×10^-10	Initial Test: 3×10^-8 max. Second Test: No increase	Initial Test: <3×10^-9 Second Test: <7×10^-10
37	Initial Test: <1×E-10	Initial Test: <1×E-10	Initial Test: <1×E-10

All of the tested heat pipe holes in this subscale Core37 braze trial passed the leak check. After the leak check, metallography was conducted on a section of the Core37. While retrieving the sample, it was observed that the braze bond was brittle and easy to break. Figure 58 shows a microscope image of the brazed bond line. In the image, the material around the bond is noticeably different. This was attributed to boron diffusion into the block segments. Additionally, there is a noticeable difference between the edges of the bond, where it appears smooth, and the center of the bond, where the braze appears rough. This was thought to be the result of a build-up of boron that may lead to embrittlement.

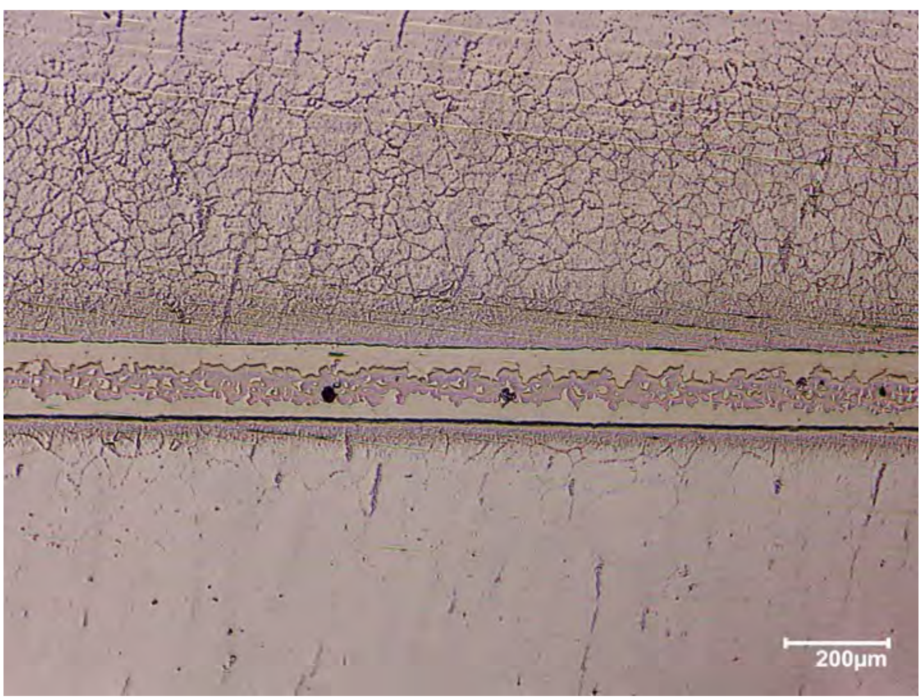

Figure 58. 200X Keyence image of brazed bond line in subscale Core37 trial.

Braze trials on eBlock7 units and a subscale Core37 unit yielded consistently strong bonds and closed asperities in the webbing, and the units passed all helium leak tests. Based on these results, AMS 4777 braze foils materials were purchased and cut into the Core37 shape for use in the full-scale Core37.

7.7 Full-Scale Braze

After successful attempts to braze two subscale eBlock7s and one successful Core37 trial assemblies that produced structurally sound and hermetically sealed bonds across the margins and the web, the process was used on the full-scale Core37. The full-scale Core37 consisted of 11 3-in.-thick segments and 1 4.5-in. segment. The drawings of these segments are shown in Appendix A. The segments were covered in a thin nickel strike to increase wetting of the braze material. The flatness and parallelism of the blocks were measured, and results are shown in Appendix B. Given the results of the inspection and the embrittlement observed in the two braze foil trials, subject matter experts (SMEs) advised using a single 0.0015-in.-thick AMS 4777 foil between the segments.

Before the core was heated, a successive dilution using liquid argon boil off and a vacuum pump was performed. Upon recommendation from braze SMEs, a three-phase heating process was used. All phases had a maximum ramp rate of 5.5°C/min. The first phase brought the Core37 to 540°C and held it there for 30 to 40 min. The second phase brought the Core37 to 950°C and held it there for another 30 to 40 min. The final phase brought the Core37 to 1065°C and held it for 40 min. After this, the Core37 was vacuum cooled to 540°C and the argon fan cooled it to below 100°C.

To achieve the best results possible, the following steps were performed.

1. Machine Core37 bond surfaces flat in to minimize joint gap clearance.
2. Insert dowel pins between Core37 blocks to maintain alignment.
3. Ensure dowel pins properly seat into adjacent alignment holes.
4. Apply 2-µm nickel strike on Core37 bond surfaces to enhance wettability.
5. Clean Core37 bond surfaces with acetone using lint-free cloth.
6. Place nickel braze foil layer at each Core37 bond line (spot weld to retain).
7. Perform high-temperature clean fire furnace burn out and vacuum leak up just before assembly of eBlock37 on furnace grating.
8. Inspect Core37 segments to ensure surfaces are flat.
9. Use lapping paper on a granite table to remove any possible high points (see Figure 59).

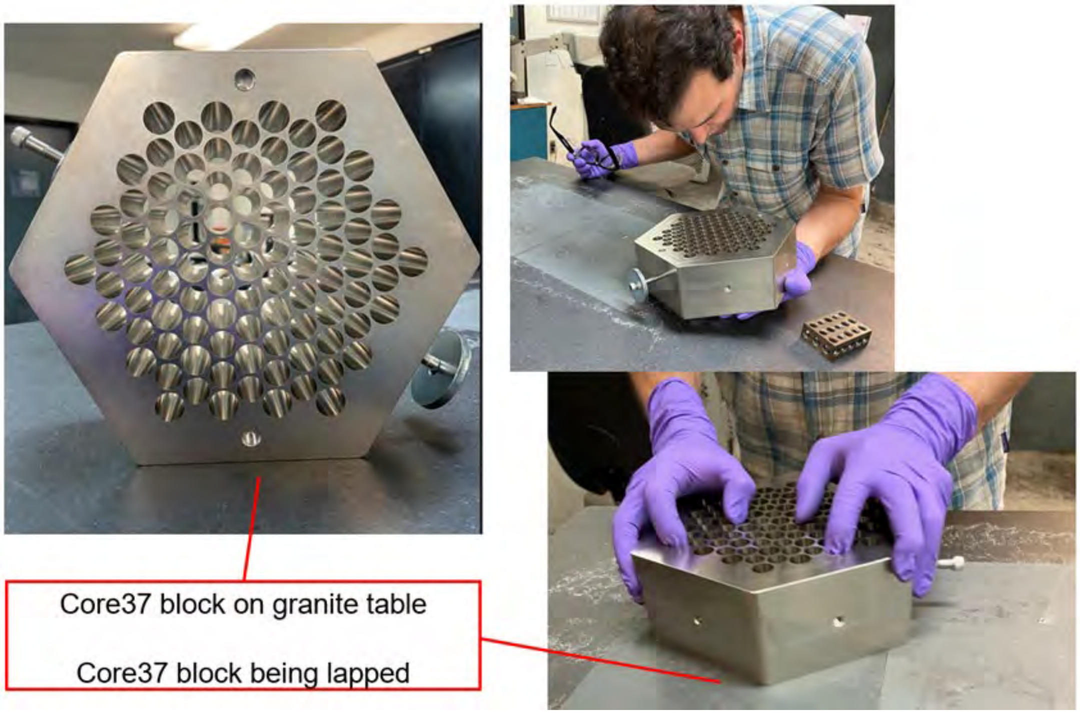

Figure 59. Core37 segment lapping and inspection process.

10. Verify dowel pin position.

11. Clean Core37 segments to ensure they are free of oil and debris (see Figure 60).

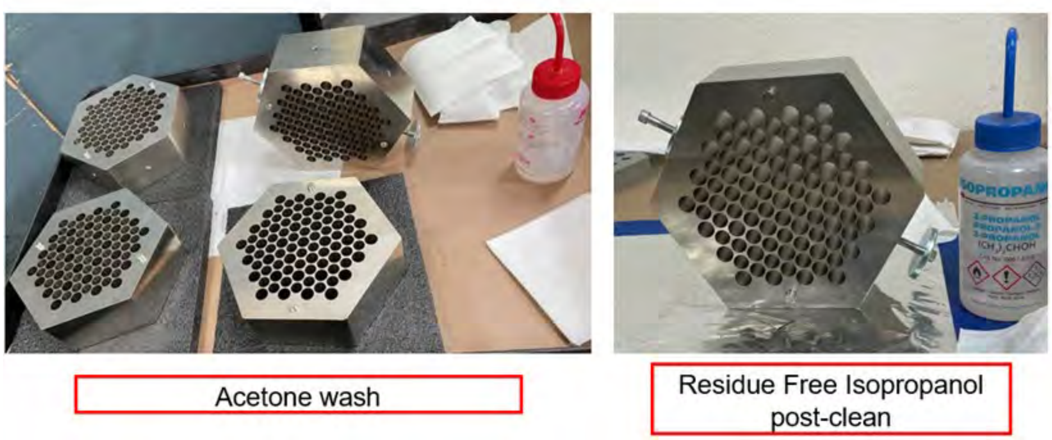

Figure 60. Core37 segment cleaning process.

12. Inspect Core37 assembly to verify there are no fit-up issues that will cause blocks to not seat during the braze process.

13. Install braze foils onto surface of Core37 segments (see Figure 61).

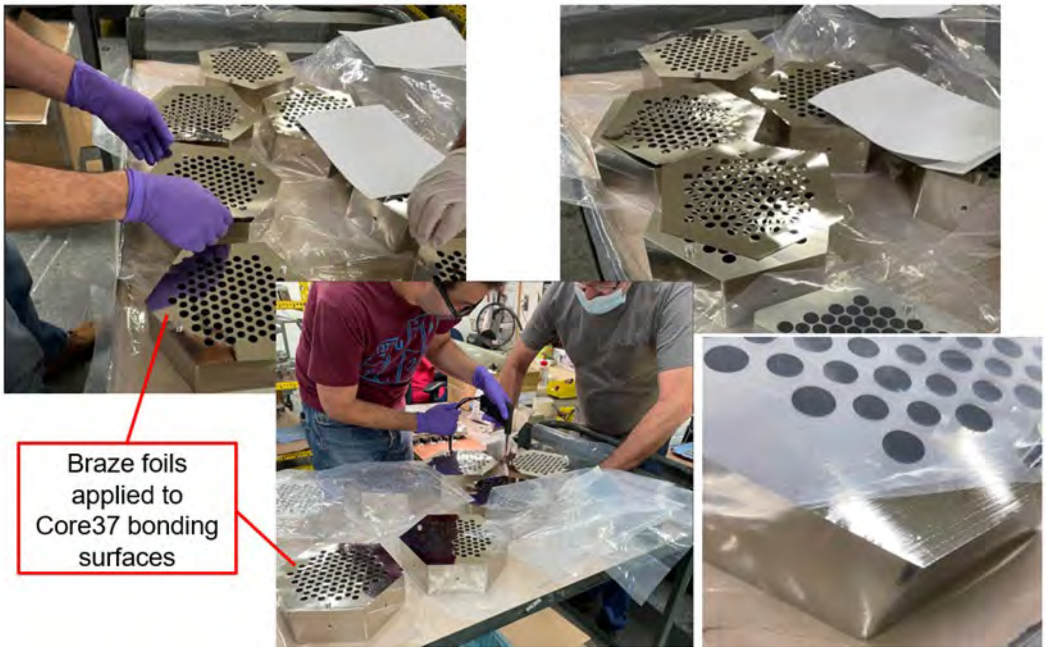

Figure 61. Braze foil installation onto Core37 segments.

14. Stack and tamp Core37 assembly on furnace grating (see Figure 62).

Figure 62. Core37 stacking process.

15. Inspect Core37 assembly to confirm fit.

16. Stack and tamp a Core37 witness assembly.

17. Place process control thermocouples in Core37 assembly.
18. Apply pressure to Core37 and witness block bond lines using block stack and weights (see Figure 63).

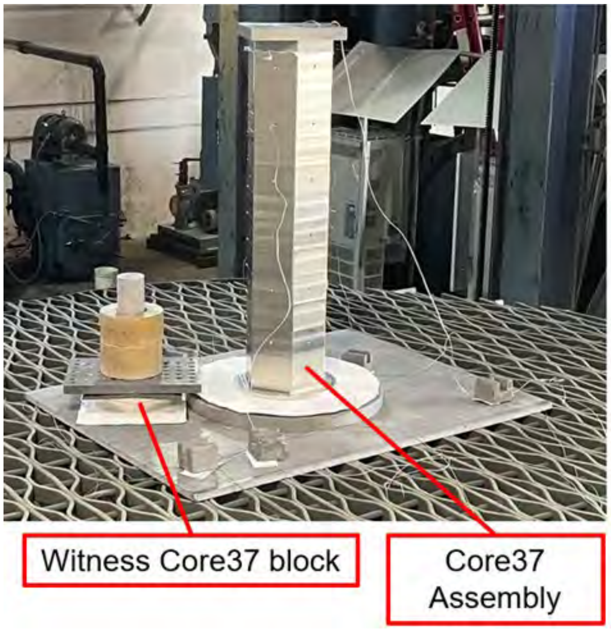

Figure 63. Core37 assembly and witness Core37 assembly instrumented and weighted.

19. Perform vacuum pump down and back fill furnace to atmospheric pressure with liquid argon boil off.
20. Repeat the above step three times before braze cycle.
21. Hold Core37 assembly at recommended braze temperature. Heat assembly slowly, extending soak and hold times by one third.
22. Vacuum cool Core37 assembly to intermediate hold temperature and then convective cool with liquid argon boil off.

After cooling, the assembly was visually inspected and removed from the furnaces using a crane. The assembly passed visual inspection and held together without issue when lifted from the top. Figure 64 shows the Core37 being moved with a crane and a bond line from the outside of the assembly.

Figure 64. Core37 assembly being moved by a crane and a bond line from the outside of the assembly.

When it was received, the core was visually inspected for any damage that may have occurred during shipping and was then helium leak checked. Although the brazed Core37 assembly passed the initial visual inspection, it did not pass helium leak checking. The baseline leak rate was too high in all holes to proceed with spraying helium. The smallest baseline leak rate, 9.8E-7 Torr L/s, was located in Hole 10, whereas the largest baseline leak rate, 1.0E-4 Torr L/s, was located in Hole 30. A table of initial leak rates can be seen in Appendix C. After the results of the helium leak test, a borescope was used to complete an internal inspection of the bond lines present in the 37 heat pipe holes. During this internal inspection, 0.002-in. cracks at the bond lines were observed. See Figure 65.

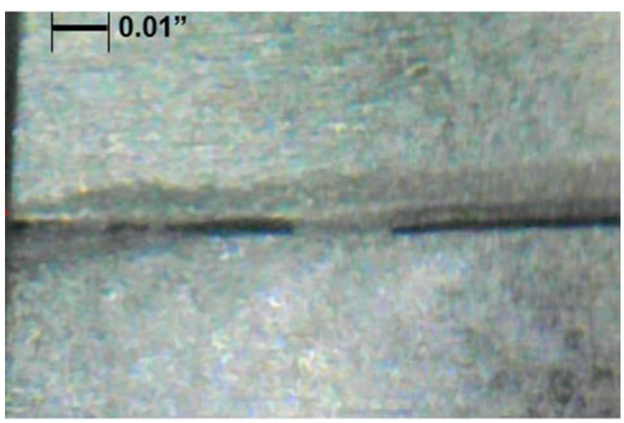

Figure 65. Crack at bond line in heat pipe holes of brazed Core37.

Brazing the Core37 produced structurally sound and hermetically sealed bonds across the margins but did not fully seal the heat pipe cavities within the web. This occurred because of unanticipated radial thermal gradients produced in the braze furnace between the relatively hotter margins (that sealed) and the relatively cooler web (that did not). Thermal gradients in the full-scale Core37 distorted the line-to-line contact between each of its segments by approximately 0.001 in. This distortion moved braze alloy away from the web bond lines.

7.8 Braze Repair

When it was discovered that the Core37 heat pipe cavities were leaking, an attempt to repair them was made with the AMI internal orbital arc welder after it was proven on the condenser tube test welds. A visual inspection using a borescope determined that repairs were needed on each of the 37 heat pipe cavities at all 11 braze bond lines (for a total of 407 welds). Initially, weld parameters for the repair were determined using welding trials in the witness core and previous subscale Core37 trial pieces. Each weld during the trial was visually inspected and was helium leak checked. When the parameters were determined, all 407 welds had to be completed before inspection because of time constraints.

7.8.1 Weld Development

Initial braze repair weld development was conducted on the subscale braze test blocks. It was initially supposed that the low fraction of braze material (~2% of the melt pool) and similarity to the substrate would be sufficient to produce acceptable welds. The first welds showed some small cracking, but tunning the weld schedule eliminated them in a few iterations. Welds that had cracked previously could be rewelded and successfully sealed. This indicated that a block repair could be successful. Figure 66 shows the weld progression on the sub-scale block.

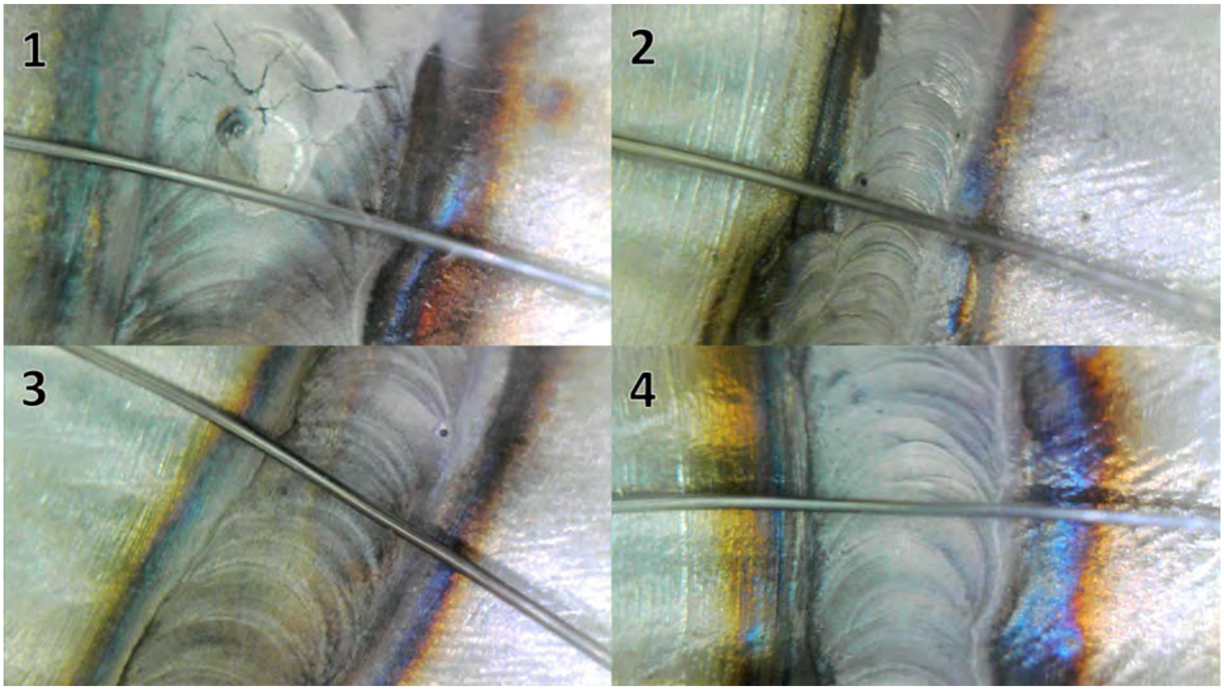

Figure 66. Test weld progression on the subscale block with 0.010-in. wire for scale.

Weld failures appeared mostly as segregation cracks or chevron cracks, but we expect both to be caused by the concentration of low melting temperature impurities from the braze foil being drawn toward the center of the cooling weld.

Figure 67 shows an example of these weld failures. Weld development progressed with the objective of diluting and dispersing the braze contaminant to reduce the thermal gradients and stop cracking. Strategies included hotter welds, deeper welds, alternating cold and hot welds, and double-pass welding.

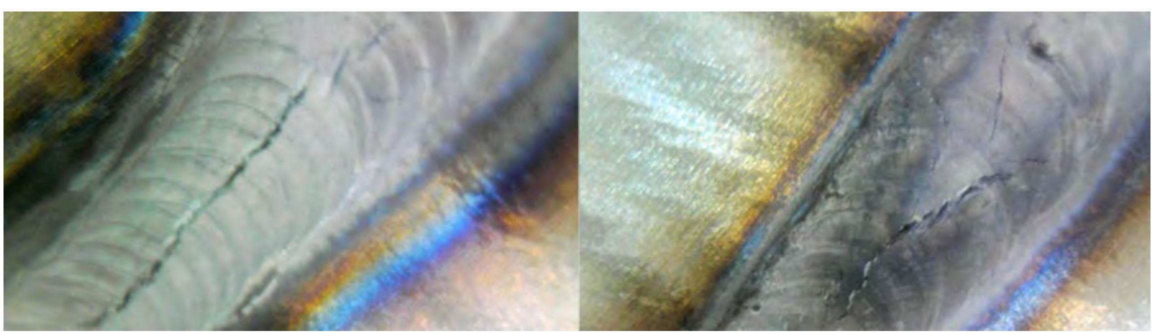

Figure 67. (Left) segregation crack and (right) chevron crack.

7.8.2 Leak Checking

Each weld was visually inspected, but some cracks were too small to see. To locate leaking welds, insertable expansion plugs with an internal vacuum path were created, shown in Figure 68.

Figure 68. Insertable, individual bond line leak checking plugs.

When leak checking, a series of bond lines can be tested at once and then the range can be quickly adjusted to find the problem.

7.8.3 Repair Discussion and Results

The center heat pipe cavity was the first to be welded. Bond lines 1–10 sealed, with 1 being closest to the heat exchanger. Bond line 11 proved impossible to seal even after several iterations of weld schedule. Next were a corner and edge pipe that showed similar results except that bond line 9 was leaking too. This precipitated a discussion of cutting off the last 1 to 3 sections of the block if that was where all the problem welds were. Welding proceeded under the expectation that most weld failures would be contained within the last three bond lines. In-line weld inspection was suspended because of time pressure.

After completing the 407 welds in the block, a visual inspection of all welds showed a failure rate of 26%. Then individual leak checking and weld re-work began on layer 2 (pipes 31–36) with the goal of getting minimally 7 or 19 sealed heat pipe holes. Unfortunately, after leak checking and repair attempts, layer 2 contained unrepairable welds distributed through the block. A table of repair results is shown in Appendix D. Welding and leak checking attempts were then suspended. Including removing layer 11, the final failure rate was 30%.

7.9 Alternative Core37

Figures 69–77 show two versions of an alternative Core37 block. Both versions are constructed from 316L stainless steel and consist of an array of 37 heat pipe evaporator tubes internally welded to a flange plate at the evaporator exit. A total of 37 heat pipe condenser tubes is internally welded to the same flange plate. A total of 54 fuel tubes is TIG welded to a plate at the evaporator entrance. Following sodium charge in the eFill37, the 37 heat pipe condensers are sealed by vacuum laser welds.

The Core37a version uses welded construction to form a hexagonal 316L stainless steel enclosure to contain a NaK-77 intermediary working fluid. The weight of the 316L stainless steel material is 148 kg. The open volume in the hexagonal enclosure is 6.5 L. There is a ~24% volumetric thermal expansion of NaK-77 working fluid from 30°C to 700°C. Allowing for expansion the initial NaK-77 volume at room temperature should be under 4.8 L. This charge corresponds to 4.1 kg of NaK-77 at room temperature. By comparison, each heat pipe in the eBlock37 contains 55 g of sodium, with a 37-heat-pipe array containing 2.0 kg.

Figure 69. (Top) NaK-77 filled Core37 block showing Version A with containment formed from welded hex plates and (bottom) Version B with containment formed from cylindrical seamless pipe.

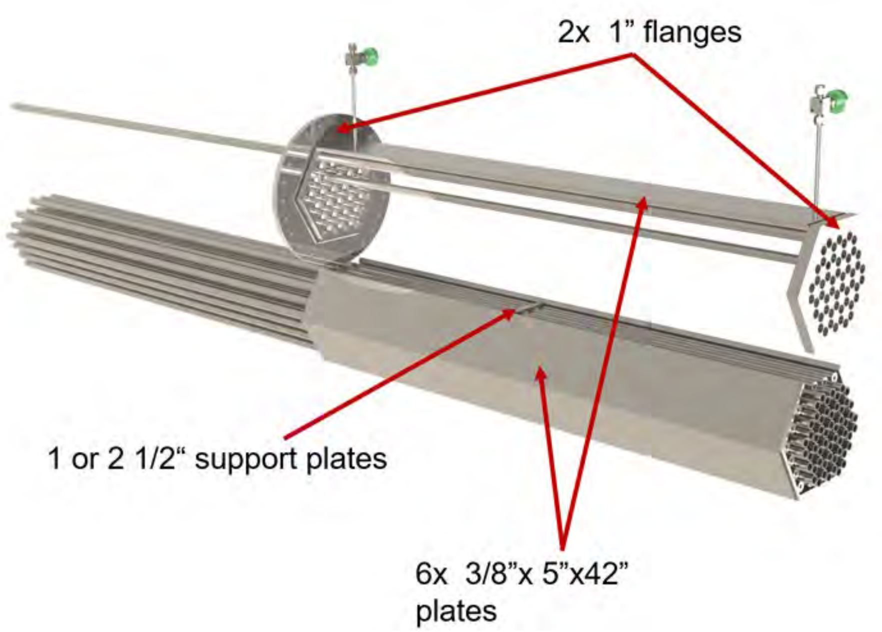

Figure 70. NaK-77 filled Core37 block showing cutaway view and assembly detail.

Figure 71. NaK-77 filled Core37 block cross-sectional view.

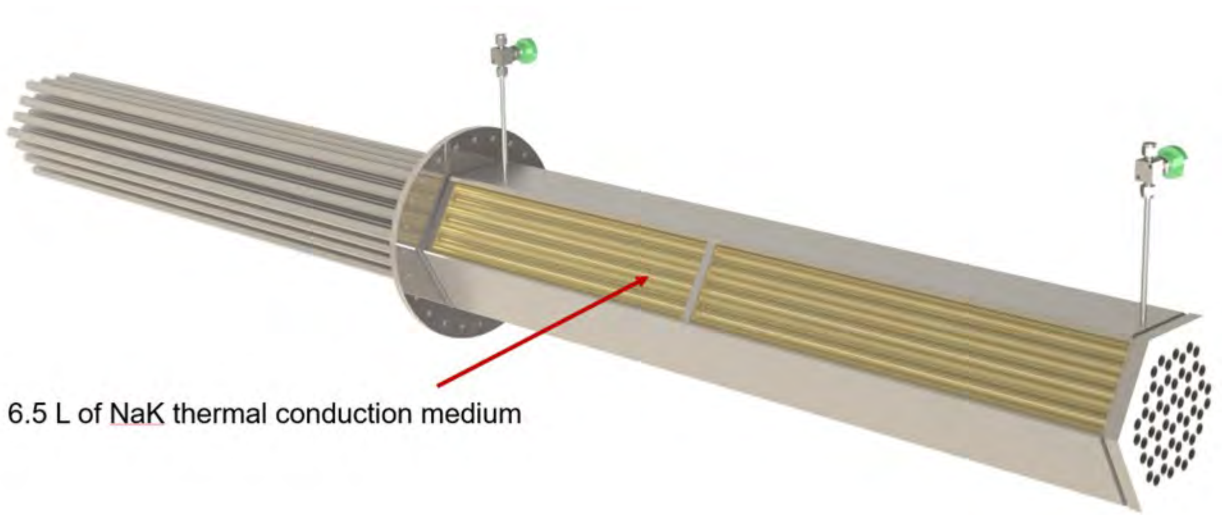

Figure 72. NaK-77 filled Core37 block showing panel cutaway.

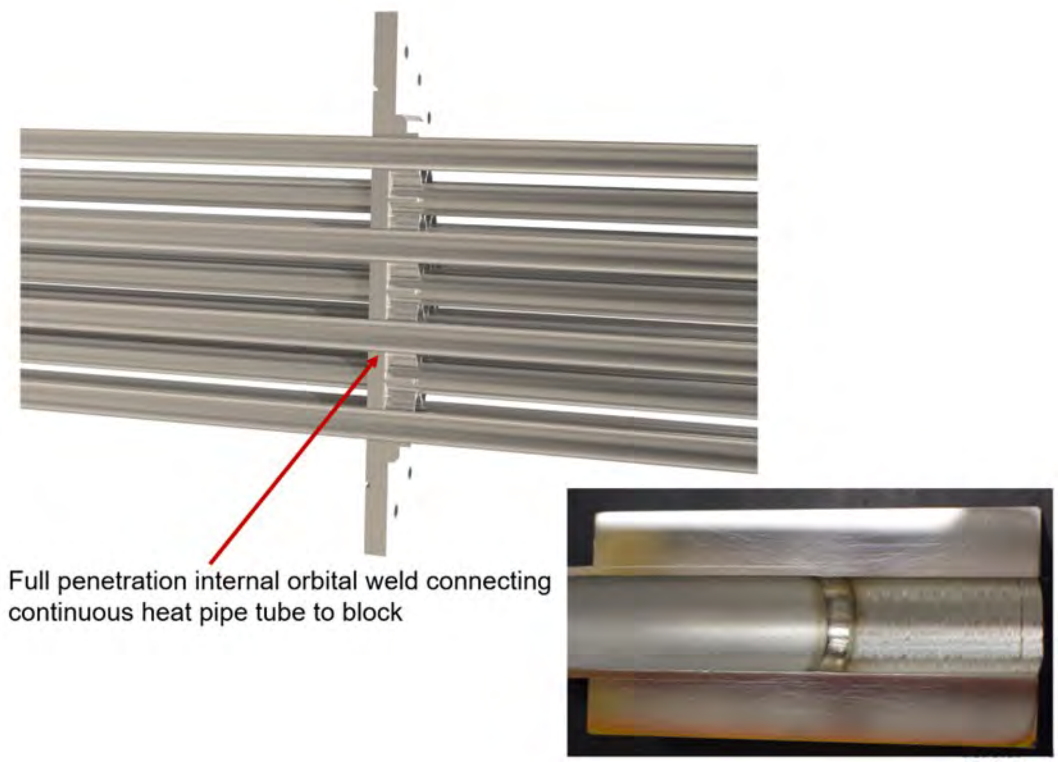

Figure 73. NaK-77 filled Core37 block showing heat pipe array cutaway at evaporator exit.

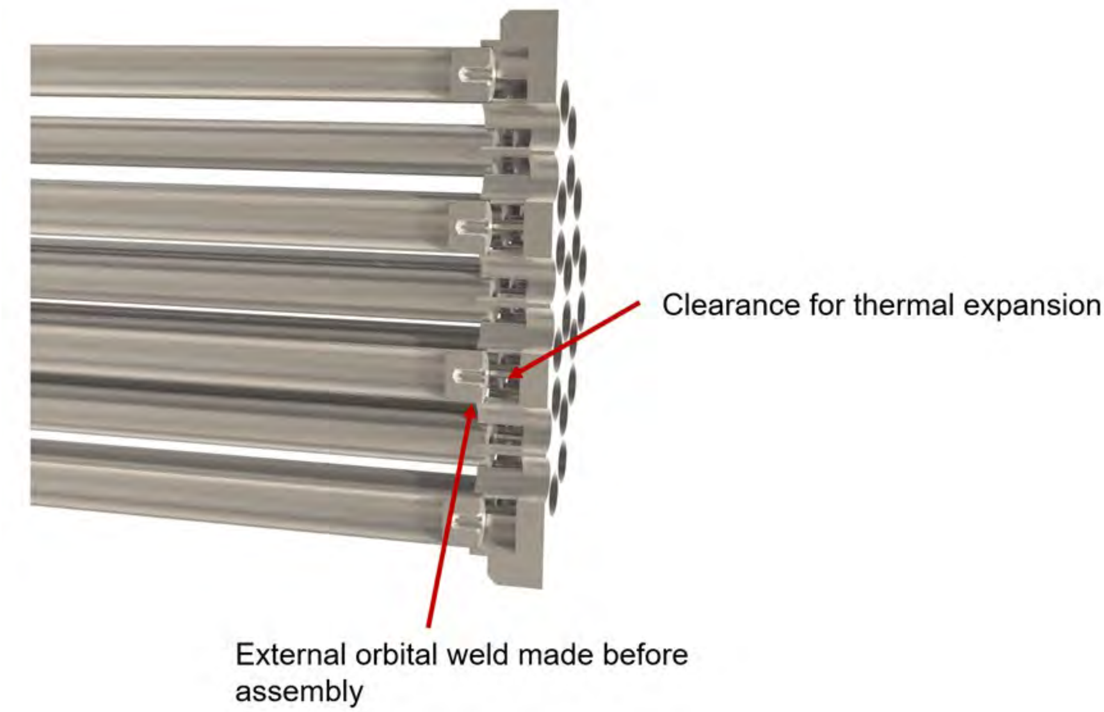

Figure 74. NaK-77 filled Core37 block showing heat pipe cutaway at evaporator entrance.

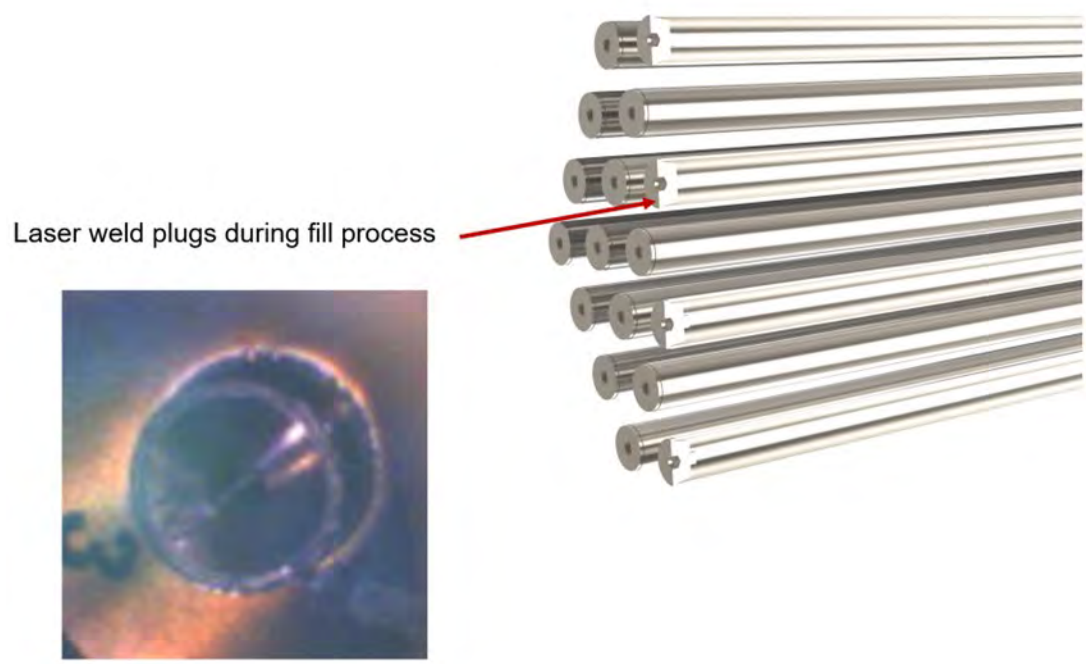

Figure 75. NaK-77 filled Core37 block showing heat pipe array cutaway at condenser end.

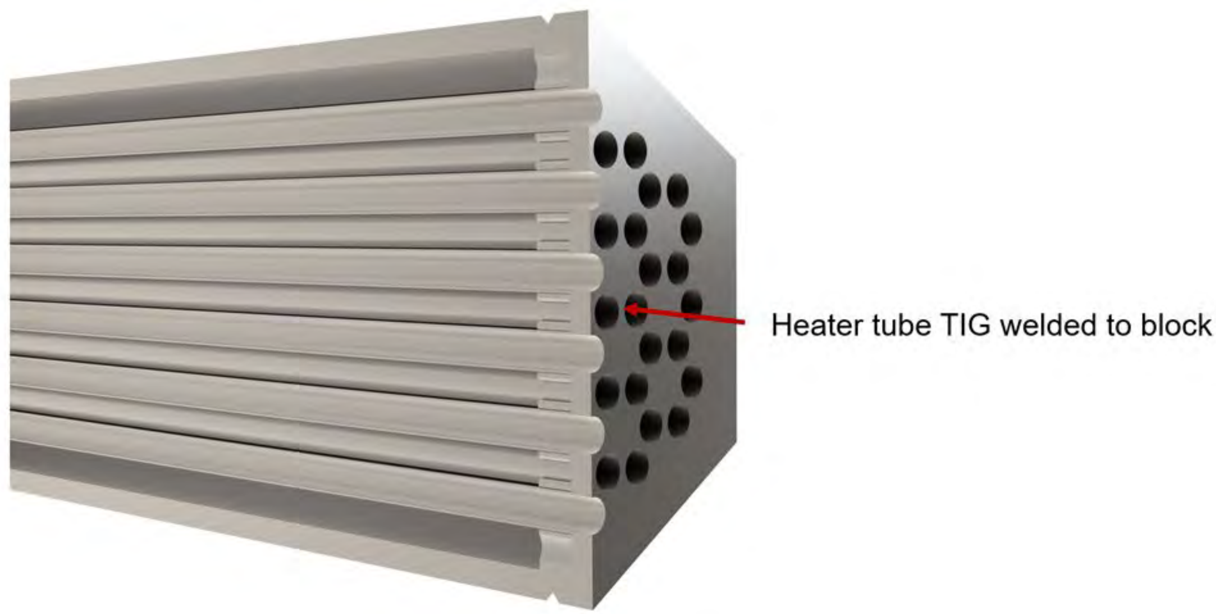

Figure 76. NaK-77 filled Core37 block showing heater cutaway at evaporator entrance.

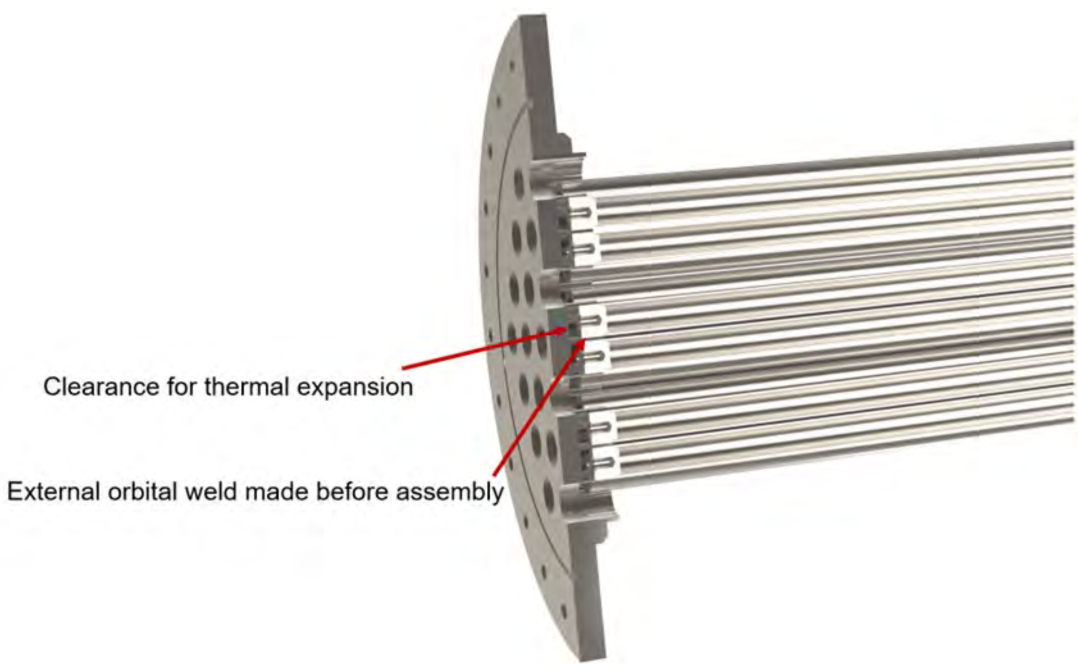

Figure 77. NaK-77 filled Core37 block showing heater cutaway at evaporator exit.

8.0 POTENTIAL PATHS FORWARD

The existing Core37 and eXchanger37 assembly can be immediately sent to Idaho National Laboratory (INL) for heater integration regardless of any other future work that is performed. The overall assembly can be dimensionally testing while being heated with cartridge heaters. Heaters in the Core37 and eXchanger37 can approximate the stress state and allow instrumentation and sensor measurement objectives to be met. Five additional potential paths forward for heat pipe/heat exchanger testing consist of the following.

8.1 Path Forward 0

A new core will be fabricated based on the current Core37 block design, the braze step will be repeated with improvements, and the fabrication sequence will be completed as originally planned. This path allows for the original stainless steel monolithic heat pipe core block to be studied. Alternative Path 0 allows for complete exercise of the eFill37 and realistic test of the original high-temperature heat pipe array design in the Microreactor AGile Non-nuclear Experimental Testbed (MAGNET) facility. The information gained from these tests may be used in models for reactor feedback control. The following technical risks apply.

- The subscale Core37 blocks brazed satisfactorily on every attempt. The previous problem encountered with the full-scale Core37 was related to temperature equalization of the blocks before the Core37 assembly reached the braze foil solidus temperature.
- As an additional precaution, thicker braze foil (not available at time because of COVID-19 shortages) can be used along with a study to confirm the appropriate furnace heating profile for the subscale and full-scale Core37.

8.2 Path Forward 1

An alternative Core37 using NaK as a heat transfer medium can be assembled. Much of the work hinges on less expensive, trained welders. The welds and inspections should go faster than for the existing eBlock37 repair (as we are not continually reworking contaminated welds). Alternative Path 1 allows for complete exercise of the eFill37 and realistic test of a high-capacity, high-temperature heat pipe array in the MAGNET facility.

8.3 Path Forward 2

Individual sodium heat pipes can be constructed from the eWick37 batch and charged with the eFill37. These heat pipes can be individually tested and integrated into MAGNET test articles. This path uses existing eWick37 and eFill37 infrastructures. Minor modifications to the eFill37 to charge individual heat pipes will be required. Tube and closure materials can be procured and undergo appropriate chemical clean and vacuum fire steps. Alternative Path 2 allows for the complete exercise of the eFill37 and the construction of one or more alternative heat-pipe-cooled MAGNET test articles.

8.4 Path Forward 3

Core37 and eXchanger37 would need to be retained at LANL. Thin-walled tubes can be hydroformed into the existing Core37, sealing off the weld cracks. The thin-walled tubes allow thermosiphons to be welded into the core block. The thermosiphons can be charged with sodium. Thermosiphons are necessary because heat pipe wicks will not fit into heat pipe cavities covered with hydroformed thin-walled tubes. This path uses eFill37 infrastructure and the existing Core37. Minor modifications to the eFill37 to charge individual heat pipes will be required. Tube and closure materials will be procured and undergo appropriate chemical clean and vacuum fire steps. Alternative Path 3 allows for complete exercise of the eFill37 and testing of a lower power thermosiphon array in the MAGNET facility. However, thermosiphons require large working fluid inventory, and their qualitative behavior is not representative of heat pipe behavior.

8.5 Path Forward 4

This path consists of the fabrication of a heat pipe graphite core block with fewer heat pipes. This would allow for the eFill37 infrastructure to be used and for a prototypic graphite heat pipe core to be tested at the MAGNET facility. This path forward requires the following.

- The use of low voltage heaters to avoid potential for dielectric breakdown (especially acute with graphite)
- Design and build of a compatible heat exchange structure
- Information related to carbon diffusion through the stainless steel heat pipes
  - To mitigate this, TZM tubes and wicks may be purchased; however, this may be time-consuming and expensive. Additionally, the heat pipe designs may need to be altered to compensate for the difference in coefficients of thermal expansion if TZM walls are used with the existing stainless steel wicks.

The sections below discuss the advantages and disadvantages of each path forward and provide rough estimates of required time and costs.

8.6 Proposed Path 0

The existing Core37 can be immediately sent to INL for heater integration and dimensional testing while being heated with cartridge heaters. The block would not be cooled by heat pipes, but high-temperature measurement objectives may be met by this approach. A replacement Core37 using lessons learned from the first one would be fabricated. The key changes are increased braze foil thicknesses and increased soak time in the furnace. The experience of sourcing, building, transporting, and filling the current Core37 will significantly improve operational efficiency toward building another.

Below are advantages and disadvantages for Proposed Path 0, which consists of a Core37 re-do.

- Advantages

- Allows immediate hot test of Core37 and eXchanger37 with heaters (instrumentation)
- Allows realistic test of modified eBlock37 heat pipe array in MAGNET facility
- Allows exercise of eFill37 infrastructure

- Disadvantages
  - Residual risk associated with braze (study mitigates)
  - Lengthy lead time in manufacturing and brazing assembly

8.7 Proposed Path 1

The existing Core37 can be immediately sent to INL for heater integration and dimensional testing while being heated with cartridge heaters. The block would not be cooled by heat pipes, but high-temperature measurement objectives may be met by this approach. An alternative Core37 using NaK as a heat transfer medium can be assembled. The figures below represent a design concept. An assembly sequence would need to be generated to estimate time to completion. The welds and inspections should go faster than for the existing eBlock37 repair (as we are not continually reworking contaminated welds). Alternative Path 1 allows for complete exercise of the eFill37 and realistic testing of a high-capacity, high-temperature heat pipe array in the MAGNET facility.

Below are advantages and disadvantages for Proposed Path 1, which consists of a NaK Core37.

- Advantages
  - Allows immediate hot test of Core37 and eXchanger37 with heaters (instrumentation)
  - Allows realistic test of modified eBlock37 heat pipe array in MAGNET facility
  - Allows exercise of eFill37 infrastructure
  - Uses inexpensive materials
  - Proposed welds are conventional or have been demonstrated by team members
- Disadvantages
  - Requires build of affordable substitute Core37
  - May requires additional safety measurements to operate NaK at MAGNET
  - Requires alkali metal (NaK) inventory ~2X that of heat pipes

8.8 Proposed Path 2

The existing Core37 can be immediately sent to INL for heater integration and dimensional testing while being heated with cartridge heaters. The block would not be cooled by heat pipes, but high-temperature measurement objectives may be met by this approach. Individual sodium heat pipes can be constructed from the eWick37 batch and charged with the eFill37. These heat pipes can be individually tested and integrated into MAGNET test articles. Path 2 uses existing eWick37 and eFill37 infrastructures. Minor modifications to the eFill37 to charge individual heat pipes will be required. Tube and closure materials can be procured and undergo appropriate chemical clean and vacuum fire steps. Alternative Path 2 allows for the complete exercise of the eFill37 and the construction of one or more alternative heat-pipe-cooled MAGNET test articles.

Below are advantages and disadvantages for Proposed Path 2, which consists of using existing infrastructure to build component-level heat pipes.

- Advantages
  - Allows exercise of eFill37 infrastructure
  - Allows immediate hot test of Core37 with heaters (instrumentation)
  - Allows testing of alternative heat pipe systems in MAGNET
- Disadvantages
  - Does not allow integrated test of eBlock37 system in MAGNET
  - Does not use eXchanger37 or energy conversion hardware at MAGNET

8.9 Proposed Path 3

It may be possible to hydroform thin-walled tubes into the existing Core37 to seal off the weld cracks. The thin-walled tubes allow thermosiphons to be welded into the core block. The thermosiphons can be charged with sodium. Thermosiphons are necessary because heat pipe wicks will not fit into heat pipe cavities covered with hydroformed thin-walled tubes. This path uses eFill37 infrastructure and the existing Core37. Minor modifications to the eFill37 to charge individual heat pipes will be required. Tube and closure materials will be procured and will undergo appropriate chemical clean and vacuum fire steps. Alternative Path 3 allows for complete exercise of the eFill37 and testing of a lower power thermosiphon array in the MAGNET facility. ***However, thermosiphons require large working fluid inventory and their qualitative behavior is not representative of heat pipe behavior.***

Below are advantages and disadvantages for Proposed Path 3, which consists of a thermosiphon version of the Core37.

- Advantages

- – Allows exercise of eFill37 infrastructure
- – Allows modification of existing Core37

- Disadvantages
  - – Does not permit hot test of Core37 with heaters (instrumentation)
  - – Thermosiphon operation not representative of heat pipes
  - – Requires alkali metal (sodium) inventory >5X that of heat pipes

8.10 Proposed Path 4

This path would involve assembling a 36-in.-long sodium heat pipe carbon core block with heat pipes and a heat exchanger. This carbon core block uses fewer heat pipes than the current eFill37 infrastructure. However, because of the difference in the number of heat pipes and the design, shown in Figures 78 and 79, a new heat exchanger will need to be designed and fabricated. Additionally, this configuration may require TZM tubes and wicks, leading to additional costs and time.

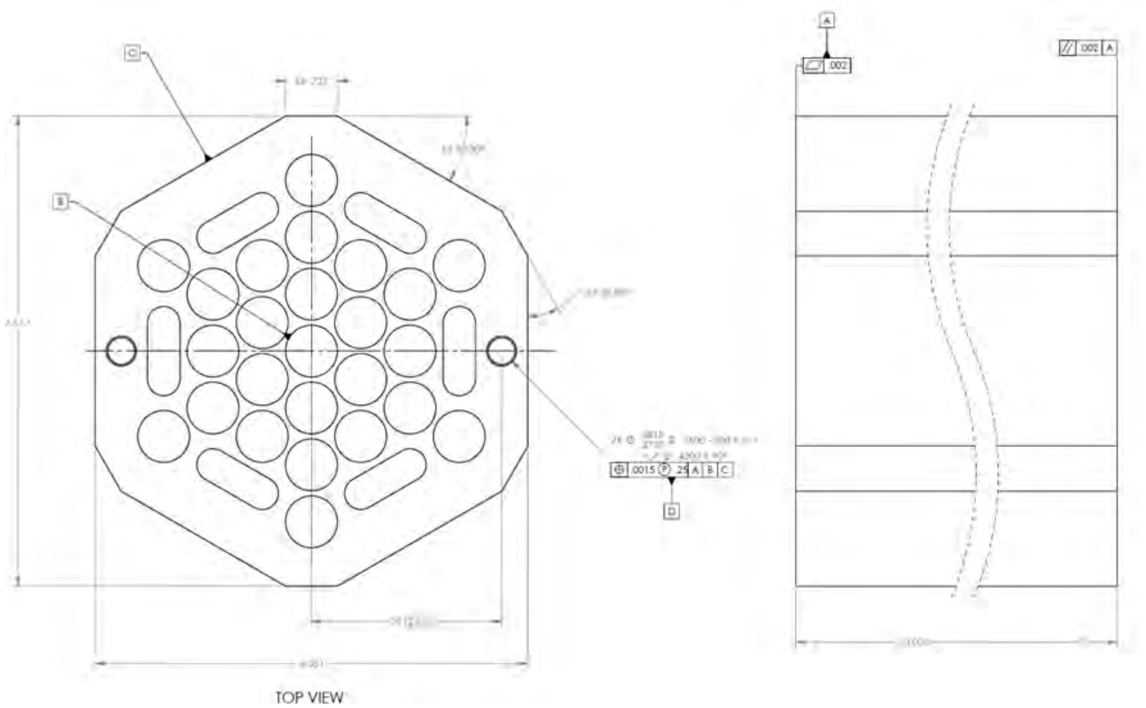

Figure 78. Carbon core block design.

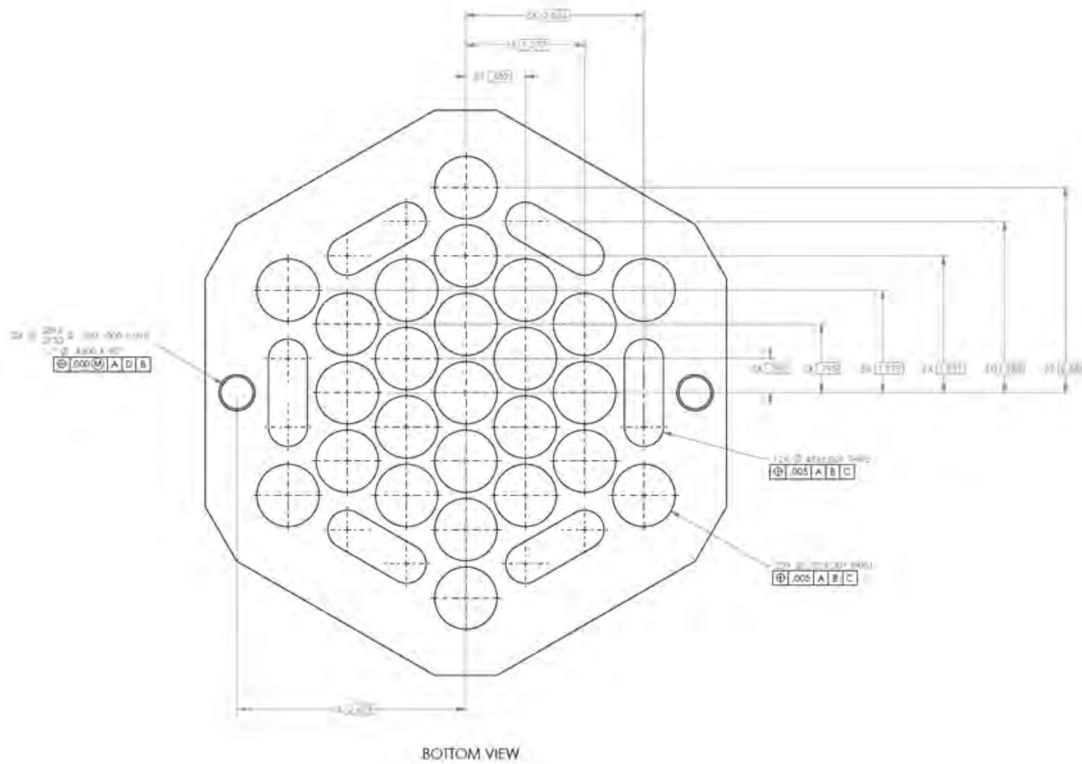

Figure 79. Carbon core block hole sizing.

Below are advantages and disadvantages for Proposed Path 4, which consists of a heat pipe carbon core block design.

- Advantages
  - Allows exercise of eFill37 infrastructure
  - Requires fewer heat pipes to be filled
- Disadvantages
  - Requires use of low voltage heaters to avoid potential for dielectric breakdown (especially acute with graphite)
  - Requires design and build of compatible heat exchange structure
  - Concerns related to carbon diffusion through wall of stainless steel heat pipes
  - Procurement of TZM material expensive and time-consuming
  - Concerns related to thermal expansion if heat pipes with TZM walls and stainless steel wicks are used

9.0 SUMMARY

A variety of fabrication and bonding methods was investigated to manufacture and fill a 37-heat-pipe monolithic core test article. From this effort, three steps in the process, the eFill37, the eWick37, and the eXchanger37, were successfully manufactured and represent major accomplishments in advancing microreactor technology. However, the final step of creating a fully bonded Core37 article with holes for heaters and heat pipes could not be completed and thus the article was ultimately not finished.

After several successful subscale trials that met geometric tolerances, created a strong bond between segments, and sealed every heat pipe hole, brazing was selected to bond the full-scale Core37 assembly. Although this process maintained tolerances and created a bond in the full-scale test, it did not successfully seal the web between the holes. Problems occurred because of unanticipated radial thermal gradients produced in the braze furnace between the relatively hotter material outside (that sealed) and the relatively cooler web (that did not). Thermal gradients in the full-scale Core37 distorted the line-to-line contact between each of its segments by approximately 0.001 in. This distortion moved braze alloy away from the web bond lines. Bond line repair was attempted with the internal OTW but was abandoned because of time constraints and the partial success rate.

Five alternative block methods have been presented as substitutes for the unsealed Core37. Table 9 summarizes the work completed in this project and is broken down by main component and major tasks for each component.

Table 9. Work Completed Throughout This Project by Component and Major Task.

Component	Percent Completed
eFill37	**99%**
Design of all components	100%
Fabrication of custom parts	100%
Design of mock block for testing	100%
Fabrication of mock block for testing	100%
Assembly of lower chamber stages	100%
Assembly of sodium charge subassembly	100%
Assembly of plug subassembly	100%
Assembly of laser weld assembly	100%
Test of sodium charge subassembly	90%
Test of plug loader subassembly	100%
Test of laser subassembly	100%
eWick37	**100%**
Design	100%
Fabrication	100%
Quality test	100%
eXchanger37	**100%**
Design	100%
Stress analysis	100%
Thermal analysis	100%

Component	Percent Completed
CFD analysis	100%
Fabrication	100%
Core37	**96%**
Design	100%
Stress analysis	100%
Thermal analysis	100%
Manufacturing processes trials	100%
Bonding trials	100%
Segment fabrication	100%
Segment inspection	100%
Full assembly bond	100%
Full assembly seal	60%
Average Completion	**99%**

The following is from a memorandum by Hyman Rickover in June 1953 that summarizes a distinction in nuclear reactor designs and describes the challenges faced in building these assemblies.

> *Important decisions about the future development of atomic power must frequently be made by people who do not necessarily have an intimate knowledge of the technical aspects of reactors. These people are, nonetheless, interested in what a reactor plant will do, how much it will cost, how long it will take to build and how long and how well it will operate. When they attempt to learn these things, they become aware of confusion existing in the reactor business. There appears to be unresolved conflict on almost every issue that arises.*
>
> *I believe that this confusion stems from a failure to distinguish between the academic and the practical. These apparent conflicts can usually be explained only when the various aspects of the issue are resolved into their academic and practical components. To aid in this resolution, it is possible to define in a general way those characteristics which distinguish the one from the other.*
>
> *An academic reactor or reactor plant almost always has the following basic characteristics: (1) It is simple. (2) It is small. (3) It is cheap. (4) It is light. (5) It can be built very quickly. (6) It is very flexible in purpose ("omnibus reactor"). (7) Very little development is required. It will use mostly "off-the-shelf" components. (8) The reactor is in the study phase. It is not being built now.*
>
> *On the other hand, a practical reactor plant can be distinguished by the following characteristics: (1) It is being built now. (2) It is behind schedule. (3) It is requiring an immense amount of development on apparently trivial items. Corrosion, in particular, is a problem. (4) It is very expensive. (5) It takes a long time to build because of the engineering development problems. (6) It is large. (7) It is heavy. (8) It is complicated.*

The tools of the academic-reactor designer are a piece of paper and a pencil with an eraser. If a mistake is made, it can always be erased and changed. If the practical-reactor designer errs, he wears the mistake around his neck; it cannot be erased. Everyone can see it.

The academic-reactor designer is a dilettante. He has not had to assume any real responsibility in connection with his projects. He is free to luxuriate in elegant ideas, the practical shortcomings of which can be relegated to the category of "mere technical details." The practical- reactor designer must live with these same technical details. Although recalcitrant and awkward, they must be solved and cannot be put off until tomorrow. Their solutions require manpower, time and money.

Unfortunately for those who must make far-reaching decisions without the benefit of an intimate knowledge of reactor technology and unfortunately for the interested public, it is much easier to get the academic side of an issue than the practical side. For a large part those involved with the academic reactors have more inclination and time to present their ideas in reports and orally to those who will listen. Since they are innocently unaware of the real but hidden difficulties of their plans, they speak with great facility and confidence. Those involved with practical reactors, humbled by their experiences, speak less and worry more.

Yet it is incumbent on those in high places to make wise decisions, and it is reasonable and important that the public be correctly informed. It is consequently incumbent on all of us to state the facts as forth-rightly as possible. Although it is probably impossible to have reactor ideas labelled as "practical" or "academic" by the authors, it is worthwhile for both the authors and the audience to bear in mind this distinction and to be guided thereby.

Yours faithfully
H. G. Rickover
Naval Reactors Branch
Division of Reactor Development
U. S. Atomic Energy Commission

10.0 REFERENCES

1. L.M. Gaspar, D.A. Giordano, N.A. Greenfield, S.J. Kim, F.A. Kubic, M.R. Middlemas, A.J. Pizzarro, W.J. Saeger, K.M. Sweetland, and R.S. Reid, *eBlock37 Microreactor Electrical Demonstration Unit*, Los Alamos National Laboratory document LA-UR-21-22647 (January 26, 2022).

2. H.R. Trellue, J. O'Brien, J.S. Carpenter, R.S. Reid, D. Guillen, and P. Sabharwall, *Microreactor Demonstration and Testing Progress in FY19*, Los Alamos National Laboratory document LA-UR-19-28768 (September 23, 2019).

3. P. J. Linstrom and W.G. Mallard, Eds., “NIST Chemistry WebBook, NIST Standard Reference Database Number 69” (available URL: https://webbook.nist.gov/chemistry/) (accessed March 2, 2021).

APPENDIX A: DRAWINGS

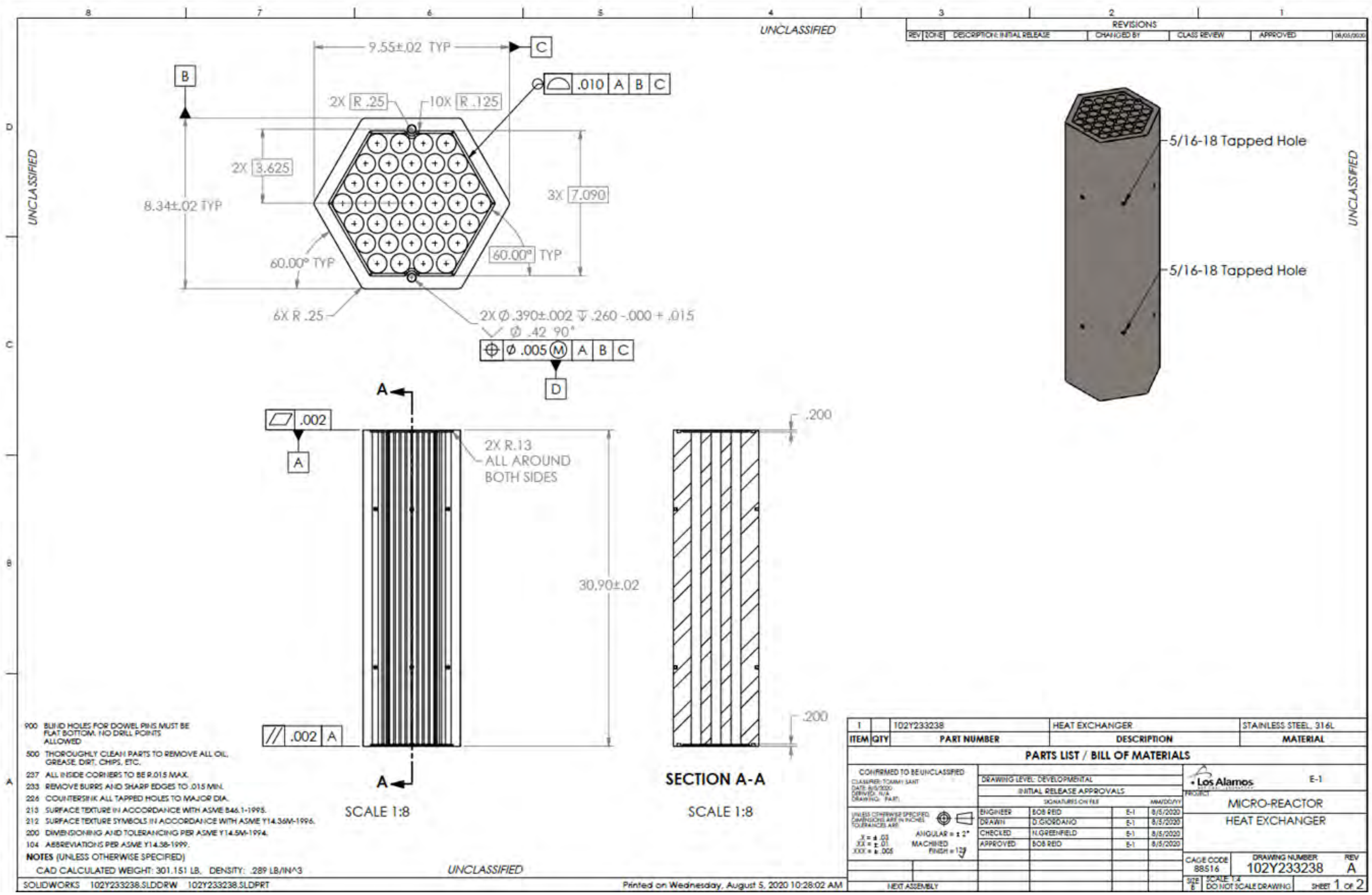

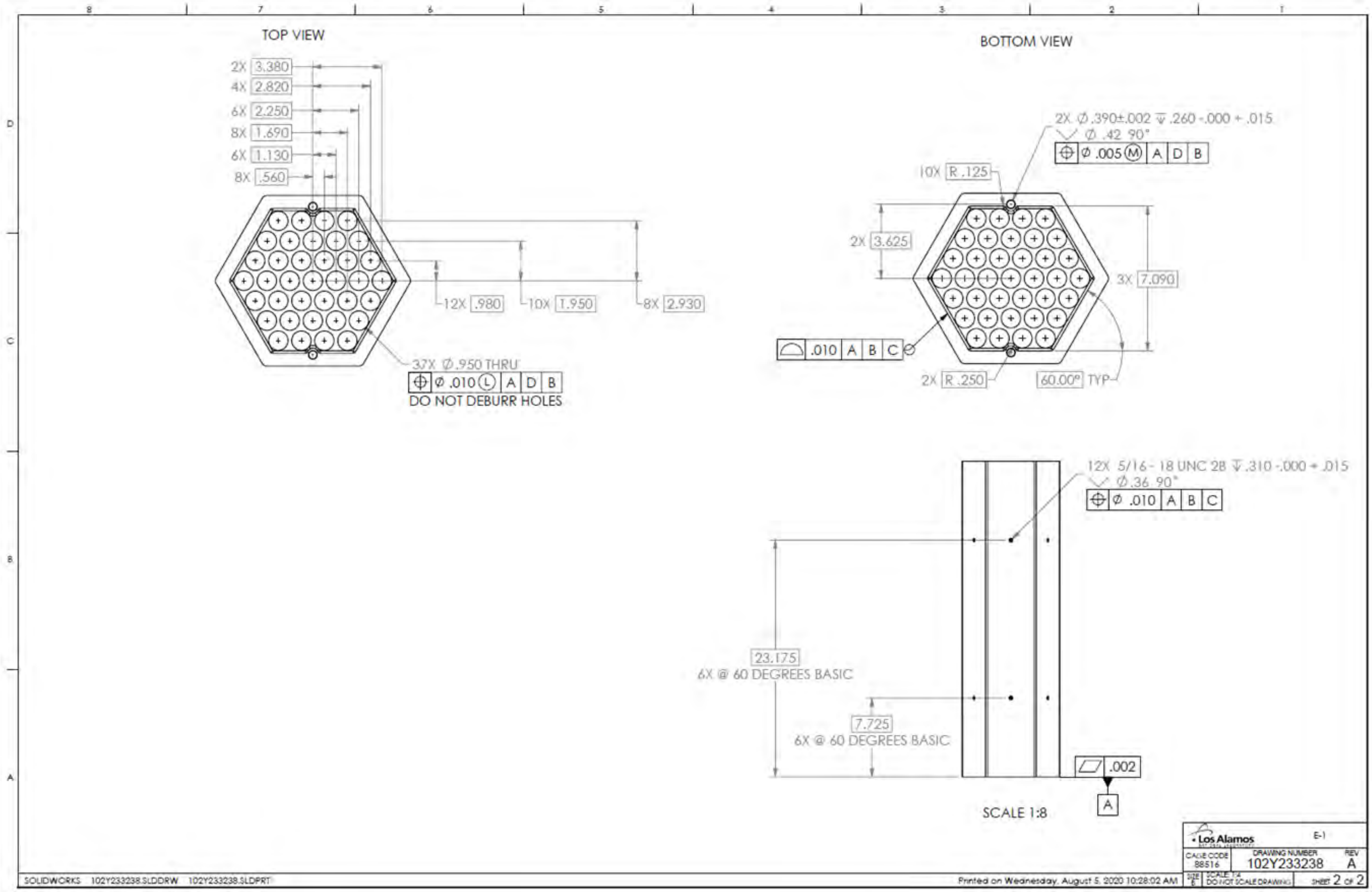
TOP VIEW
2X 3.380
4X 2.820
6X 2.250
8X 1.690
6X 1.130
8X .560
12X .980
10X 1.950
8X 2.930
37X Ø.950 THRU
Ø .010 Ⓛ A D B
DO NOT DEBURR HOLES
BOTTOM VIEW
2X Ø.390±.002 ↧ .260 -.000 +.015
⌵ Ø .42 90°
Ø .005 Ⓜ A D B
10X R .125
2X 3.625
3X 7.090
.010 A B C
2X R .250
60.00° TYP
12X 5/16 - 18 UNC 2B ↧ .310 -.000 +.015
⌵ Ø.36 90°
Ø .010 A B C
23.175
6X @ 60 DEGREES BASIC
7.725
6X @ 60 DEGREES BASIC
.002
A
SCALE 1:8
Los Alamos
E-1
CAGE CODE
88516
DRAWING NUMBER
102Y233238
REV
A
SHEET 2 OF 2
SOLIDWORKS 102Y233238.SLDDRW 102Y233238.SLDPRT
Printed on Wednesday, August 5, 2020 10:28:02 AM

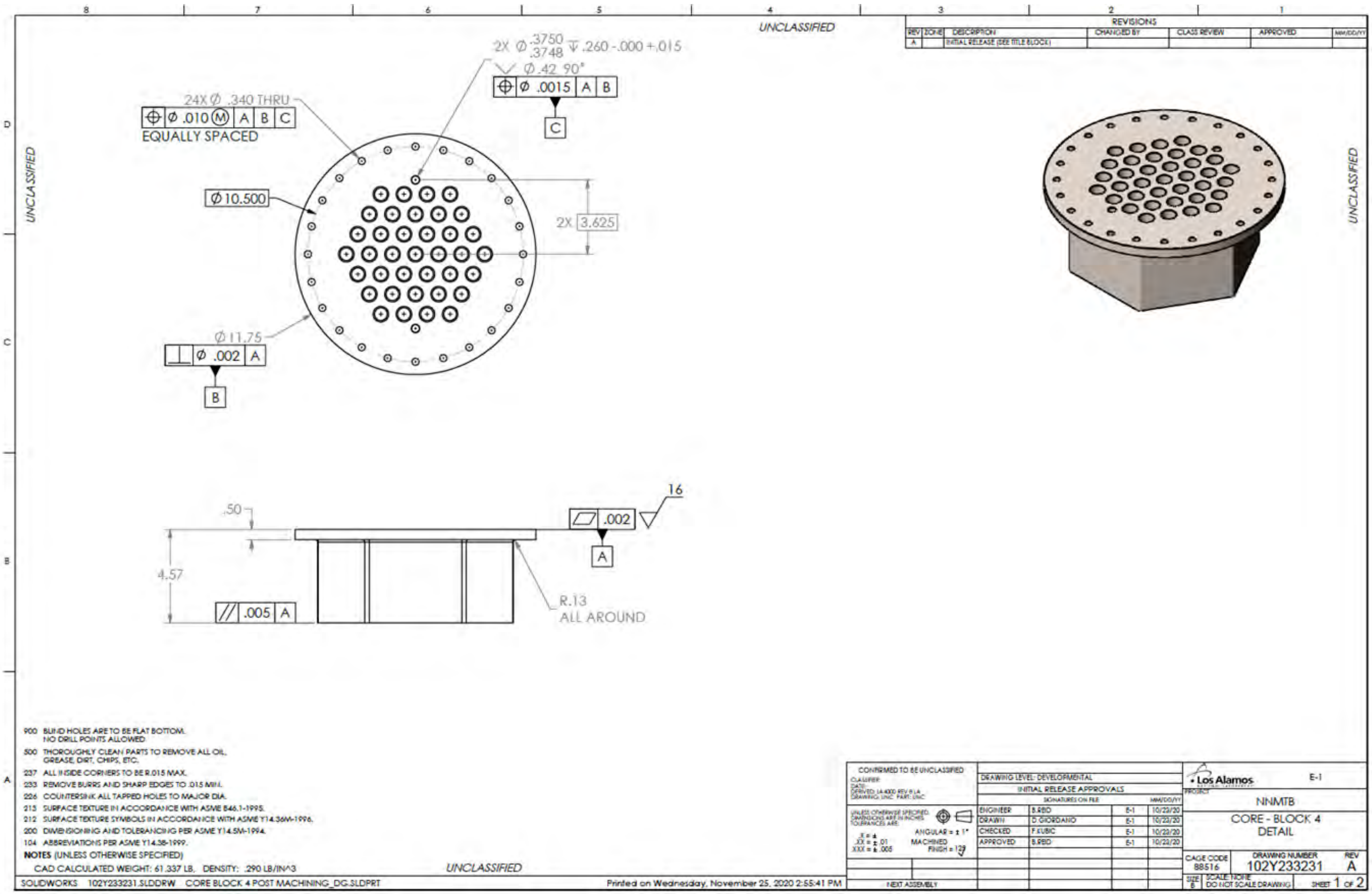
UNCLASSIFIED
REVISIONS
REV ZONE DESCRIPTION CHANGED BY CLASS REVIEW APPROVED MM/DD/YY
A INITIAL RELEASE (SEE TITLE BLOCK)
2X Ø .3750 .3748 ↧ .260 -.000 +.015
Ø .42 90°
⌖ Ø .0015 A B
C
24X Ø .340 THRU
⌖ Ø .010 Ⓜ A B C
EQUALLY SPACED
Ø 10.500
2X 3.625
Ø 11.75
⊥ Ø .002 A
B
.50
4.57
// .005 A
▱ .002
A
16
R.13
ALL AROUND
900 BLIND HOLES ARE TO BE FLAT BOTTOM. NO DRILL POINTS ALLOWED.
500 THOROUGHLY CLEAN PARTS TO REMOVE ALL OIL, GREASE, DIRT, CHIPS, ETC.
237 ALL INSIDE CORNERS TO BE R.015 MAX.
233 REMOVE BURRS AND SHARP EDGES TO .015 MIN.
226 COUNTERSINK ALL TAPPED HOLES TO MAJOR DIA.
215 SURFACE TEXTURE IN ACCORDANCE WITH ASME B46.1-1995.
212 SURFACE TEXTURE SYMBOLS IN ACCORDANCE WITH ASME Y14.36M-1996.
200 DIMENSIONING AND TOLERANCING PER ASME Y14.5M-1994.
104 ABBREVIATIONS PER ASME Y14.38-1999.
NOTES (UNLESS OTHERWISE SPECIFIED)
CAD CALCULATED WEIGHT: 61.337 LB. DENSITY: .290 LB/IN^3
UNCLASSIFIED
SOLIDWORKS 102Y233231.SLDDRW CORE BLOCK 4 POST MACHINING_DG.SLDPRT
Printed on Wednesday, November 25, 2020 2:55:41 PM
CONFIRMED TO BE UNCLASSIFIED
DRAWING LEVEL: DEVELOPMENTAL
INITIAL RELEASE APPROVALS
SIGNATURES ON FILE MM/DD/YY
ENGINEER B.REID E-1 10/23/20
DRAWN D.GIORDANO E-1 10/23/20
CHECKED F.KUBIC E-1 10/23/20
APPROVED B.REID E-1 10/23/20
ANGULAR = ± 1°
.XX = ± .01
.XXX = ± .005
MACHINED FINISH = 125
NEXT ASSEMBLY
Los Alamos
E-1
PROJECT
NNMTB
CORE - BLOCK 4
DETAIL
CAGE CODE 88516
DRAWING NUMBER 102Y233231
REV A
SIZE B
SCALE: NONE
DO NOT SCALE DRAWING
SHEET 1 OF 2

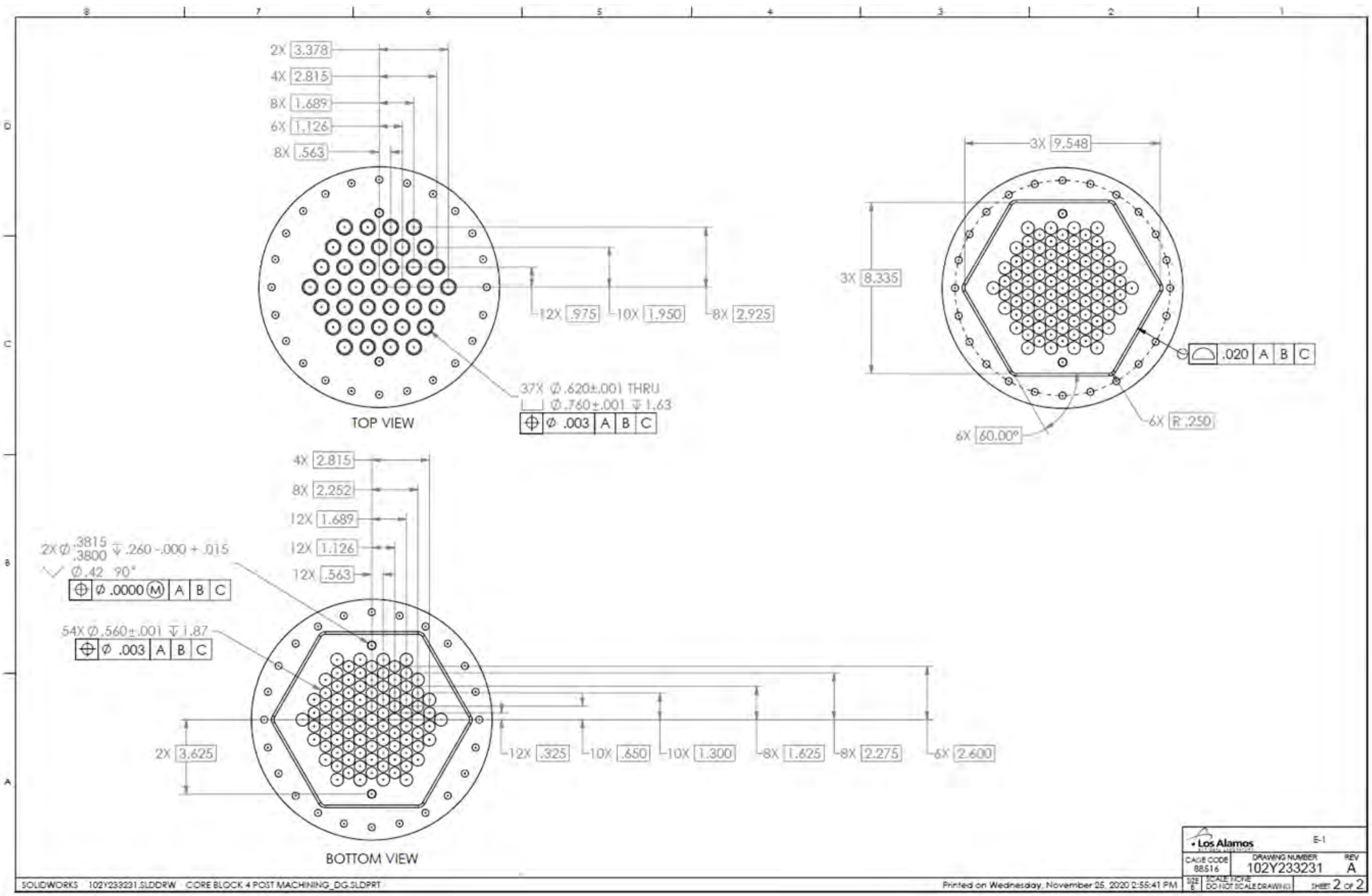

2X 3.378
4X 2.815
8X 1.689
6X 1.126
8X .563
12X .975
10X 1.950
8X 2.925
37X Ø .620±.001 THRU
Ø .760±.001 ↧ 1.63
⌖ Ø .003 A B C
TOP VIEW
3X 9.548
3X 8.335
.020 A B C
6X R .250
6X 60.00°
4X 2.815
8X 2.252
12X 1.689
12X 1.126
12X .563
2X Ø .3815 .3800 ↧ .260 -.000 +.015
⌵ Ø .42 90°
⌖ Ø .0000 Ⓜ A B C
54X Ø .560±.001 ↧ 1.87
⌖ Ø .003 A B C
2X 3.625
12X .325
10X .650
10X 1.300
8X 1.625
8X 2.275
6X 2.600
BOTTOM VIEW
Los Alamos
E-1
CAGE CODE 88516
DRAWING NUMBER 102Y233231
REV A
SCALE: NONE DO NOT SCALE DRAWING
SHEET 2 OF 2
SOLIDWORKS 102Y233231.SLDDRW CORE BLOCK 4 POST MACHINING_DG.SLDPRT
Printed on Wednesday, November 25, 2020 2:55:41 PM

UNCLASSIFIED

REV	ZONE	DESCRIPTION	CHANGED BY	CLASS REVIEW	APPROVED	MM/DD/YY

REVISIONS

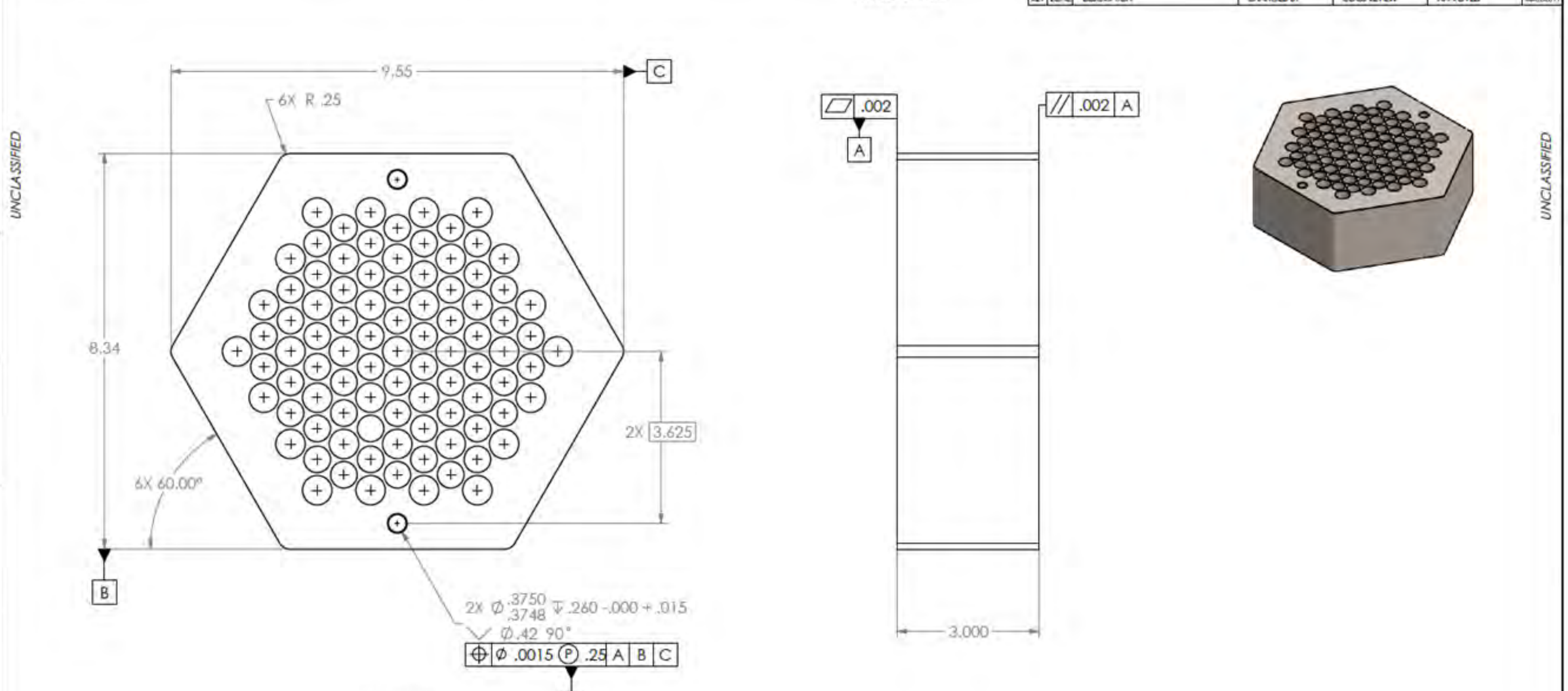

TOP VIEW

[illegible] ENGRAVE PART NUMBER AND REVISION LEVEL TO FIT APPROXIMATELY WHERE SHOWN. CHARACTERS .160 HIGH MAXIMUM. EXAMPLE: 4Y17612XX REV A

900 BLIND HOLES FOR DOWEL PINS MUST BE FLAT BOTTOM. NO DRILL POINTS ALLOWED

500 THOROUGHLY CLEAN PARTS TO REMOVE ALL OIL, GREASE, DIRT, CHIPS, ETC.

237 ALL INSIDE CORNERS TO BE R.015 MAX.

233 REMOVE BURRS AND SHARP EDGES TO .015 MIN.

226 COUNTERSINK ALL TAPPED HOLES TO MAJOR DIA.

213 SURFACE TEXTURE IN ACCORDANCE WITH ASME B46.1-1995.

212 SURFACE TEXTURE SYMBOLS IN ACCORDANCE WITH ASME Y14.36M-1996.

200 DIMENSIONING AND TOLERANCING PER ASME Y14.5M-1994.

104 ABBREVIATIONS PER ASME Y14.38-1999.

NOTES (UNLESS OTHERWISE SPECIFIED)

CAD CALCULATED WEIGHT: 31.008 LB, DENSITY: .290 LB/IN^3

UNCLASSIFIED

ITEM	QTY	PART NUMBER	DESCRIPTION	MATERIAL
1	1	102Y233230		STAINLESS STEEL, 316L

PARTS LIST / BILL OF MATERIALS

CONFIRMED TO BE UNCLASSIFIED
CLASSIFIER:
DATE:
DERIVED:
DRAWING: PART

UNLESS OTHERWISE SPECIFIED, DIMENSIONS ARE IN INCHES. TOLERANCES ARE:
.X = ± .030
.XX = ± .010
.XXX = ± .005
ANGULAR = ± 1°
MACHINED FINISH = 63

DRAWING LEVEL: PRODUCT

INITIAL RELEASE APPROVALS

	SIGNATURES ON FILE		MM/DD/YY
ENGINEER	BOB REID	E-1	03/09/20
DRAWN	DAVID GIORDANO	E-1	03/09/20
CHECK	M. MCKAMEY	SIGMA-2	03/09/20
APPROVED	BOB REID	E-1	03/09/20

NEXT ASSEMBLY

Los Alamos E-1

PROJECT: NNMTB

CORE - BLOCK 3 DETAIL

CAGE CODE	DRAWING NUMBER	REV
88516	102Y233230	A

SIZE B SCALE 1:2 DO NOT SCALE DRAWING SHEET 1 OF 3

SOLIDWORKS 102Y233230.SLDDRW 102Y233230.SLDPRT

Printed on Wednesday, July 1, 2020 11:26:27 AM

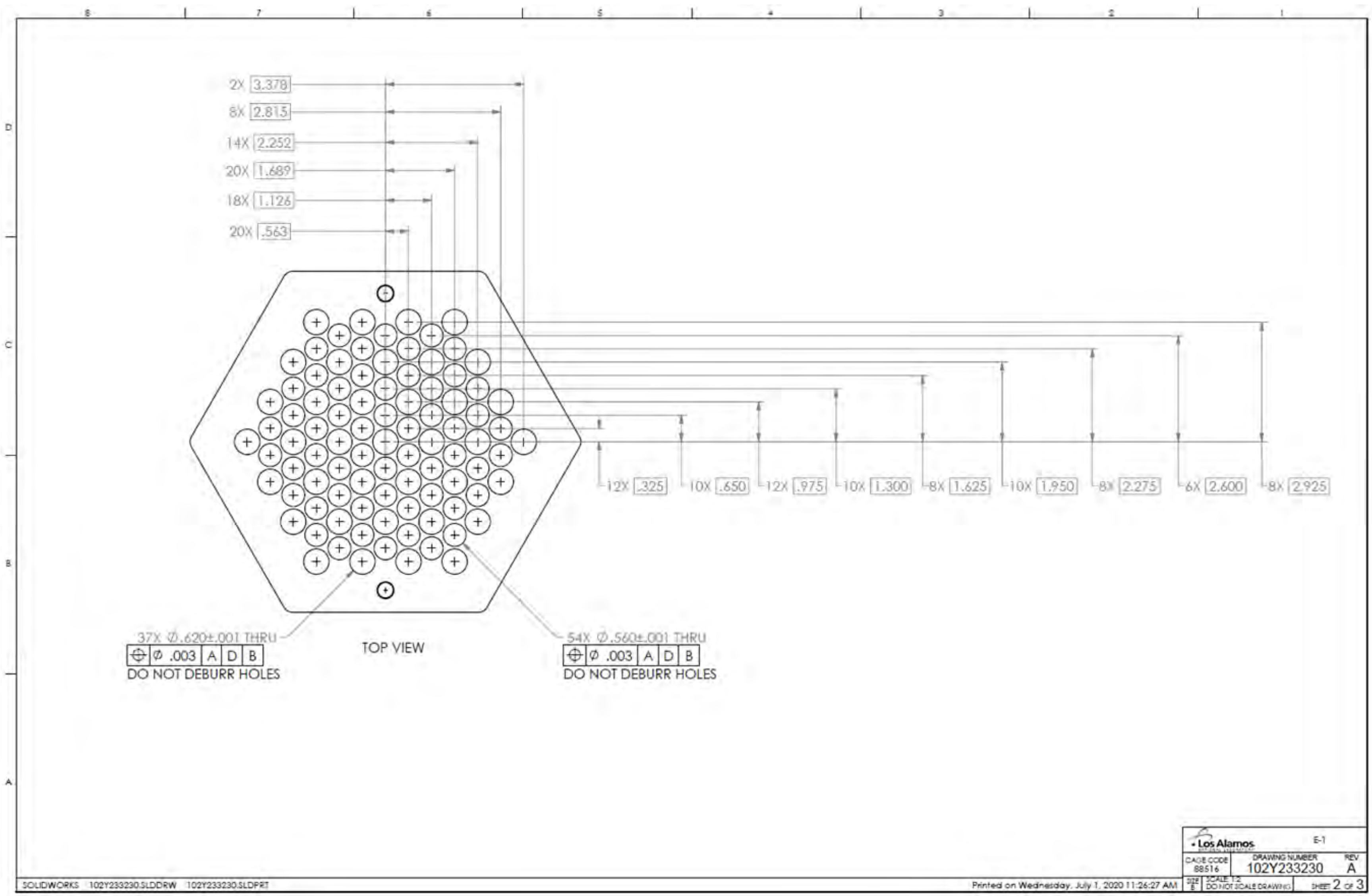
2X 3.378
8X 2.815
14X 2.252
20X 1.689
18X 1.126
20X .563
12X .325
10X .650
12X .975
10X 1.300
8X 1.625
10X 1.950
8X 2.275
6X 2.600
8X 2.925
37X Ø.620±.001 THRU
Ø .003 A D B
DO NOT DEBURR HOLES
TOP VIEW
54X Ø.560±.001 THRU
Ø .003 A D B
DO NOT DEBURR HOLES
Los Alamos
E-1
CAGE CODE 88516
DRAWING NUMBER 102Y233230
REV A
SHEET 2 OF 3
SOLIDWORKS 102Y233230.SLDDRW 102Y233230.SLDPRT
Printed on Wednesday, July 1, 2020 11:26:27 AM

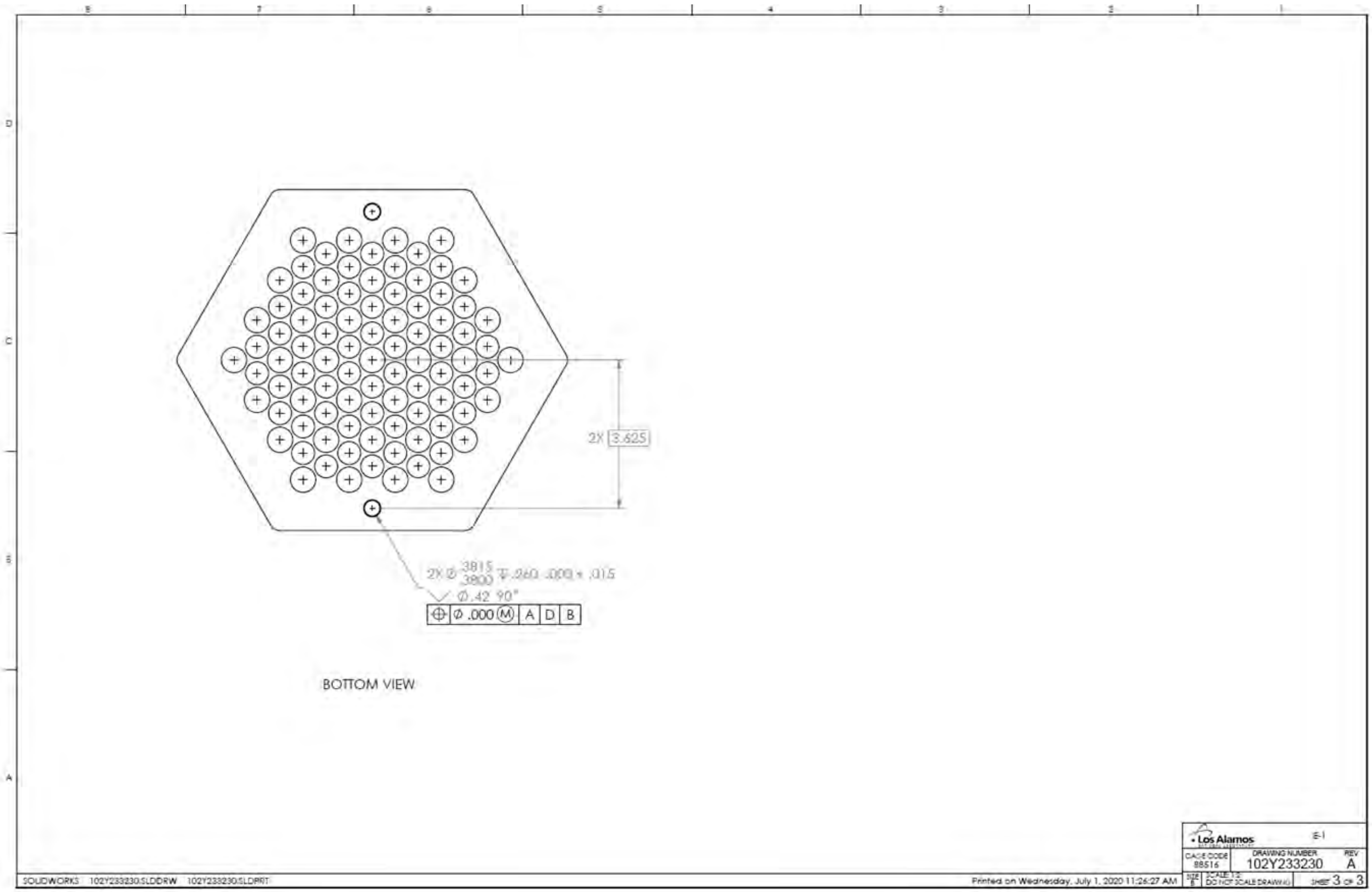

2X 3.625
2X Ø .3815 .3800 ↧ .260 .000 + .015
Ø .42 90°
⌖ | Ø .000 Ⓜ | A | D | B
BOTTOM VIEW
Los Alamos
E-1
CAGE CODE 88516
DRAWING NUMBER 102Y233230
REV A
SCALE 1:2
DO NOT SCALE DRAWING
SHEET 3 OF 3
SOLIDWORKS 102Y233230.SLDDRW 102Y233230.SLDPRT
Printed on Wednesday, July 1, 2020 11:26:27 AM

APPENDIX B: Core37 SEGMENT INSPECTION

Table B-1. Inspection Report for Flanged Core Segment.

Final Inspection Report

Form-022 Rev. 9/8/2022

Jaguar Precision Machine, LLC

1. Part Number	2. Part Name	Temperature	Relative Humidity	3. Lot Number	4. Revision	Serial No.
102Y233231	CORE - BLOCK 4 DETAIL	68.5 F	39%	NA	A	NA

5. Char No.	6. Reference Location	7. Characteristic Designator	8. Quantity	9. Requirement	9a. UoM	9b. Upper Limit	9c. Lower Limit	10. Results 1	11. Gage No.	12. Non-Conformance Number	15. Notes, Tool Description
Characteristic Accountability								Inspection / Test Results			Other Fields
1	pg.1, Zone B.3		1	.002 FLATNESS	in	0.002	0.000	0.001502	96		CMM
2	pg.1, Zone B.4		1	.005 PARALLELISM	in	0.005	0	0.003532	96		CMM

The uncertainties are beyond the resolution of indicated values except when noted. Uncertainty numbers available upon request. PO # EP80115

13. Prepared By Brendan Mead — 14. Date 9/19/2022

Table B-2. Inspection Report for Core Segments.

Final Inspection Report

Form-022 Rev. 9/8/2022

Jaguar Precision Machine, LLC

1. Part Number	2. Part Name	Temperature	Relative Humidity	3. Lot Number	4. Revision	Serial No.
102Y233230	CORE - BLOCK 3 DETAIL	68.7 F	40%	NA	A	NA

5. Char No.	6. Reference Location	7. Characteristic Designator	8. Quantity	9. Requirement	9a. UoM	9b. Upper Limit	9c. Lower Limit	10. Results 1	2	3	4	5	6	7	8	9	10	11	11. Gage No.	12. Non-Conformance Number	15. Notes, Tool Description
Characteristic Accountability								Inspection / Test Results													Other Fields
1	pg.1, Zone D.2		1	.002 FLATNESS	in	0.002	0.000	0.000572	0.000495	0.000723	0.000606	0.000608	0.00068	0.000625	0.000502	0.000799	0.000555	0.00075	96		CMM
2	pg.1, Zone D.2		1	.002 PARALLELISM	in	0.002	0.000	0.000412	0.001552	0.000237	0.000086	0.000186	0.001724	.001463	0.001589	0.00091	0.000295	0.00043	96		CMM

The uncertainties are beyond the resolution of indicated values except when noted. Uncertainty numbers available upon request. PO # EP80115

13. Prepared By Brendan Mead — 14. Date 9/19/2022

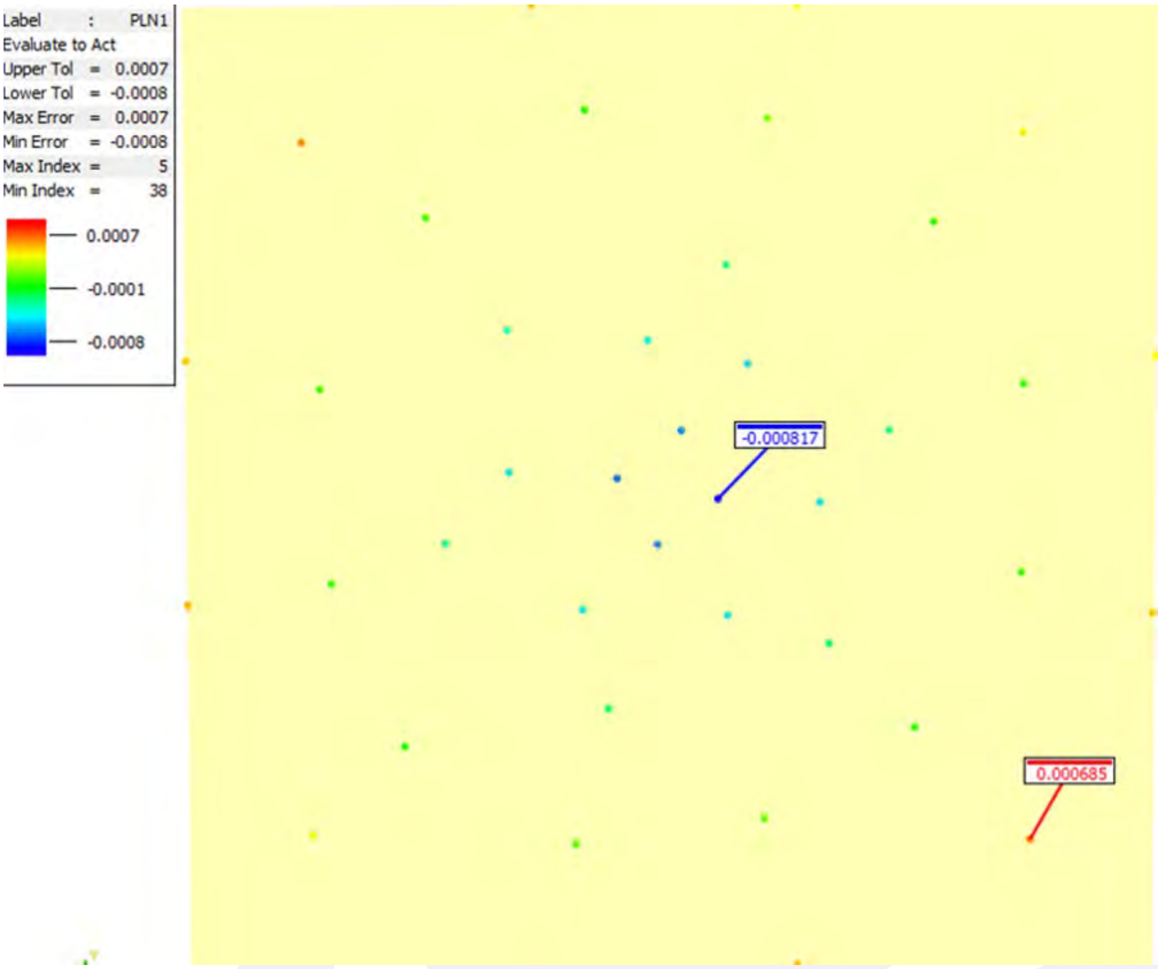

Figure B-1. Flatness heat map for flanged Core37 segment.

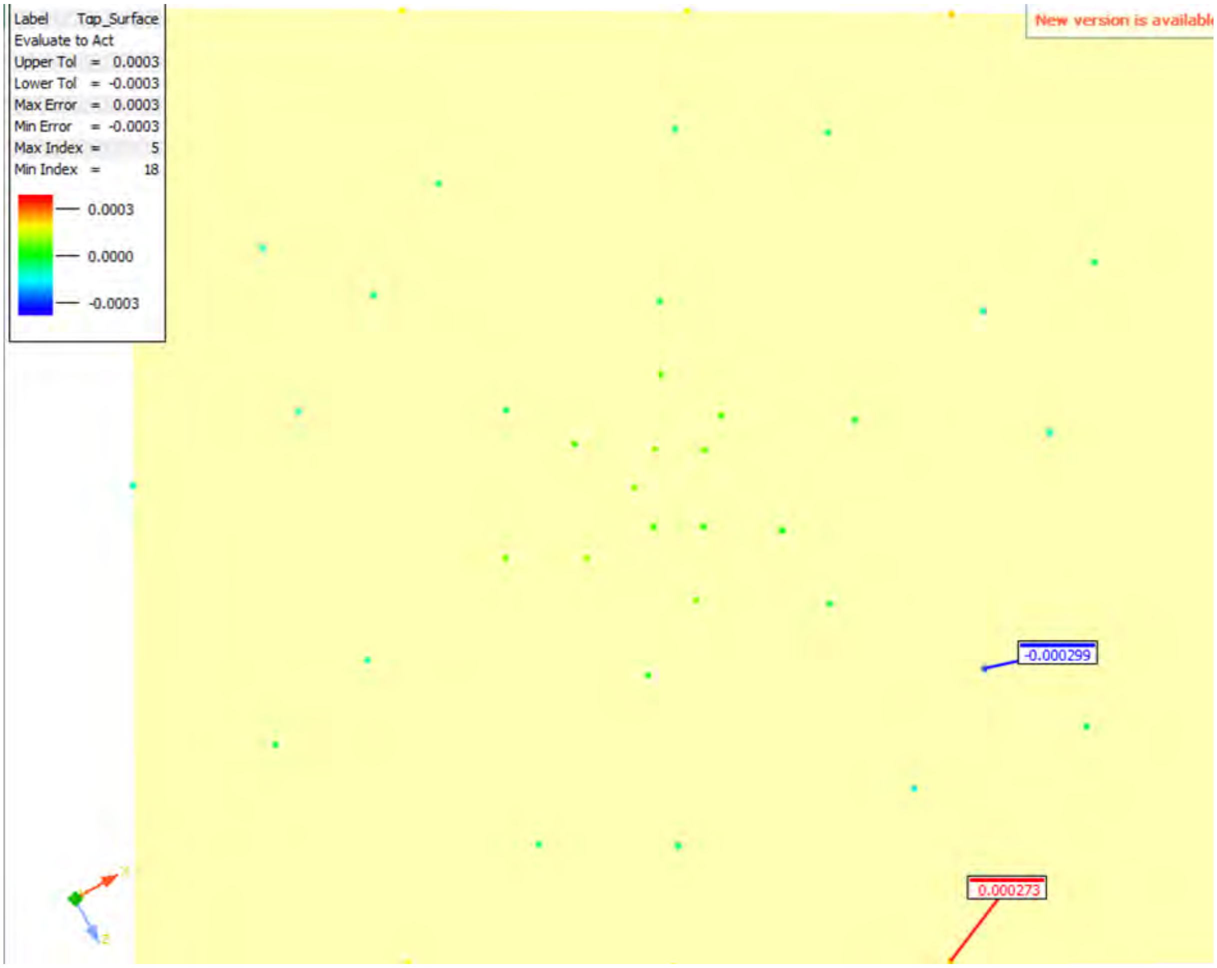

Figure B-2. Flatness heat map for Core37 segment number 1.

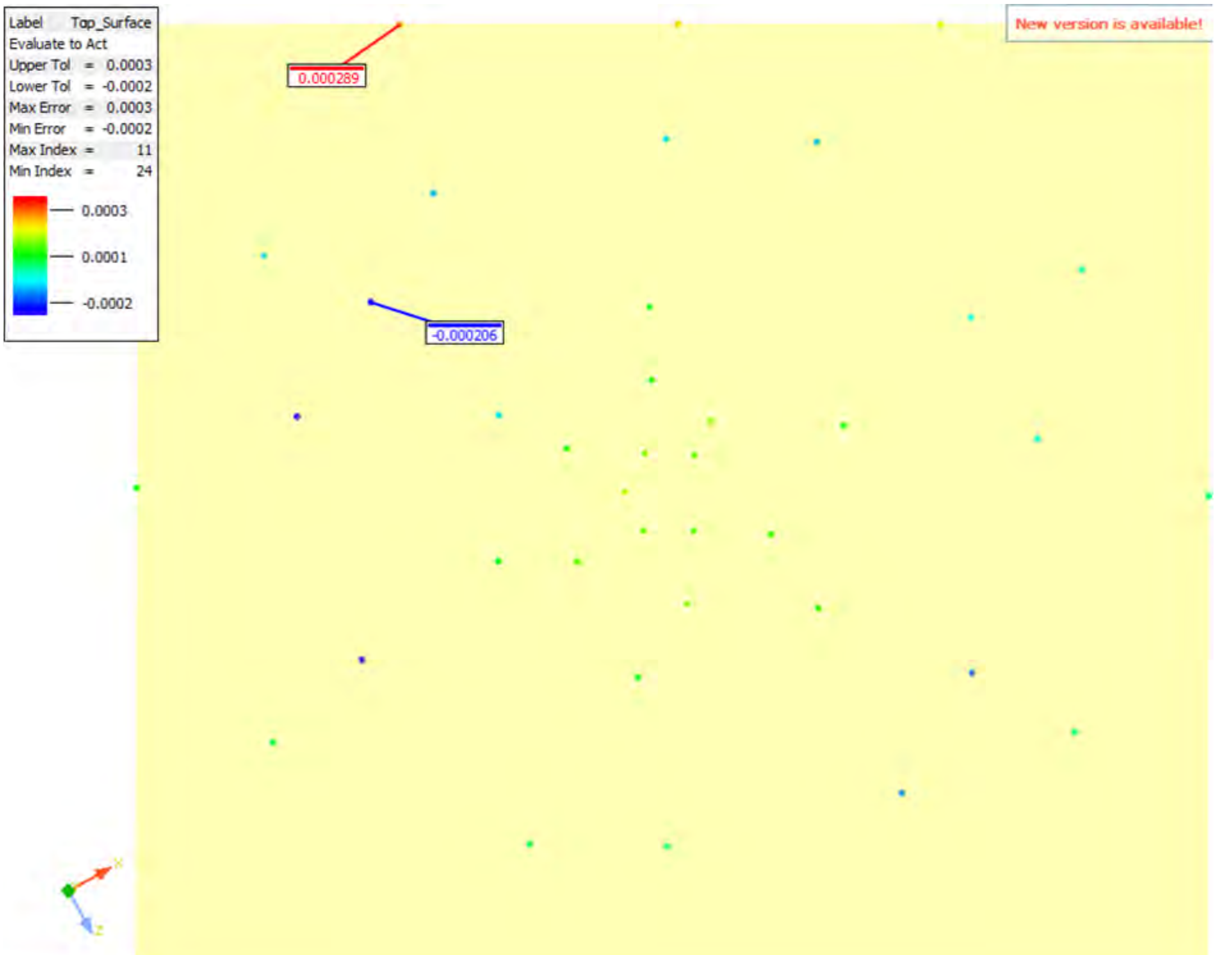

Figure B-3. Flatness heat map for Core37 segment number 2.

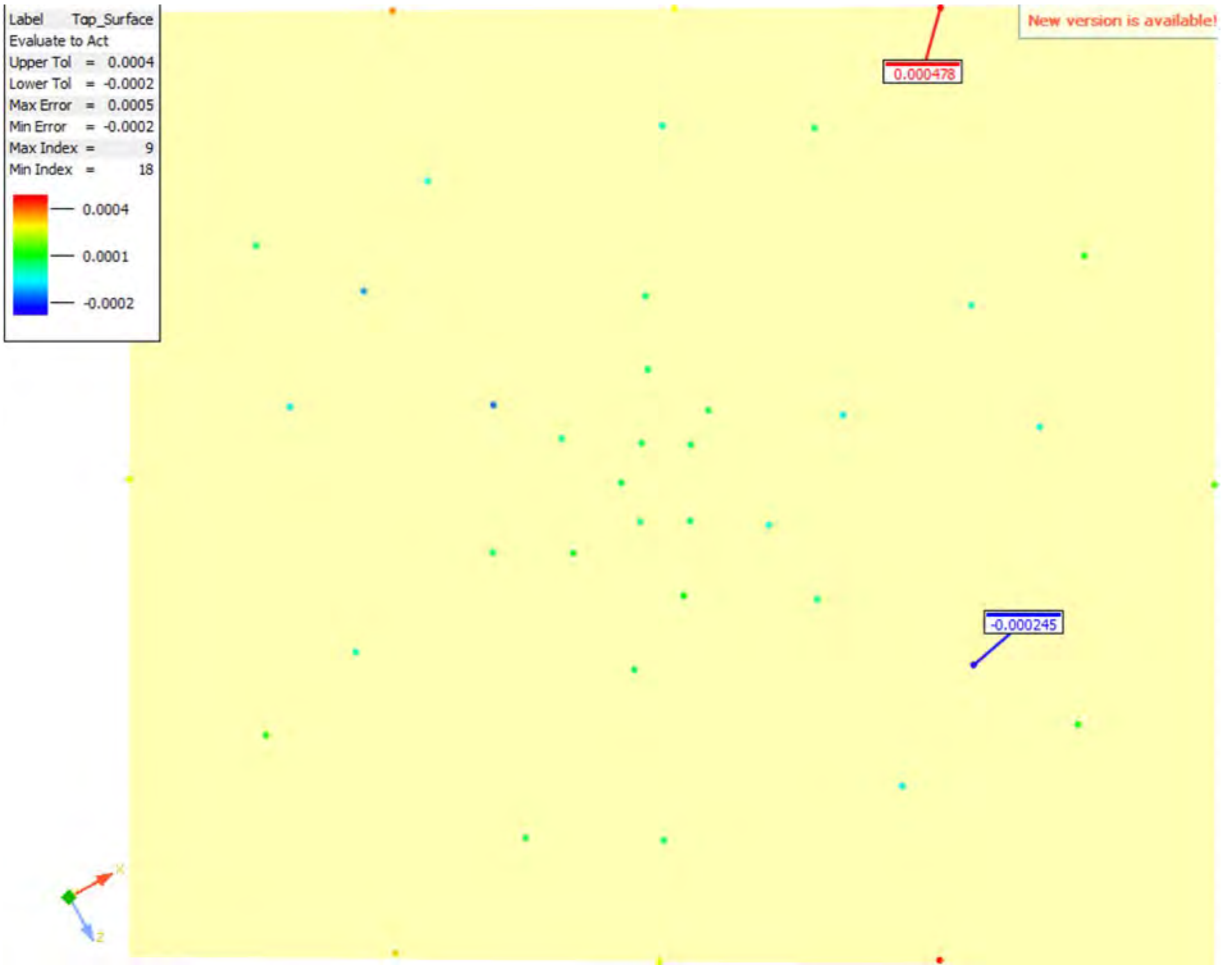

Figure B-4. Flatness heat map for Core37 segment number 3.

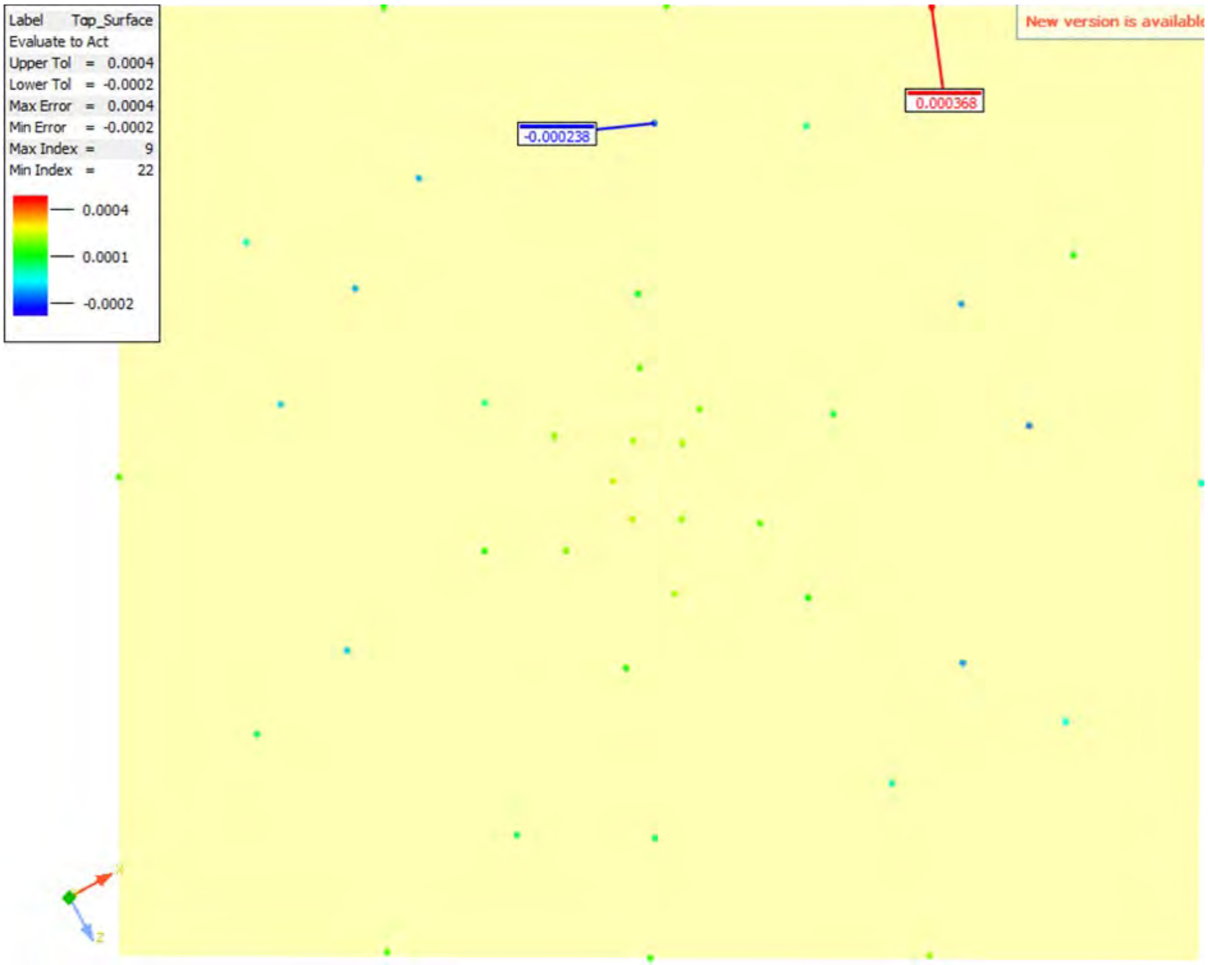

Figure B-5. Flatness heat map for Core37 segment number 4.

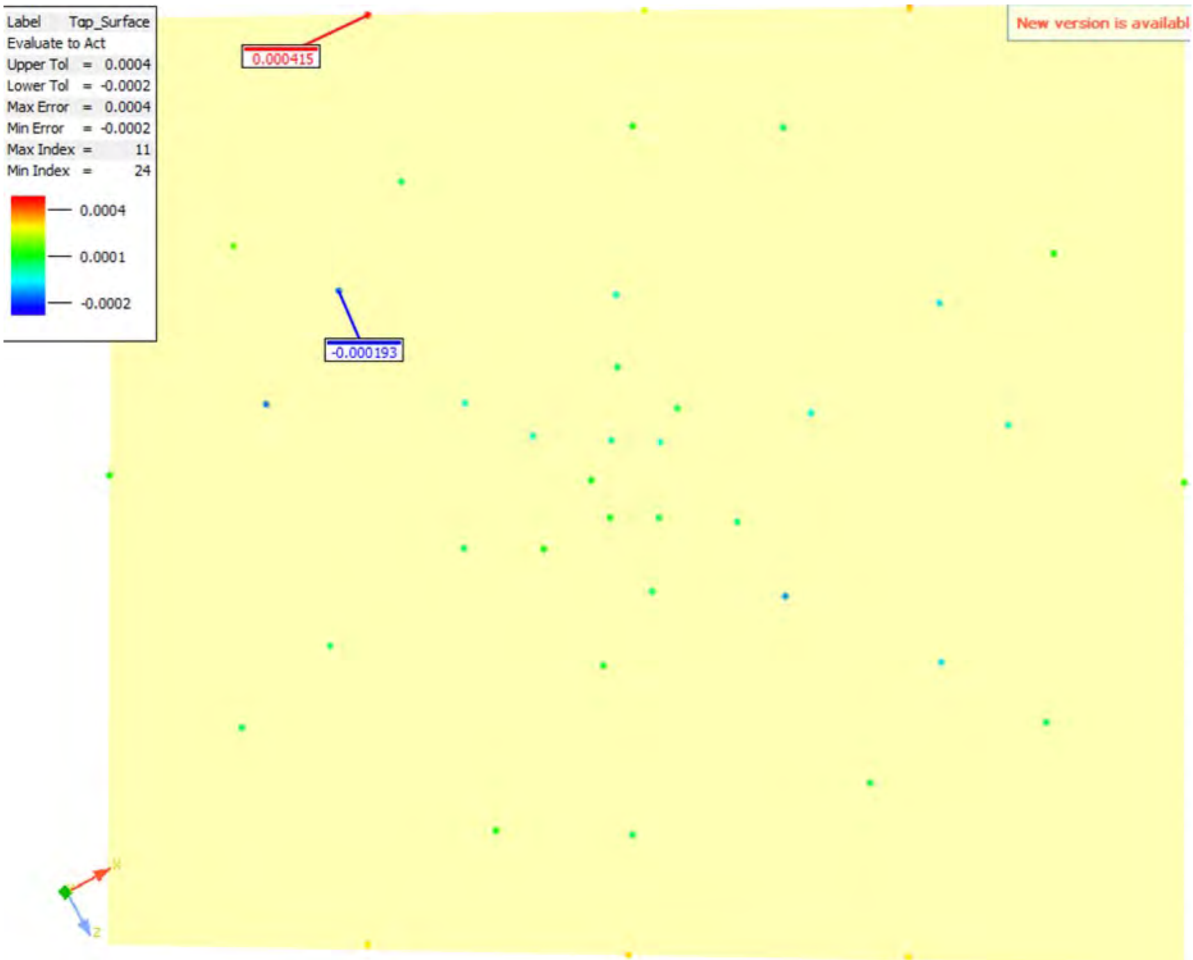

Figure B-6. Flatness heat map for Core37 segment number 5.

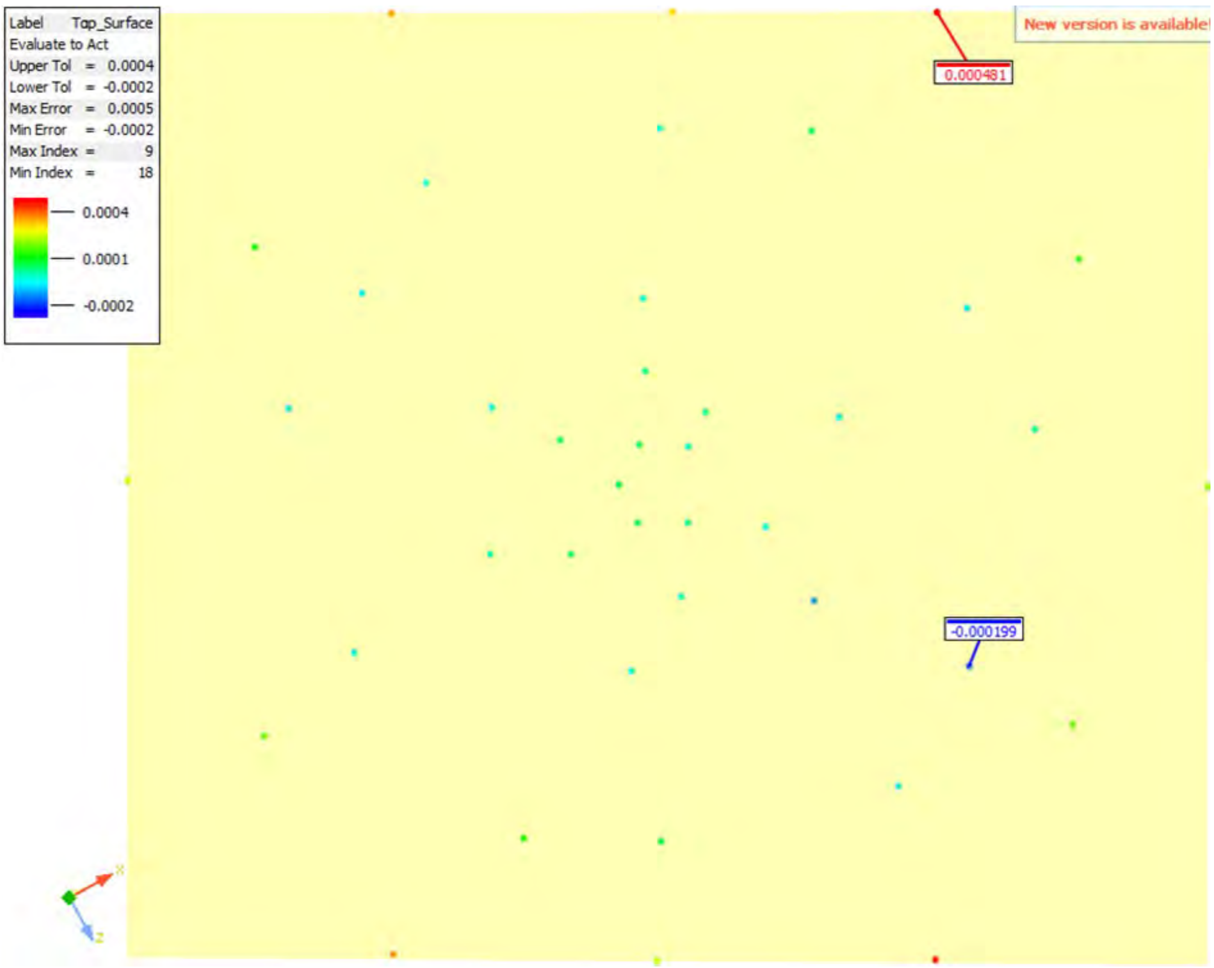

Figure B-7. Flatness heat map for Core37 segment number 6.

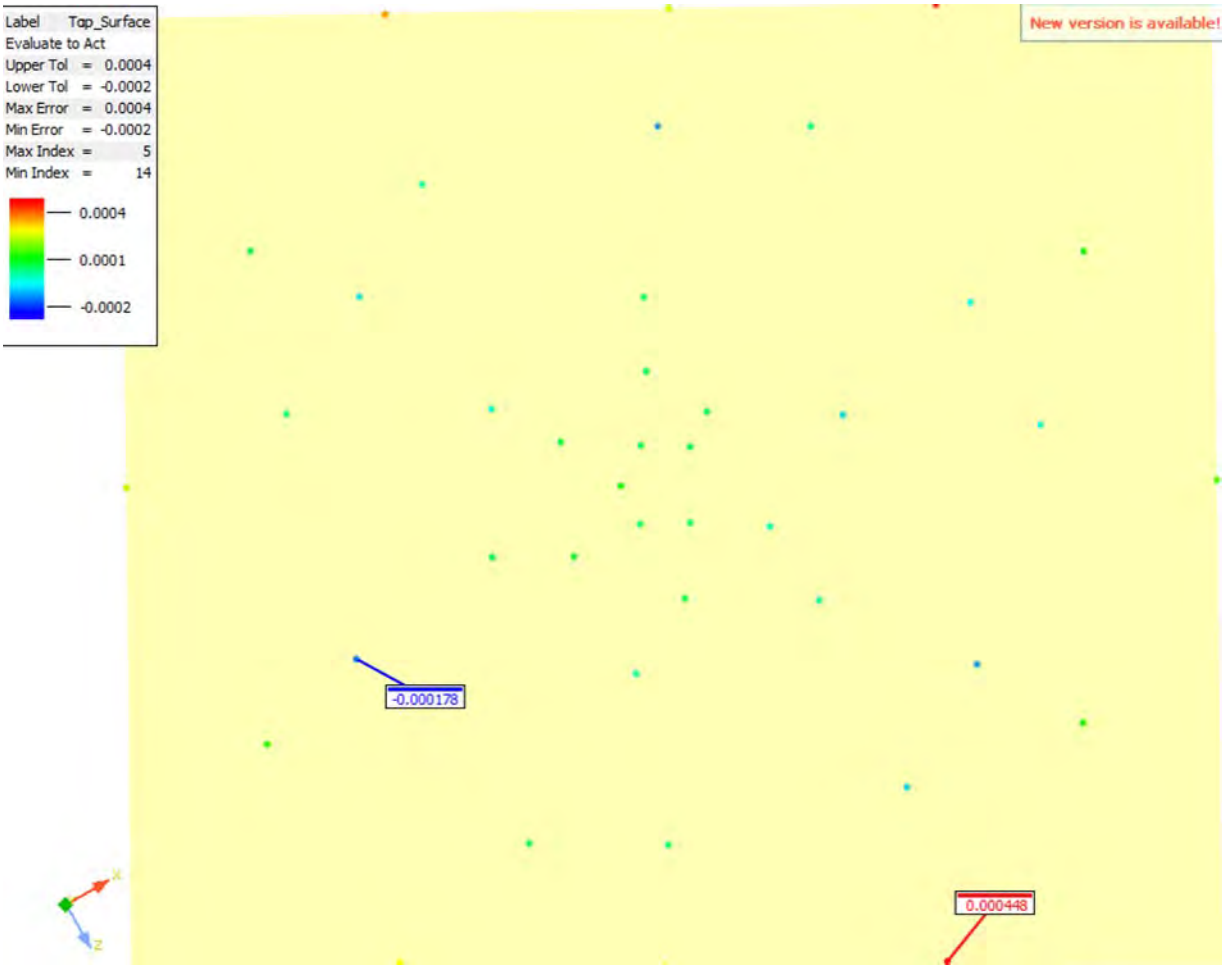

Figure B-8. Flatness heat map for Core37 segment number 7.

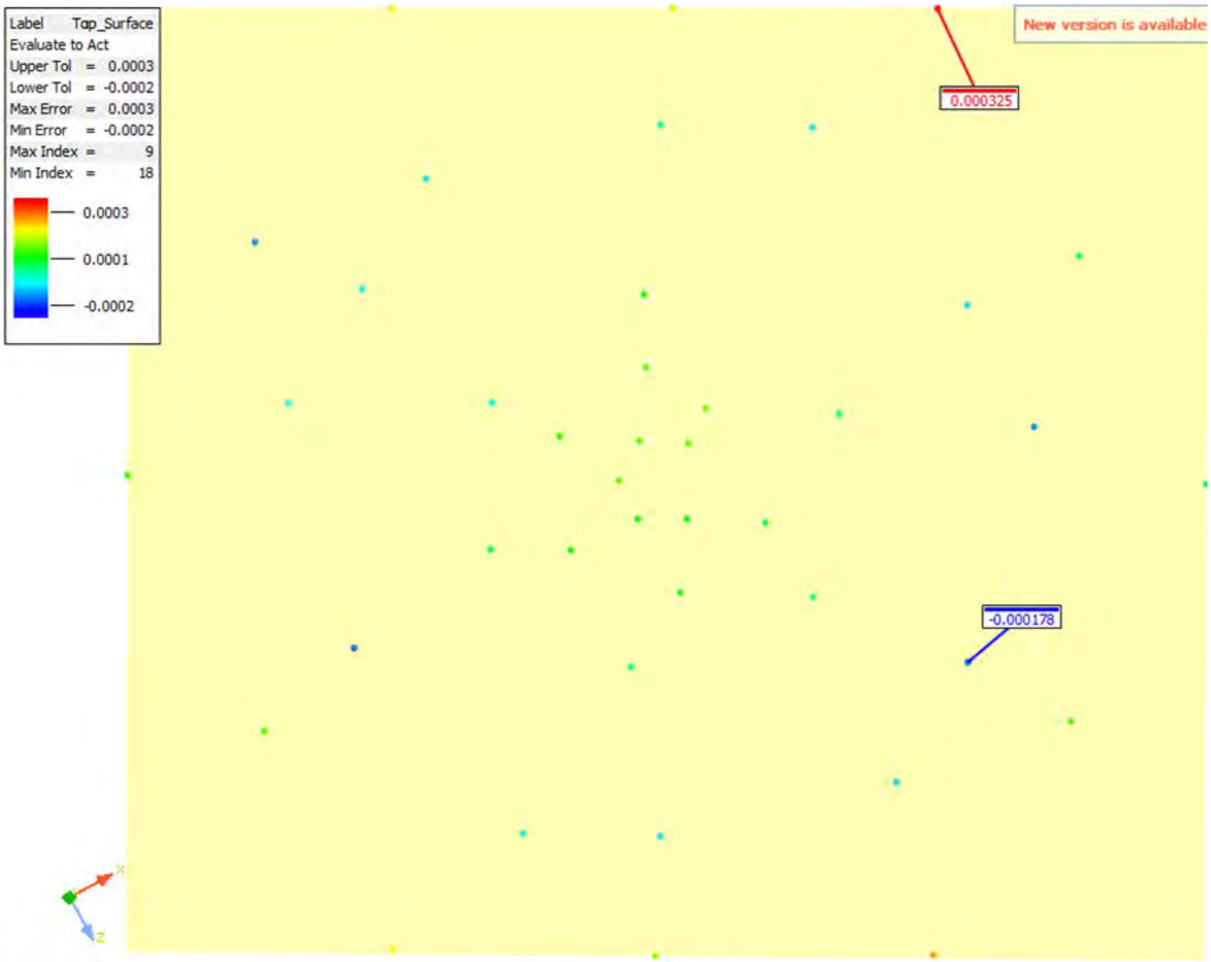

Figure B-9. Flatness heat map for Core37 segment number 8.

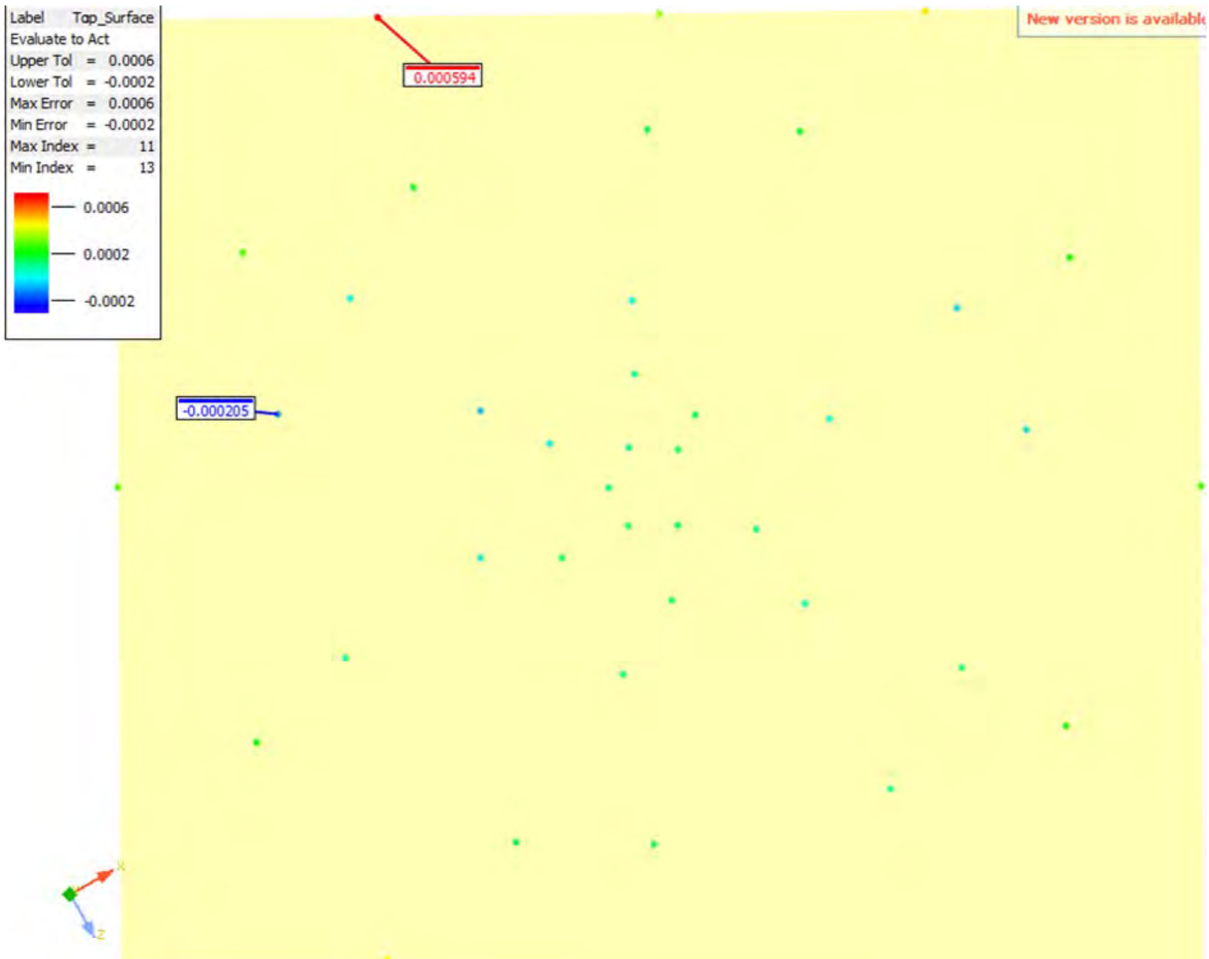

Figure B-10. Flatness heat map for Core37 segment number 9.

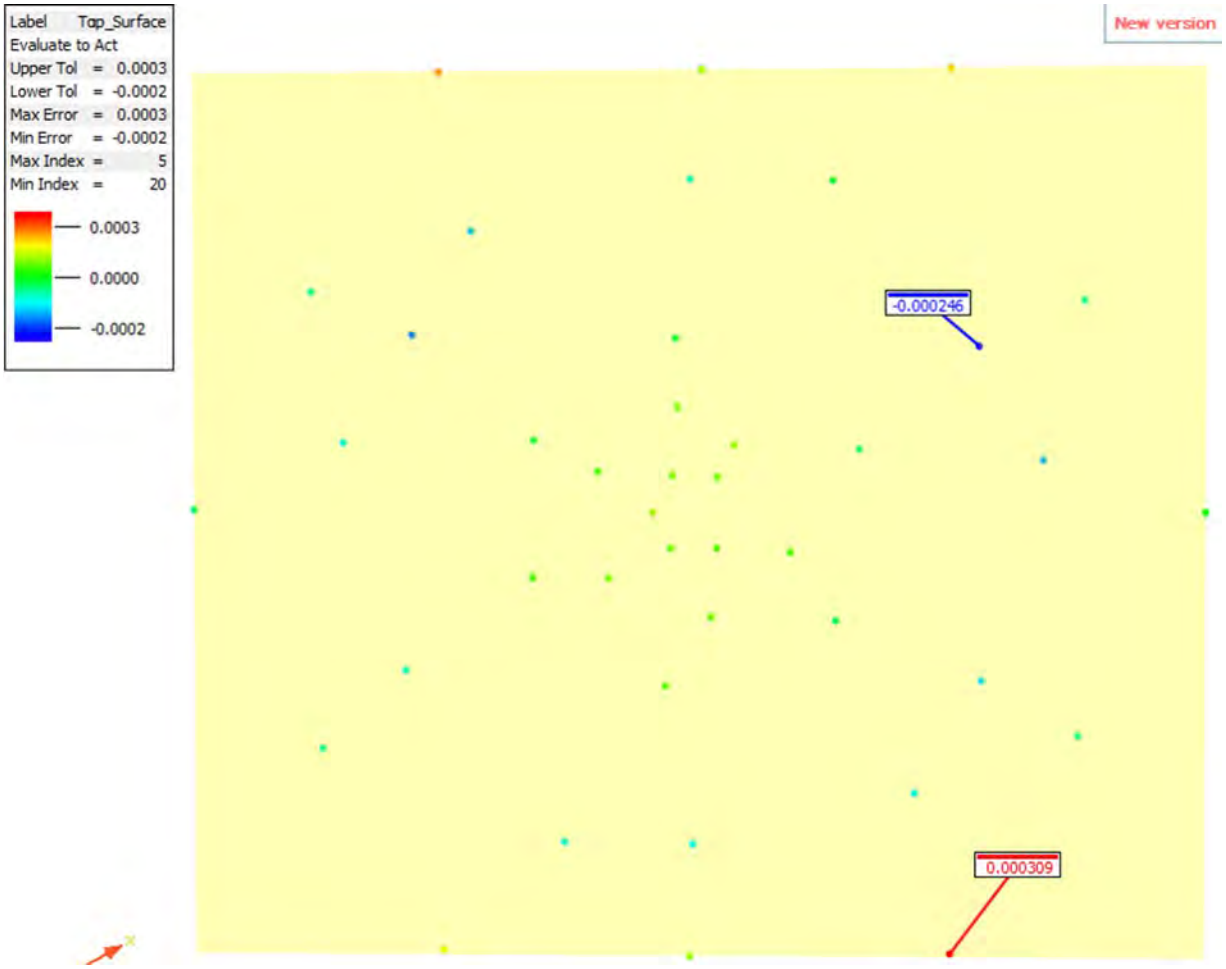

Figure B-11. Flatness heat map for Core37 segment number 10.

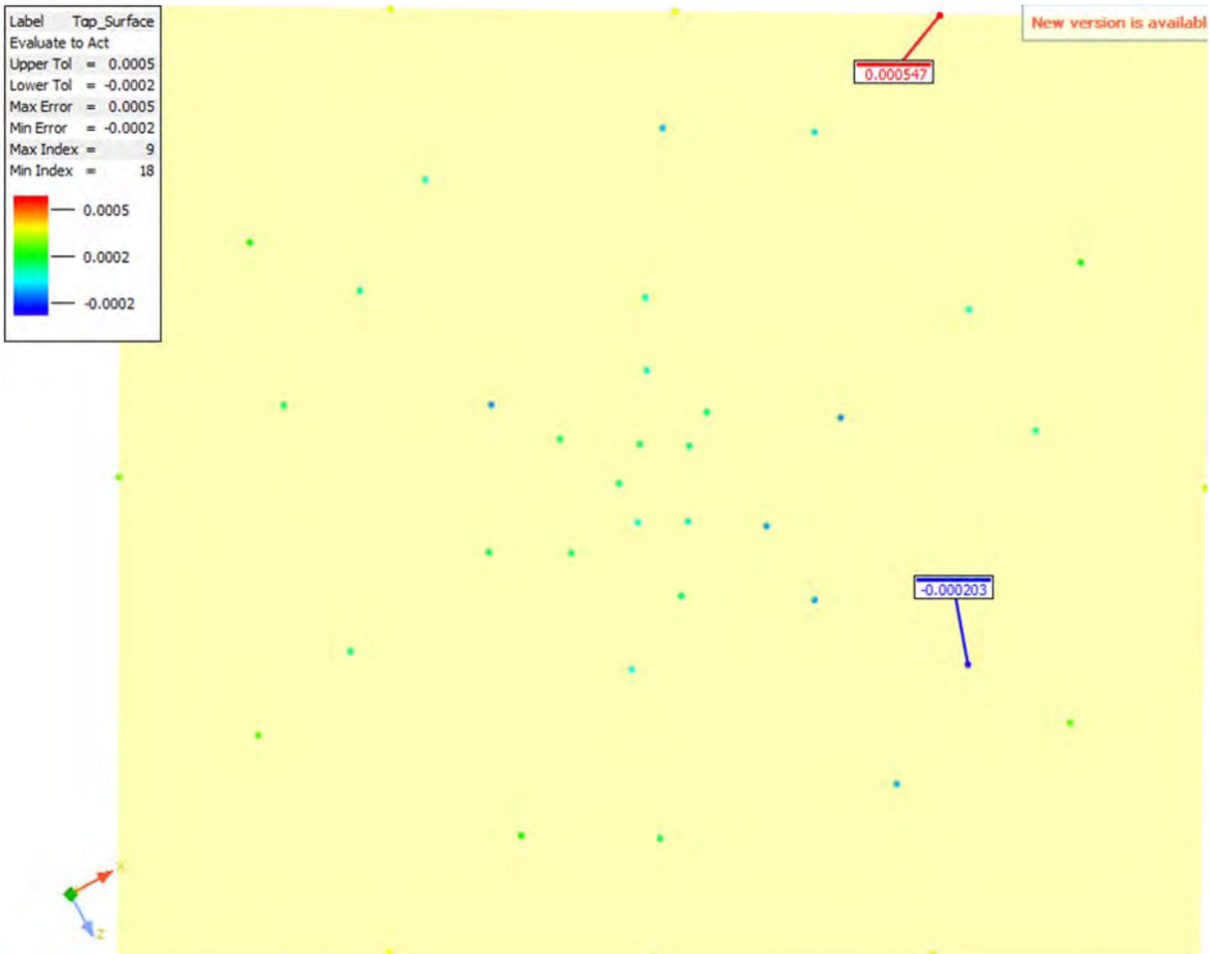

Figure B-12. Flatness heat map for Core37 segment number 11.

APPENDIX C: INITIAL Core37 HELIUM LEAK TEST RESULTS

Table C-1. Initial Core Helium Leak Test Results.

Hole Number	Leak Rate (Torr L/s)	Hole Number	Leak Rate (Torr L/s)
1	7.46E-06	20	4.24E-05
2	1.11E-05	21	4.81E-05
3	1.68E-05	22	6.89E-05
4	3.21E-05	23	3.86E-05
5	1.60E-05	24	2.72E-05
6	5.37E-06	25	1.25E-05
7	4.60E-06	26	3.72E-05
8	4.89E-06	27	4.03E-05
9	7.37E-06	28	3.03E-05
10	9.84E-07	29	4.23E-05
11	1.15E-05	30	1.05E-04
12	6.52E-06	31	8.81E-06
13	4.11E-06	32	7.71E-06
14	1.35E-05	33	1.55E-05
15	7.09E-06	34	2.70E-06
16	2.14E-06	35	4.99E-06
17	4.40E-06	36	1.11E-05
18	1.94E-05	37	1.24E-05
19	4.62E-05		

APPENDIX D: BRAZE REPAIR RESULTS

Table D-1. Braze Repair Results.

Hole/Bond Line	1	2	3	4	5	6	7	8	9	10	11
1	1	1	1	1	1	1	1	1	1	1	x
2	1	1	1	1	x	x	x	1	1	1	x
3	1	x	x	x	1	1	1	1	1	1	1
4	1	1	1	1	x	1	1	1	1	1	1
5	1	1	x	x	x	x	1	1	1	1	1
6	x	x	1	1	x	1	x	1	1	1	x
7	1	x	1	1	1	1	x	1	1	1	1
8	1	1	1	1	1	1	x	1	1	1	x
9	2	L	1	1	1	1	1	1	L	1	x
10	1	L	1	1	1	1	1	1	1	1	1
11	x	1	1	1	1	1	1	x	x	x	x
12	L	L	1	1	1	1	1	1	1	1	x
13	1	1	1	1	1	1	x	x	x	1	x
14	1	1	1	x	x	1	x	x	x	1	x
15	1	x	x	x	x	x	x	1	x	1	x
16	1	1	x	x	1	1	x	1	1	1	x
17	2	L	1	1	1	1	1	1	1	1	x
18	1	1	1	1	x	1	1	1	1	1	x
19	1	1	1	1	x	1	x	1	1	1	1
20	1	1	1	x	x	1	1	x	1	1	1
21	1	1	1	1	1	1	1	x	1	1	1
22	1	x	1	1	1	1	1	1	1	1	1
23	1	1	1	1	1	1	1	1	1	1	1
24	1	1	1	1	1	1	x	1	1	1	x
25	2	L	1	1	1	1	1	1	1	1	1
26	2	L	L	1	1	1	1	1	1	1	1
27	1	x	x	1	1	x	x	x	1	x	1
28	1	1	1	1	1	1	1	1	x	x	1
29	1	1	x	1	x	x	1	x	x	x	1
30	1	x	x	x	x	x	1	1	1	1	x
31	2	2	2	2	2	2	L	2	L	2	1
32	2	L	2	x	2	x	x	x	x	2	1
33	x	x	x	x	L	x	L	x	x	L	x
34	2	x	L	L	x	x	L	L	L	2	1
35	L	L	x	L	L	x	L	2	2	2	1
36	x	x	x	x	x	2	x	2	x	2	1
37	1	1	1	1	1	1	1	1	1	1	x

Key	1	x	2	L
	Visual Pass	Visual Fail	Leak Pass	Leak Fail